CONFOCAL MICROSCOPY OF DYNAMIC PROCESSES IN THE CORNEA OF CONSCIOUS HUMANS

A thesis submitted to
the University of London
for the degree of Doctor of Medicine

Jeremy Prydal

St. George's Hospital Medical School

London

BIBL.
LONDIN.
UNIV.

Volume 2 is a video
Please apply to
university

ABSTRACT

This thesis is concerned with the results of imaging the cornea in conscious human subjects using a tandem scanning confocal microscope. The work was made possible by very recent, or ongoing, advances in optical, video and computer technologies. New methods of computer image analysis were developed to quantify structures in images. These techniques enabled, for the first time, examination of ongoing dynamic processes in undisturbed living tissue. Observations were made *in vivo* of the structure of normal human cornea, its response to injury, and changes in a number of pathological conditions.

Healthy cornea was examined for thickness of the epithelium and for morphology of keratocytes. Epithelial thickness varied from 38 to 53 μm. No variation was found across the central 5mm. Density of keratocytes was greatest near the stromal surface and reduced sharply towards posterior cornea. Approximately 50 μm from the endothelium there was an increase in cellularity. Cell size remained approximately constant throughout the stroma.

Tissue reaction to injury was studied after excimer laser photoablation to correct for myopia. Changes in keratocyte morphology, and the formation of scar tissue were quantified. Cell density, cell size and density of subepithelial scarring followed similar patterns, increasing to a maximum at 2-4 weeks. Regeneration of subepithelial nerves was examined up to 2.5 years after laser treatment. Almost no regeneration of subepithelial nerves was detected.

Confocal microscopy seemed to offer the opportunity to measure thickness of tear fluid between contact lens and epithelium. However, reproducible measurements were not obtained or possible.

Applications of the technique to the diagnosis of clinical disorders, as well as monitoring the effects of treatment, was examined. Observations were made in cases of infection by *Acanthamoeba*, and *Herpes simplex*, and in patients with *Herpes zoster*, Keratoconus, Leprosy, and Irido-corneal-endothelial syndrome.

PREFACE

This dissertation has not been submitted in whole, or part, to any other university.

I am very grateful to my supervisor, Professor P.N. Dilly, for his enthusiastic support, advice and help, both during the period spent doing the work presented here, and at many other times.

Special thanks are due to Professor J. Marshall, for his support, and for enabling me to examine patients undergoing excimer laser treatment. I appreciate the help of members of his research group, Miss M. Corbett and Miss S. Verma, who carried out the laser surgery and made measurements of refractive errors. Thanks are also due to Dr. F. Franc, for his advice in writing computer programs. All other work presented here was done by the author alone.

I am very grateful to Mr. M. Kerr Muir, Mr. D.J. Spalton, Mr. T. ffytche and Professor A. Boyde. They have shown much interest in the work, offered help, advice and made patients available for study.

The work would not have been possible without the generous support of the Iris Fund and Special Trustees of St. Thomas' Hospital.

I am especially grateful to Professor D.W. Kennard for numerous valuable discussions, his continual support, and great encouragement throughout.

VOLUME 1

TABLE OF CONTENTS 1

1 INTRODUCTION 14
1.1 Introduction 15
1.2 History of confocal microscopy 16
1.3 Confocal microscopy of the eye 18
1.4 Earlier work by author 20
1.5 Current Work 21
1.5.1 Epithelial thickness 21
1.5.2 Keratocyte density and orientation 22
1.5.3 Cellular response to injury 22
1.5.4 Re-innervation of the cornea after injury 23
1.5.5 Tear layer thickness between contact lenses and epithelium 24
1.5.6 Clinical conditions 24

2 EQUIPMENT AND METHODS 25
2.1 Optics 26
2.2 Surface reflections 29
2.3 Confocal microscope 30
2.3.1 General features 30
2.3.2 Alignment of holes in disk 30
2.3.3 Pattern of holes in disk 31
2.3.4 Illumination 31
2.3.5 Objective 32
2.4 Video recording 33
2.5 Image processing 35
2.6 Calibration 36
2.7 Procedures 37
2.7.1 Alignment 37
2.7.2 Examination of patients 37

3 VIDEO: CONFOCAL MICROSCOPY OF THE NORMAL CORNEA ... 38
3.1 Introduction 39
3.2 Orientation of optical sections 39
3.2.1 Tangential optical sections 39
3.2.2 Oblique optical sections 41
3.3 VIDEO 43
3.3.1 Tangential optical sections 43
3.3.2 Oblique optical sections 47

4 MEASUREMENT OF EPITHELIAL THICKNESS USING OBLIQUE OPTICAL SECTIONS....48
4.1 Introduction....49
4.2 Contact lenses for calibration....50
4.3 Method of measurement from oblique optical sections....51
4.4 Tests of accuracy....53
4.4.1 Curvature of corneal surface....53
4.4.2 Image distortion....55
4.3.3 Model of eye surface....55
4.5 Measurements in normal humans....57
4.5.1 Oblique optical sections....57
4.5.2 Tangential optical sections....62
4.6 Oblique optical sections without contact lenses....63
4.7 Discussion....64
4.8 Conclusions....66

5 DENSITY SIZE AND ORIENTATION OF KERATOCYTES....67
5.1 Introduction....68
5.2 Examination of subjects....69
5.3 Digitising of images....69
5.4 Density and size of cells....70
5.4.1 Problems in analysis of images....70
5.4.2 Procedure for image analysis....71
5.4.2 Results....77
5.5 Orientation of cells....83
5.5.1 Image analysis....83
5.5.2 Results....83
5.6 Discussion....86

6 WOUND HEALING....88
6.1 Introduction....89
6.2 Methods....91
6.2.1 Patients....91
6.2.2 Treatment....92
6.2.3 Examination....92
6.2.4 Image analysis....92
6.3 Results....95
6.4 Discussion....102

7 NERVE REGENERATION AFTER EXCIMER LASER.....104
7.1 Introduction.....105
7.2 Method.....106
7.2.1 Patients.....106
7.2.2 Laser treatment.....106
7.2.3 Microscopy.....106
7.3 Results.....108
7.4 Discussion.....111

8 THICKNESS OF TEAR FLUID BETWEEN SOFT CONTACT LENSES AND EPITHELIUM.....113
8.1 Introduction.....114
8.2 Author's earlier work.....114
8.3 Confocal microscopy for measurement of tear thickness under lenses.....116
8.3.1 Observations using immersion objectives.....116
8.3.2 Observations using dry objectives.....118
8.4 Discussion.....119

9 CLINICAL APPLICATIONS.....120
9.1 Introduction.....121
9.2 Corneal abrasion.....121
9.3 Infective keratitis.....123
9.3.1 *Acanthamoeba*.....123
9.3.2 *Herpes simplex*.....127
9.3.3 *Herpes zoster* keratitis.....129
9.3.4 Leprosy.....131
9.4 Endothelial disease.....132
9.5 Keratoconus.....134

REFERENCES.....135

TABLE OF CONTENTS 2

FIGURES

Figure 2.1.....27

Optics of tandem scanning confocal microscope.

S light source, D rotating disk, I illumination side of disk, O observation side of disk, M_1 half silvered mirror, L objective lens, C cornea,. M_2 Mirror, V video camera

Figure 3.1.....40

Diagram of alignment giving 'tangential' optical sections

OB objective, OS optical section, OA optical axis of objective, EP epithelium, ST stroma.

Figure 3.2.....40

Sample image of optical section tangential to epithelial surface in normal cornea.

Figure 3.3.....42

Diagram of alignment of objective to eye surface to give 'oblique' optical sections. OB objective, OS optical section, OA optical axis of objective, EP epithelium, ST stroma.

Figure 3.4.....42

Sample image of optical section at oblique angle to eye surface showing cross section through epithelium and stroma. The subepithelial nerve plexus is clear.

(a) Surface of epithelium

(b) Surface of stroma

Figure 3.5.....45

Tangential optical section through the subepithelial nerve plexus in a normal cornea.

Figure 3.6.....46

Optical section through stroma of a healthy cornea showing stromal nerve fibre with adjacent Schwann cell (arrow).

Figure 4.1.....51
Diagram of optics showing oblique optical section through contact lens, epithelium and superficial stroma. Objective at angle of 30° to normal. Optical section assumed to be flat, and contact lens and epithelium to be of same refractive index. Distances x' and y' determined from images and radial epithelial thickness, y, calculated from the ratio: x/y=x'/y' using known value of x, radial thickness of the contact lens.

Figure 4.2.....54
Error in estimation of epithelial thickness resulting from assumption that contact lens and epithelium are flat parallel layers. The ratio x'/y' is plotted against the angle of the objective to normal. Radius of curvature of stromal surface taken to be 7.5 mm. Contact lens and epithelium each taken to be 50μm thick and thus the ratio x'/y' would be 1.0 if the surfaces were flat.

Figure 4.3.....58
Confocal optical section through the eye surface.
(a) External surface of contact lens
(b) surface of epithelium
(c) dark band reflected from near stromal surface
(d) lighter band reflected from near stromal surface
The section marked is that used for determining separation of surfaces.

Figure 4.4.....59
Mean pixel intensity in each column of section marked in figure 4.3 plotted against horizontal position across image.
a: Front surface of contact lens
b: Interface between contact lens and epithelium
c: Dark band at stromal surface
d: Bright band at stromal surface
Letters correspond to structures marked in figure 4.3.

Figure 4.5.....61
Mean epithelial thickness in 4 subjects. Two values were calculated for each subject (see text). Error bars are +95% confidence limits.

Figure 4.6.....61
Epithelial thickness at 5 positions across the cornea: Centre (0), two positions below centre (-1.25 and -2.5 mm) and two positions above centre (+1.25 and +2.5 mm). Error bars are +95% confidence limits.
Figure 4.7.....63
Confocal optical section through epithelium and superficial stroma without contact lens.
(b) Surface of epithelium
(c) Dark band in reflection at stromal surface
(d) Lighter band at stromal surface
Subepithelial nerves are mostly within the dark band at the stromal surface
Figure 5.1.....70
Grey scale confocal image of keratocytes in superficial stroma. Full size image 768 by 512 pixels.
Figure 5.2.....75
Correlation of threshold values against mean intensity of image. Best threshold level determined 'by eye' plotted against mean intensity. Units of intensity were arbitrary, range 0-255. Linear regression line shown, constant -0.216, co-efficient 0.481, correlation co-efficient 0.92. Dashed lines are 95% confidence limits.
Figure 5.3.....78
Images before and after processing. The central region of images 256 x 256 pixels (210 x 210 µm) were processed. (a) Grey scale image. Section through superficial stroma. The full sized image is shown in Fig. 5.1. (b) Binary image, result of processing image 5.3a. Grey areas are of value 0, white of value 1.
Figure 5.4.....79
Images before and after processing. (a) Grey scale image. Section 25 µm superficial to Descemet's membrane. From same subject as images in Fig. 5.3. (b) Binary image after processing of image shown in 5.4a. Grey areas are of value 0, white of value 1.

Figure 5.5.....80

Density of cells (number / mm^2) plotted against depth of image from epithelial surface in each of 4 subjects.

Figure 5.6.....81

Percentage area of images occupied by cells plotted against depth of image from epithelial surface in each of 4 subjects.

Figure 5.7a.....85

Two dimensional Fourier transform of optical section just deep to Bowman's membrane (Fig 5.3a).

Figure 5.7b.....85

Two dimensional Fourier transform of optical section just superficial to Descemet's membrane (Fig 5.4a).

Figure 6.1.....94-95

Threshold level selected 'by eye' plotted against mean intensity of sample images (a) of keratocytes before laser treatment, (b) keratocytes after treatment, (c) subepithelial scar tissue (see section 6.1). Units of intensity on ordinates and abscissas are arbitrary, range 0 to 255. Linear regression (solid line) and 95% confidence limits (dashed lines) are shown.
Linear regression:
(a) Constant=-0.216 co-efficient=0.481 r=0.92
(b) Constant=5.504 co-efficient=1.383 r=0.87
(c) Constant=8.302 co-efficient=1.330 r=0.88

Figure 6.2.....96

Grey scale and binary images of keratocytes in superficial stroma at one month after laser treatment. Images are 210 x 210 μm, the central region 256 by 256 pixels from full image, size 768 by 512 pixels. In binary images grey areas are of value 0, white of value 1.

Figure 6.3.....97

Grey scale and binary images of subepithelial scarring one month after treatment. The full sized grey scale image is shown in figure 7.1.

Figure 6.4.....98
Results for each subject after photokeratectomy are plotted against time in months after the treatment. Size of cells (open circles, left ordinate), cell density (solid stars, right ordinate) and density scar tissue (solid squares, right ordinate) are plotted. Time zero is before treatment.

Figure 6.5.....99
Results in subject LC as plotted in figure 6.3 to show error bars, ±95% confidence limits. Cell density, cell size and density of scar tissue are plotted against time after treatment.

Figure 7.1.....109
Optical section tangential to scar material 1 month after Excimer laser treatment.. No nerves were seen superficial to this layer.

Figure 7.2.....109
Structures shown in Fig 7.1 with optical section at oblique angle to eye surface.

Figure 7.3.....110
Single subepithelial nerve fibre as found in 2 of the 19 subjects examined.

Figure 7.4.....110
Tortuous nerve fibre in the superficial stroma as found in one subject following Excimer laser treatment.

Figure 8.1.....117
Oblique optical section through cornea.
(a) Outer surface of contact lens
(b) Inner surface of contact lens
(c) Surface of epithelium

Figure 8.2.....118
Non contact dry objective: Oblique optical section through contact lens and eye surface.
(a) Outer surface of contact lens

(b) Surface of epithelium

(c) Surface of stroma

Subepithelial nerves and stromal keratocytes can be identified.

Figure 9.1.....122

Epithelial cell surface 2 days after corneal abrasion showing elongated cells (Normal structure is shown in figure 3.2)

Figure 9.2.....125

Optical section through deep epithelium in patient with *Acanthamoeba* keratitis. The organism (arrow) is about 35 µm in diameter.

Figure 9.3.....126

Optical section through stroma in patient with *Acanthamoeba* keratitis showing nerve of normal diameter, approximately 8 µm.

Figure 9.4.....127

Optical section through surface of epithelium in patient with *Herpes simplex* keratitis.

Figure 9.5.....128

Optical section tangential to subepithelial nerve plexus in patient with *Herpes simplex* keratitis. Only small fragments of nerves remain.

Figure 9.6.....129

Optical section oblique to corneal surface in patient with *Herpes simplex* keratitis. No subepithelial nerves can be identified.

Figure 9.7.....131

Thickened subepithelial nerve fibres in case of lepromatous leprosy.

Figure 9.8.....133

Junction of normal and abnormal cells in Irido-corneal-endothelial syndrome (arrows). The overlying stroma and epithelium were hazy due to oedema.

Figure 9.9.....134

Thickened stromal nerve in a case of keratoconus.

TABLE OF CONTENTS 3

TABLES

Table 6.1.....101

Refractive errors in each subject before and 6 months after excimer laser treatment

VOLUME 2

VHS video

ERRATA

Page	Line	
2	30	For "Keratoconnus" read "Keratoconus"
34	3	For "tack" read "track"
37	2	For "every each" read "each"
46	2	For "keratocytes" read "keratocyte"
69	16	For "subject" read "subjects"
72	9	For "where" read "were"
76	3	For $S = \frac{4a}{p^2}$ read $S = \frac{4\pi a}{p^2}$
84	5	For "fourier" read "Fourier"
92	15	For "section 5.4.2" read "section 5.4.1"
93	1	For "opf" read "of"
111	18	For "Lawresnson's" read "Lawrenson's"
126	4	For "re-examination" read "re-examined"
129	3	For "reduced" read "reduce"
137	16	For "veranderungen" read "Veränderungen"
137	16	For "reflexbild" read "Reflexbild"
145	6	For "Cambride" read "Cambridge"

CHAPTER 1

1 INTRODUCTION

1.1 Introduction

1.2 History of confocal microscopy

1.3 Confocal microscopy of the eye

1.4 Earlier work by author

1.5 Current work

1.5.1 Epithelial thickness

1.5.2 Keratocyte density and orientation

1.5.3 Cellular response to injury

1.5.4 Density of the sub-epithelial nerve plexus

1.5.5 Tear layer thickness between contact lenses and epithelium

1.5.6 Clinical conditions

1.1 Introduction

Confocal microscopy is a modification of reflected light microscopy (Boyde and Petran 1983, Petran and Hadravsky 1986). Living tissue in conscious humans can be examined at high resolution, contrast and magnification. Conventional histological techniques of fixation and staining are not required. The ability to examine undisturbed tissue at high magnification in living humans is unique. Confocal microscopy is a significant advance in the methodology available. It enables study of structural changes in ongoing physiological and pathological processes.

This thesis is concerned with results of imaging the cornea in conscious subjects using a tandem scanning confocal microscope (TSCM). Structure in healthy and diseased eyes, dynamic processes during wound healing, and changes in disease states were quantified. The results are presented.

The theoretical possibility of using confocal microscopy has been realised for many years. However it is only recently been possible to build a system to examine eyes of conscious humans. The equipment is very different from earlier conventional microscopes. Light levels are low and images blurred due to eye movement. Images can not be viewed through an eye piece. Special optical devices, sensitive video cameras, video recorders with fine search facilities and computer processing are necessary to give clear images. Advances in these technologies have only recently made the work presented here possible. The problems are similar to those of astronomical imaging. Objects can not be seen by the naked eye, but can be revealed by optical and computer processing.

1.2 History of confocal microscopy

Confocal microscopy was invented by Minsky in 1955 (Minsky 1988). He built the first confocal microscope, although images were too transient for it to be of practical use. A small point of light was focused in specimens and only light from that point used to form images. Light reflected from above and below the plane of focus was excluded. Images were thin optical 'sections' or slices through the specimen. As a result, detail in images was not obscured by out of focus reflections from other layers. The object was moved to scan the beam across an area and enlarge the field of view beyond the size of the single illuminated point. A radar screen with slow decay was used to display images. However, they were short-lived, only parts were visible at one time, and they could not be recorded for publication.

In 1960 Petran built the first functional microscope (Petran et al. 1968). The object was illuminated by several points of light at one time. Each was the image of a small hole in a disk, exposed on one side to direct sunlight. Light reflected from each point was imaged in another hole on the opposite side of the disk. The disk rotated to scan the object and build up an image. An advantage of this system was that images of stable objects could be viewed through the eye piece in 'real time'. However, they were dim - it was necessary for the eye to be fully dark adapted before using the microscope. Also alignment of holes on the illumination and observation sides of the disk had to be within tolerances of a few microns. This design is known as the 'two-sided' TSCM.

Egger used a similar design to that of Petran (Egger et al. 1969). He replaced the holes in the disk with radial slits. Thus alignment was simplified.

In 1971 Davidovits and Egger described a confocal microscope in which a laser was used as the light source. The object was scanned by movement of the objective lens. However the time required to build up an image was too long to examine moving tissue in living animals.

A laser scanning confocal microscope in which the beam was scanned in a raster pattern at standard TV rates was developed by Draaijer and Houpt in 1988. Use of coherent laser light reduced chromatic aberration. Also the size of the beam could be changed which gave optical sections of varying thickness. Selection of the appropriate wavelength of light also makes laser microscopes suitable for fluorescent microscopy. Fluorescent stains can be used to identify specific structures (Poole et al. 1993) and to measure intracellular ionic concentrations (Lohmeyer et al. 1994). In these applications confocal microscopy is used because of the high resolution, not to enable examination of whole specimens. Most laser confocal microscopes require several minutes per scan and they have not yet been used successfully to examine eyes in conscious humans.

Another type of confocal microscope was built by Kino (Xiao and Kino 1987, Kino et al. 1988, Xiao et al. 1988). This was again a modification of Petran's design, but used the same hole in the disk for both illumination of the object and imaging of light reflected from it. A system of cross polarising filters and half silvered mirrors was required to separate the two light paths. The advantage of this design was that alignment of holes in the disk was not necessary. However images were of lower contrast than those by Petran's original 'two-sided' design (Boyde, Xiao et al. 1990).

1.3 Confocal microscopy of the eye

Maurice, in 1968, described a simple form of confocal microscopy in which half the objective lens was used for illumination and half for observation (Maurice 1968). Later, resolution was improved by using two stationary slits in each light path. The specimen was advanced across the illuminated slit (Maurice 1974).

Improvements in the methods used to scan the object have lead to instruments suitable for clinical use, the specular microscope (Laing et al. 1975 and Bourne et al. 1976). They give images of the surfaces of the epithelial and endothelial layers in conscious patients. However they are limited to examining the outer and inner surfaces of the cornea where the change in refractive index is larger than within the cornea and thus more light is reflected.

Petran examined enucleated chicken eyes using a TSCM. However, again, imaging was limited to the epithelial and endothelial cell layers (Petran et al. 1985). Lemp, Dilly and Boyde imaged the full thickness of cornea in excised human eyes (Lemp et al. 1985).

Dilly in collaboration with Boyde, Wright and Lemp modified a TSCM built by Petran and were able to image cornea in conscious humans (Dilly 1988). Fleeting glimpses of epithelium, endothelium as well as cells within the stroma were observed. However they were too brief to be recorded with the system available at that time. Two years later, Cavanagh and Jester et al. used a sensitive video camera and were able to record images in conscious humans with a modified TSCM (Cavanagh et al. 1990)

The author of this thesis used a Petran TSCM to measure tear thickness of layers in the cornea in eyes of freshly sacrificed animals (Prydal 1991,

Prydal and Campbell 1992). Details are given in section 8.2. Images in conscious humans were recorded using the 'one-sided' TSCM.

Koester, Auran et al. (1993) published photographs of images from living human eyes showing superficial and deep epithelial cells, subepithelial nerve fibres, stromal keratocytes and endothelial cells. They used a scanning slit design of microscope with a specially developed immersion objective (Koester et al. 1993).

In 1993 Cavanagh and Petroll et al. described further modifications of Petran's design. This microscope was manufactured by the Tandem Scanning Corporation (Reston, Virginia, USA). Particular care had been taken to ensure accurate optical alignment, the size and pattern of holes in the disk had been optimised and an objective built specifically for examining the cornea in conscious subjects.

Masters (1994) examined cornea in conscious humans using a system with confocal slits of adjustable width.

1.4 Earlier work by author

In our earlier work, a prototype Petran TSCM was used to measure the thickness of tear film and epithelium in animals (Prydal 1991, Prydal and Campbell 1992). However, at that time, clear images were only possible in immobile tissues and therefore animals were examined soon after death. The surface of the tear film, epithelium and stroma could be clearly identified. It was possible to record high resolution images using standard photographic methods, but exposures of up to two minutes were required, little light was available to form images. Also it was only possible to image superficial layers of the cornea. Structures deep to the stromal surface were of poor resolution.

Attempts were made to record images of living human cornea using sensitive cooled and intensified CCD (charge coupled display) cameras, but this was not successful. It seemed possible that the mechanical design of the microscope did not allow for sufficiently accurate alignment. Images in conscious subjects were possible using the 'one-sided' TSCM (Xiao and Kino 1987, Kino 1988) probably because it did not require accurate alignment. Images of the tear film and epithelial surfaces were recorded *in vivo* using an intensified CCD camera, but the system did not give reproducible results and again images were limited to superficial layers of the cornea.

We attempted to improve the Petran TSCM and modify it specifically for examining conscious humans. However at about that time, the TSCM manufactured by Tandem Scanning Corporation became available. The author visited Professor Cavanagh at Dallas University, Texas to evaluate the microscope. It was a substantial improvement on earlier models and gave images of high contrast and resolution throughout the cornea. One of these microscopes was used for the work presented in this thesis.

1.5 Current Work

The work presented in this thesis was made possible by very recent or ongoing advances in optical, video and computer methods. These enabled examination of the structure of the cornea in healthy and diseased eyes, as well as during wound healing. New methods were developed to quantify structures in images. Several specific studies were performed, as outlined below.

At this time Professor Marshall at St. Thomas' Hospital was studying a group of ten patients undergoing excimer laser treatment for myopia. This provided the opportunity to examine the response to injury in these patients. They were examined before treatment and at regular intervals up to 6 months afterwards. Observations were also made in subjects who had been treated up to 2.5 years earlier.

The procedure of laser treatment was carried out by members of Professor Marshall's research group, but the observations by confocal microscopy presented here were done by the author alone.

The application of confocal microscopy to diagnosis of clinical disorders as well as monitoring the effects of treatment was also examined.

1.5.1 Epithelial thickness

In earlier work (Prydal 1991, Prydal and Campbell 1992) confocal microscopy was used to measure thickness of tear film and epithelium in several animal species. Surfaces within the cornea were identified and the position of animals' heads adjusted so that images were circular. Optical sections were then tangential to surfaces. They could be accurately lo-

cated. The separation between them, radial thickness, was measured using the stage micrometer of the microscope.

However, accurate measurements by this method are not possible in conscious humans. Involuntary eye and head movements introduce unknown errors. In this work, an alternative method of measurement was developed in which measurements were made from single fields of video recordings with optical sections oblique to the eye surface. Measurements of epithelial thickness were made in the centre and at different positions across the cornea in healthy subjects.

1.5.2 Keratocyte density and orientation

Keratocytes function to maintain the collagen fibres and extra-cellular matrix of the corneal stroma (Klyce and Beuerman 1988). Earlier work concerning their density and distribution was done using conventional microscopy or biochemical methods in excised tissue (Møller-Pedersen et al. 1994, Katakami et al. 1991, Poole et al. 1993). A laser scanning confocal microscope was used by Boettcher et al. (1994) to examine isolated rabbit cornea. Images were digitised for computer analysis, but counting was done manually.

The author developed a computerised method for analysing cellular structure in optical sections through the stroma. It gave independent automated measurements cell density and size. Orientation of keratocytes at different layers in the cornea was also determined.

1.5.3 Cellular response to injury

The availability of confocal microscopy enabled, for the first time, sequential microscopical examination of tissue reaction to injury in man.

Katakami et al. (1991) examined keratocyte activity following epikeratophakia in rabbits using conventional histological methods. Laser scanning confocal microscopy was used by Ichijima et al. (1993) to study healing after trauma to the endothelium and whole cornea, but again this work was done in isolated tissue.

Excimer laser treatment for myopia reshapes the corneal surface by photoablation of superficial layers of stroma, thus changing the optical power of the external corneal surface (Marshall et al. 1986). Methods were developed by the author for digital image analysis of cells in the stroma and were used to examine ongoing processes during wound healing after excimer treatment. Measurements were made throughout the stromal thickness in the centre of the ablated area.

1.5.4 Re-innervation of the cornea after injury

There have been many studies of corneal neuroanatomy using conventional light and electron microscopy (Zander and Weddell 1951, Whittear 1960, Matsuda 1967, Rózsa and Beuerman 1982, Beuerman et al. 1982). Imaging of corneal nerves by confocal microscopy has been reported (Masters and Paddock 1990, Cavanagh et al. 1993, Koester et al. 1993).

Epithelial, subepithelial and superficial stromal nerves are destroyed by Excimer laser ablation (Trabucchi et al. 1994). Studies in animals using conventional histological techniques have found nerve regeneration to be complete within 1 month (Pallikaris et al.1990, Trabucchi et al. 1994). We followed re-growth of the subepithelial nerve plexus and superficial stromal nerves in human subjects.

1.5.5 Tear layer thickness between contact lenses and epithelium

In earlier work, the author found tear film thickness to be substantially thicker than previous estimates and to be of a different structure, composed largely of mucus (Prydal 1991, Prydal and Campbell 1992, Prydal et al. 1992). Tear film thickness on the external surface of contact lenses was measured and found to increase during adaptation to their wear.

Confocal microscopy seemed to offer the opportunity to measure thickness of tear fluid between contact lens and epithelium. Optical sections at oblique angles to the eye surface were imaged. Outer and inner surfaces of the contact lens and the surface of the epithelium could be identified. The aim was to measure thickness with different contact lenses, materials and fittings, and to follow changes as subjects adapted to their wear.

1.5.6 Clinical conditions

Infective disorders of the cornea were examined. The aim was to identify causative agents, or changes characteristic of particular infections. Patients with infections by *Acanthamoeba*, *Herpes simplex*, and *Herpes zoster* were examined.

Observations were also made in patients with Keratoconnus, Leprosy, and Irido-corneal-endothelial (ICE) syndrome .

The purpose was to find those conditions in which confocal microscopy may be useful for clinical management. It was not intended to examine sufficient numbers of patients for statistically significant results.

CHAPTER 2

2 EQUIPMENT AND METHODS

2.1 Optics

2.2 Surface reflections

2.3 Confocal microscope

- 2.3.1 General features
- 2.3.2 Alignment
- 2.3.3 Pattern of holes in disk
- 2.3.4 Illumination
- 2.3.5 Objective

2.4 Video recording

2.5 Image processing

2.6 Calibration

2.7 Procedures

- 2.7.1 Alignment
- 2.7.2 Examination of patients

2.1 Optics

Confocal images are 'optical sections', or slices, through the object. They may be several millimetres below its surface. Light reflected from above and below the plane of focus is excluded. Only reflections from the plane of focus contribute to the image.

In Petran's design of microscope (Petran et al. 1985) a disk contains hundreds of paired holes (Nipkow disk). Part of the disk is illuminated, forming several point sources of light. Each is imaged in the object and light reflected from it focused in a corresponding hole in another part of the disk. The image of the illumination hole corresponds precisely with the observation hole - they are 'confocal'.

The observation hole acts as a filter. Only light from the plane of focus can pass. Detail in images is improved because out of focus reflections do not contribute to images and obscure structure that is in focus.

The observation hole also filters light in another way. The image of an illuminated point is an Airy diffraction pattern. In conventional microscopy the outer rings of the pattern may limit resolution (Elkington and Frank 1984). In confocal systems, the observation hole blocks outer diffraction rings, passing only the central part of the pattern. It has been estimated that this results in an improvement in resolution by a factor of two (Wilson 1989).

Figure 2.1 is a diagram of the optics of a 'two-sided' TSCM, as described by Petran. A disk (D) contains several hundred holes, 50 μm in diameter. One side of the disk is used for illumination (I), the other for observation (O). Rays from one of the illuminated holes is shown imaged by the objective lens (L) in the cornea (C). Light reflected from this illuminated spot is imaged by the same objective, via a half silvered mirror (M_1) and

fully silvered mirror (M_2), in a conjugate hole on the opposite side of the disk.

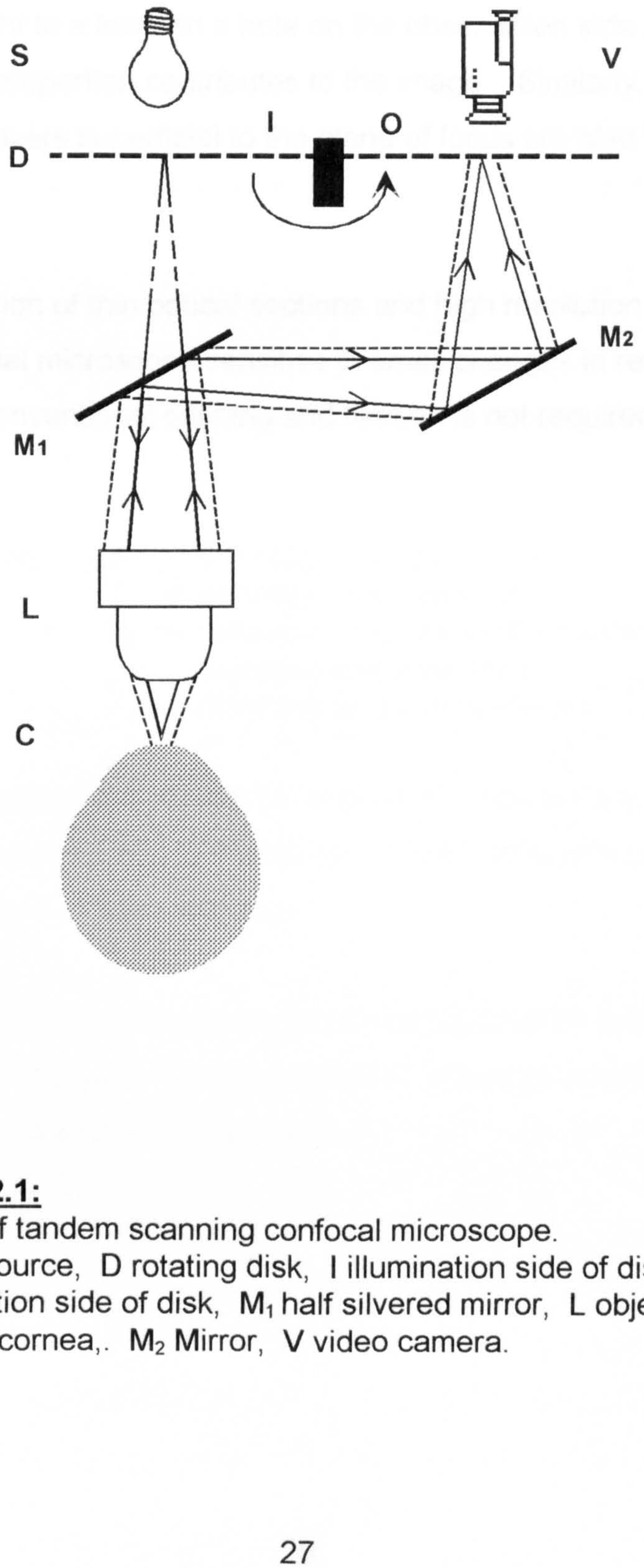


Figure 2.1:
Optics of tandem scanning confocal microscope.
S light source, D rotating disk, I illumination side of disk, O observation side of disk, M_1 half silvered mirror, L objective lens, C cornea,. M_2 Mirror, V video camera.

Images are formed on the photocathode of a video camera (V). If the object reflects sufficient light, images may be viewed directly through an eye-piece in place of the camera. The disk rotates to scan the object and build up a complete image.

Light rays reflected from below the plane of focus (dashed lines fig 2.1) are not brought to a focus in a hole on the observation side of the disk. Only a small proportion contributes to the image. Similarly, light reflected from layers superficial to the plane of focus are also largely excluded.

The combination of thin optical sections and high resolution images makes confocal microscopy sensitive to small changes in refractive index. As a result, conventional staining and fixation is not required to see detail in tissue.

2.2 Surface reflections

Filtering of axial rays is less efficient than of non-axial ones. Reflections from the external surface of the specimen, the back of the objective, as well as other optical components pass directly through holes on the observation side of the disk, reducing image contrast.

The proportion of light reflected at an interface depends in part on the difference in refractive index. At small incident angles (Jenkins and White 1985):

$$R = I\left[\frac{(n_1 - n_2)}{(n_1 + n_2)}\right]^2$$

where R = Intensity of reflected light
I = Intensity of incident light
n_1 = refractive index of medium between objective and specimen
n_2 = refractive index of specimen

Use of water immersion objectives reduces the difference in the refractive index at the outer surface of the cornea. Less light is reflected resulting in clearer images of deep structure.

Reflections from optical components can be reduced by anti-reflection coatings. Also the use of mirrors instead of prisms decreases the number of surfaces orthogonal to the light path.

2.3 Confocal microscope

A two sided TSCM designed and manufactured by the Tandem Scanning Corporation (Reston, Virginia, USA) was used for the work described in this thesis. It was based on Petran's design, but had been modified and improved by the company in several ways.

2.3.1 General features

The microscope was designed specifically for examining eyes of conscious patients. The objective was horizontal and apparatus mounted on a slit-lamp base. Patients were seated, their head supported by chin and forehead rests. The table supplied with the microscope was found to be unstable and was replaced with one made by Carl Zeiss.

2.3.2 Alignment of holes in disk

Alignment of holes on the illumination and observation sides of the Nipkow disk must be to within tolerances of a few microns. The image of holes on the illumination side should fall precisely on the conjugate holes on the opposite side of the disk. Holes were 20 µm in diameter and misalignment by this amount would prevent all light from passing through the system.

The mechanical construction of Petran's early microscope did not allow sufficiently fine adjustments. In addition, it was necessary to partly dismantle the microscope. It seemed likely that the alignment was disturbed when re-building the instrument.

In the new microscope, adjustment of the horizontal position of the disk could be done without dismantling the microscope. A special objective with a built in mirror was provided for this purpose. It gave a bright uniform image when viewed through the eye-piece. External adjustment

knobs were used to eliminate flicker in the image. The disk was then aligned in the horizontal plane.

Adjustment of the tilt of the disk and its centring was more complex. However, if little flicker was apparent when viewing the even field produced by the special alignment objective, tilt and centring where correct. The mechanical construction was stable and these more complex adjustments were not required.

Materials used for construction were chosen so that alignment was not lost as the equipment warmed and expanded.

2.3.3 Pattern of holes in disk

The arrangement of holes in the disk should give even illumination across the image. Equal spacing would give images which were brighter towards the edge. Petran arranged the holes in a modified Archimedian spiral (Petran et al. 1985b). This gave even illumination, but the moving holes caused streaks across images. These were accentuated in video recordings because of interference between the spacing of streaks and those of video scan lines.

In the new microscope the pattern of holes had been designed to give even illumination, no streaking, and no aliasing in video recordings. There were 64,000 holes in the disk, each 20 µm diameter. Its transmitted 0.25% of the incident light and rotated at 450 rpm.

2.3.4 Illumination

Illumination was from an air cooled 100W mercury arc lamp. Unfortunately, the fan introduced some vibration. In Petran's microscope the light source housing was water cooled to avoid this problem.

2.3.5 Objective

The objective was designed specifically for examining the eye in conscious humans. It was water immersion, 24x magnification, numerical aperture 0.6, with variable working distance from 0 to 1.5 mm. The tip was a glass cone tapering to a diameter of 5mm with curvature matched to that of the eye surface. The tip could contact the cornea without the body of the objective touching the eye lashes or lid.

The objective mounting could retract, taking up forward and backward eye movement without changing the plane of focus. This improved stability of images.

The plane of focus was advanced through the cornea without movement of the objective or subject. Lenses housed within the objective were positioned by a motor. This was controlled by a separate unit (Oriel). The Oriel controller could be set to move the focal plane in or out of the tissue, either continuously or in specified steps. A readout gave the distance moved by lenses in the objective. Using computer models of the optics, an equation converting this reading to the distance moved by the optical section through the stroma has been determined*:

$$D = (0.414 \times R) - (1.285 \times 10^{-5} \times R^2) + (1.914 \times 10^{-10} \times R^3)$$

where D = distance moved in cornea (μm)
R = distance moved by lenses (μm)

The accuracy of this equation was not tested as precise measurements of depth were not required in the work presented here.

---

* Personal communication, J. Hill, Tandem Scanning Corporation, Reston, Virginia, USA.

2.4 Video recording

Intensified tube cameras are more sensitive than those with silicon chip CCD's although they give images of lower contrast. Several cameras were tested: Dage 66 silicon intensified tube (SIT) camera, Dage VT1000 SIT (Alrad Instruments, Newbury, UK) Hamamatsu SIT (ImproVision, Coventry,UK), Dage intensified CCD (Alrad Instruments) and Improvision intensified CCD.

The Dage VT 1000 was found to be most sensitive and gave images of high contrast. Video tubes are more sensitive in the centre of the field. This model was fitted with additional circuitry to reduce variations in sensitivity.

Images were recorded on Super-VHS tape using a Panasonic AG7335 recorder. The Panasonic recorder enabled video recordings to be reviewed one frame at a time, running in either forward or reverse directions. Each video frame is made up of two interlaced fields. The recorder included controls to select either the first or second field. These precise search facilities enabled careful review of recordings and selection of those individual fields showing clear structure. Images were then transferred to a digital frame store within the recorder and from there to a computer.

Video recordings are at a rate of 25 frames per second. Each frame is made up of two fields and thus each of these is exposed for 20ms. An electronic shutter was tested, as it seemed possible that reduced exposure times may have given clearer images, but it was found to interact with the scanning holes in the disk.

The camera was mounted on the microscope in a higher position than had been intended and the focusing lens adjusted beyond its normal

range. This gave a wider field of view, only slightly smaller than that viewed directly through the eye piece.

The audio tack was used to record details of the experiment, subject, and depth of the optical section as given by the read out on the Oriel objective controller.

2.5 Image processing

Selected images were digitised at a resolution of 768 by 512 pixels and 256 grey levels (Imaging Technology Inc., Overlay Frame Grabber). Processing was done on a 486 or Pentium PC using 'Lucida', an image processing package (Kinetic Imaging, Liverpool, UK.).

Significant image enhancement can be achieved by averaging successive frames. However images of eye structure were continually moving. Part of the Lucida program was written specifically to overcome this problem. It enabled several frames to be repositioned so that features coincided. They could then be averaged. Unfortunately this feature was of limited value. Eye movements were not simple translations in one plane. The eye seemed to also rotate and twist and the program could not compensate for such movements.

Contrast could be improved by subtracting background noise from images. However, background varied with the structure and subject examined. It was often necessary to use different backgrounds for each subject and type of image. Background images were made by averaging up to 150 images without repositioning them to coincide features.

This gave a featureless image without structural detail. However, averaging revealed streaks caused by the scanning holes in the Nipkow disk. These were removed by a standard image averaging process in which each pixel is replaced by the average of itself and the surrounding eight pixels (Gonzalez and Wintz 1983a). This filtering process was performed 15 times and resulted in background images of smooth profile.

Image contrast was enhanced by 'normalisation' (Gonzalez and Wintz 1983b):

$$P' = 255 \times \left[\frac{(P - \min)}{(\max - \min)} \right]$$

where
P' = new pixel value
P = original pixel value
max = value of brightest pixel in original image
min = value of darkest pixel in original image

Various procedures for image enhancement and analysis were used for different observations. Details are given in the relevant chapters

Photographs could be made by sending digital images to a photographic printer (Polaroid CI3000, Polaroid UK, St. Albans, UK). This could print to Polaroid or standard 35mm film.

2.6 Calibration

Distances across images was measured in images of a silicon crystal marked with squares of periodicity 9.9 μm (Agar Scientific Ltd, Stanstead, UK). Slight pin-cushion distortion was evident. It was quantified using the same crystal.

2.7 Procedures

2.7.1 Alignment

The microscope was aligned each week using the procedure described in section 2.3.2. It was also checked before every each subject was examined by focusing the microscope on the tip of the standard objective. This gave a good indication of the accuracy of alignment. If flicker was visible, the full alignment procedure was carried out.

2.7.2 Examination of patients

The objective tip was cleaned with 70% Industrial methylated spirit (70% v/v), in keeping with the standard hospital procedure for cleaning of instruments used in contact with patients' eyes.

The nature of procedures were explained to subjects and consent obtained. The cornea was anaesthetised with 0.4% Oxybuprocaine Hydrochloride (Benoxinate) and subjects' heads supported by chin and forehead rests. They were instructed to fixate a small light. A drop of 2% methylcellulose was put on the tip of the objective to serve as an optical link - immersion fluid. After contact between objective and eye, the focal plane was advanced and the position of the microscope adjusted using its joy-stick to image superficial epithelium. Special procedures for each observation made are described in relevant chapters.

CHAPTER 3

3 VIDEO: CONFOCAL MICROSCOPY OF THE NORMAL CORNEA

3.1 Introduction

3.2 Orientation of optical sections

3.2.1 Tangential optical sections

3.2.2 Oblique optical sections

3.3 Description of video recording

3.3.1 Optical sections tangential to layers of cornea

3.3.2 Optical sections oblique to layers of cornea

3.1 Introduction

A sample video recording of confocal microscopy in a conscious human subject is included with this thesis. The subject was a 29 year old female with normal eyes.

Optical sections may be either tangential to surfaces in the cornea or oblique to them. Oblique sections give 'cross sections' through several layers in one image.

3.2 Orientation of optical sections

3.2.1 Tangential optical sections

Optical sections tangential to surfaces were obtained by focusing on the epithelial surface and adjusting the position of the microscope to give a circular image of the cell surface, at that starting level. The plane of focus was then advanced through the cornea without changing the orientation of microscope to eye surface.

Tangential optical sections were formed when the axis of the objective was aligned along the normal to the eye surface - with the objective resting flat on the eye. The diagram in figure 3.1 shows this arrangement. Figure 3.2 is a sample image of an optical section tangential to the epithelial surface.

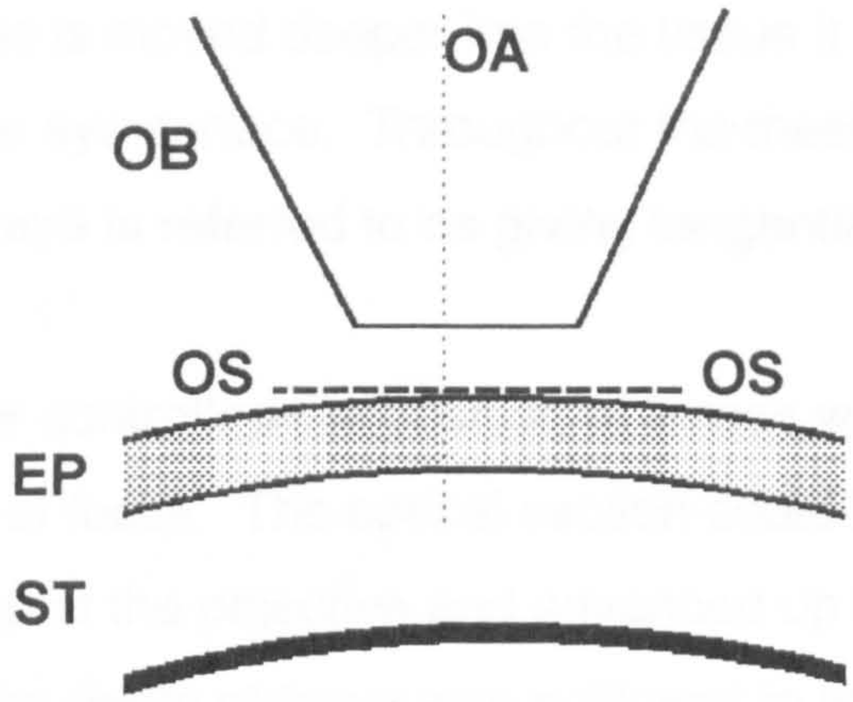


Figure 3.1
Diagram of alignment giving 'tangential' optical sections
OB objective, OS optical section, OA optical axis of objective, EP epithelium, ST stroma.

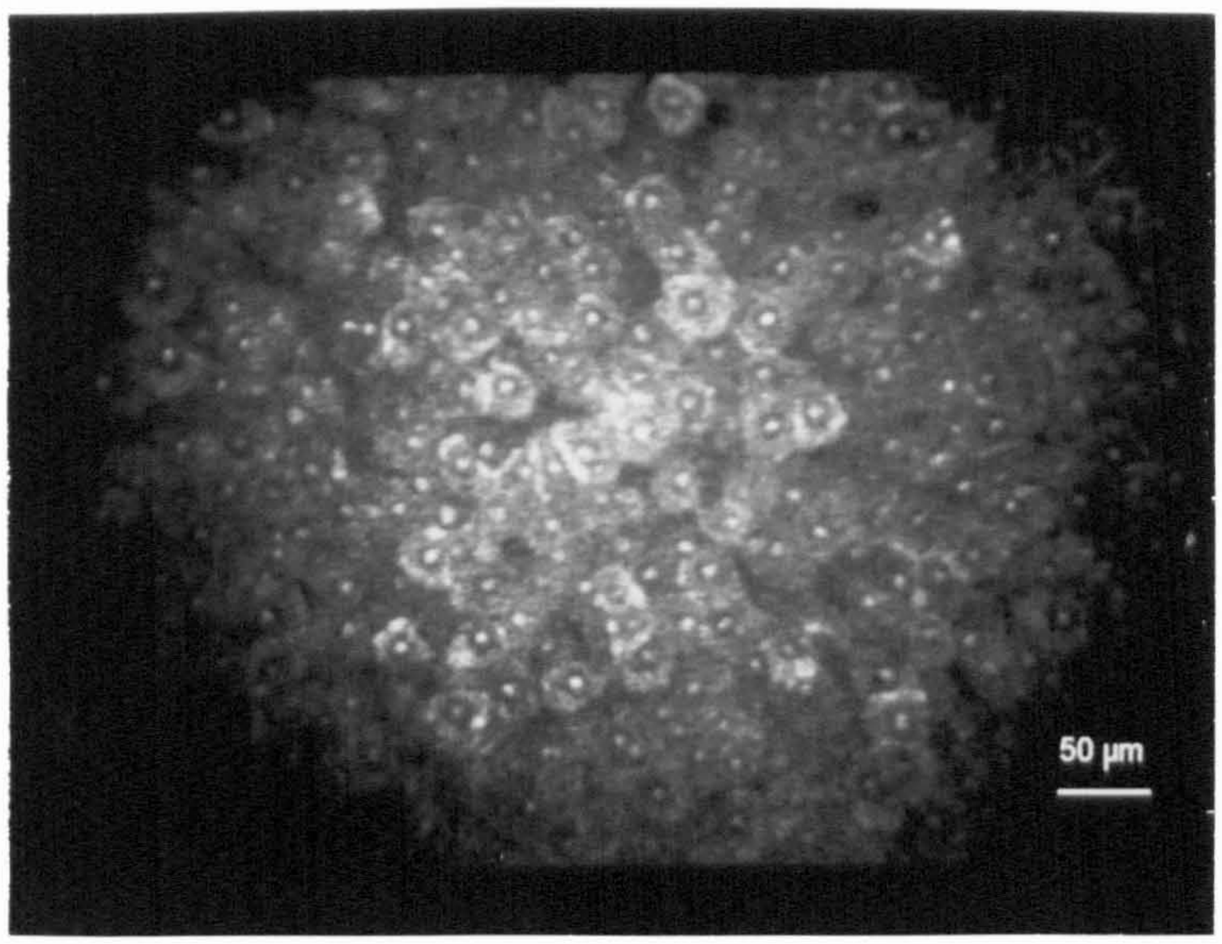


Figure 3.2
Sample image of optical section tangential to epithelial surface in normal cornea.

As the focal plane is moved deeper into the tissue it remains parallel with the tangent to the eye surface. Throughout the thesis, this alignment of microscope and eye is referred to as giving tangential optical sections.

A precision motor controlled the position of lenses within the objective to adjust the depth of focus. The optical section could be withdrawn until focused on the tip of the objective and advanced up to 1.5 mm from that position. Thus the depth of focus was sufficient to image all structures in the cornea down to endothelium.

The first part of the video recording was made with the objective positioned as in figure 3.1. The plane of focus is advanced away from the tip of the microscope objective, through epithelium and stroma, down to endothelium.

3.2.2 Oblique optical sections

Images of cross sections through the eye are obtained when the microscope objective is at an oblique angle to the tangent at the eye surface, as illustrated in figure 3.3. Such images show the surface of epithelium, Bowman's membrane and superficial stroma in single images. A sample is shown in figure 3.4. The second part of the video recording was made with the microscope in this orientation.

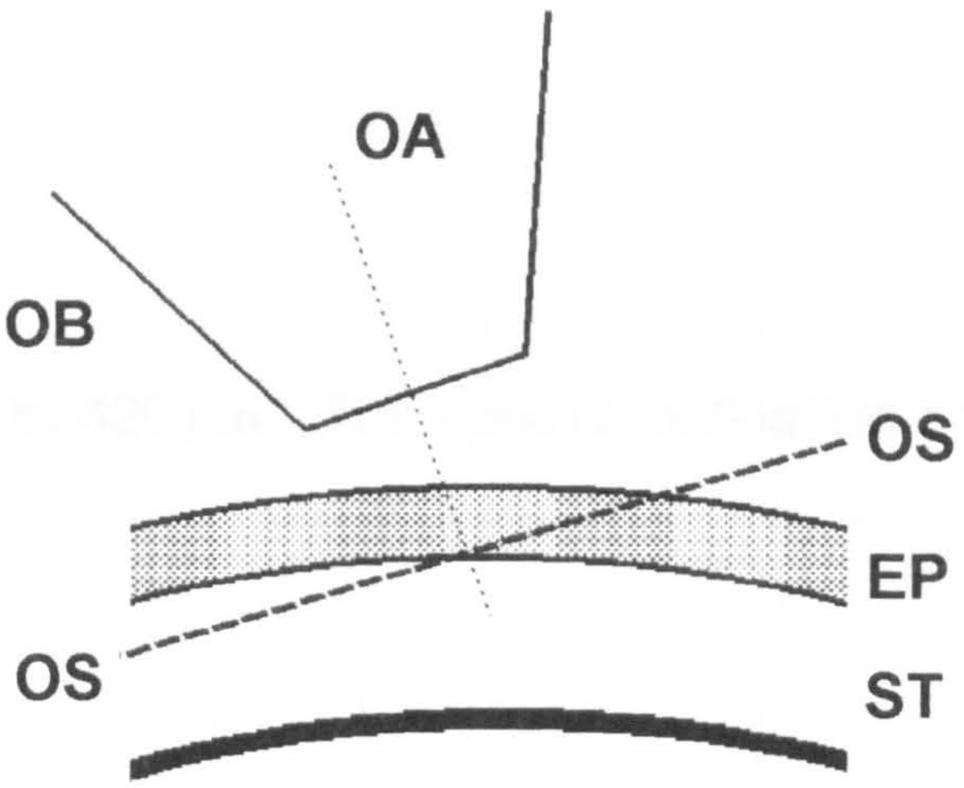


Figure 3.3
Diagram of alignment of objective to eye surface to give 'oblique' optical sections. OB objective, OS optical section, OA optical axis of objective, EP epithelium, ST stroma.

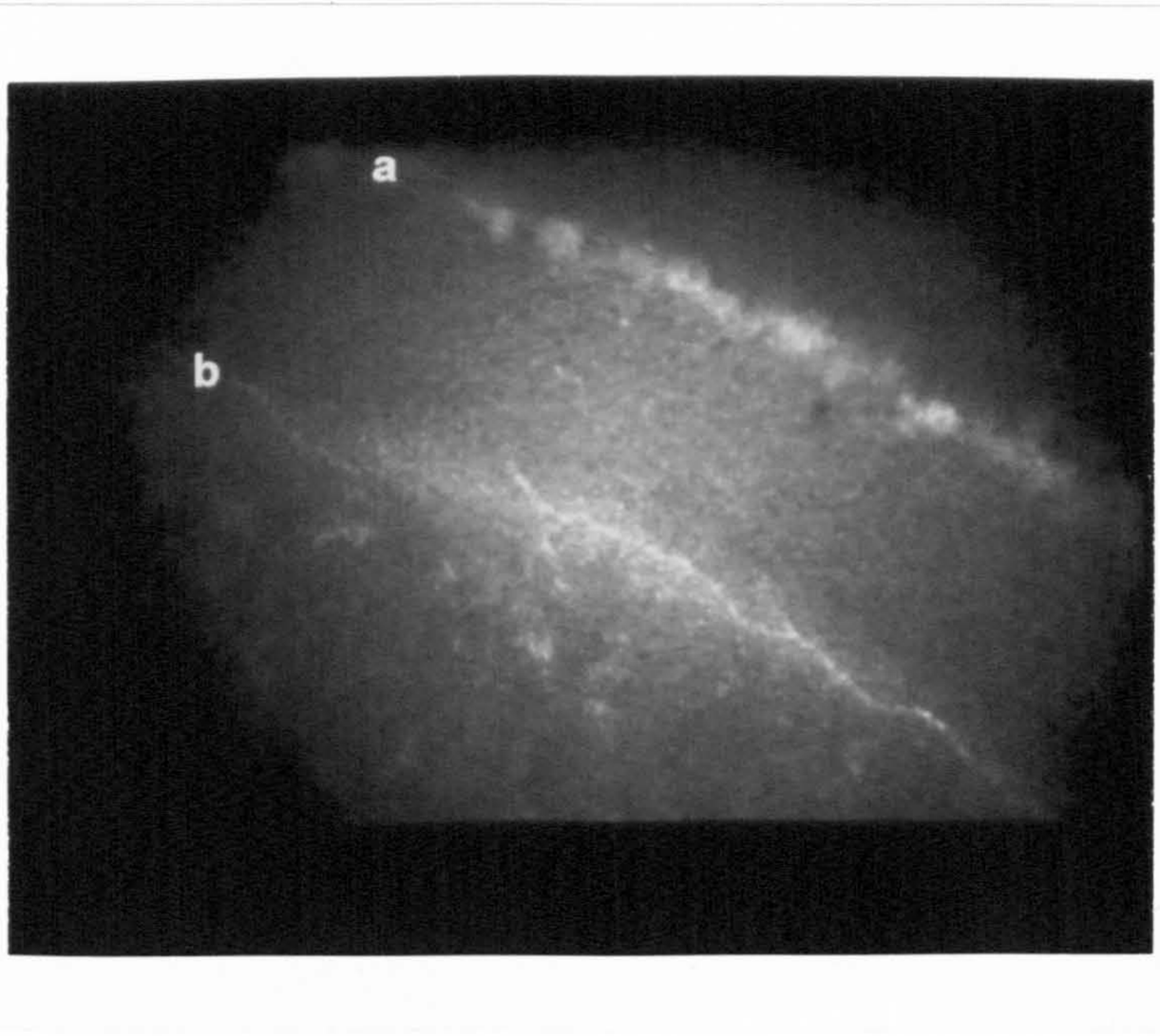


Figure 3.4
Sample image of optical section at oblique angle to eye surface showing cross section through epithelium and stroma. The subepithelial nerve plexus is clear.
(a) Surface of epithelium
(b) Surface of stroma.

3.3 VIDEO

Images are 630 by 420 µm. The video recording has not been edited or enhanced.

3.3.1 Tangential optical sections

00:10	Start of recording
00:10 to 00:14	The focal plane is advanced through immersion fluid. Bright spots are presumed to come from bubbles in the methylcellulose. The junction between immersion fluid and tear film can not be identified. There may be little difference in their refractive indices and no sharp interface between the two layers.
00:14 to 00:23	Optical section through the surface of epithelium. The optical section is tangential to the surface. Borders of cells and bright nuclei are clear. Cells are approximately 40 µm in diameter.
00:23 to 00:41	The optical section is retracted to focus on the tip of the objective, cutting through the periphery of the front of the lens. The surface of the objective is curved to match the radius of the eye. Peripheral bright rings are seen where

3.3 VIDEO

Images are 630 by 420 µm. The video recording has not been edited or enhanced.

3.3.1 Tangential optical sections

00:10	Start of recording
00:10 to 00:14	The focal plane is advanced through immersion fluid. Bright spots are presumed to come from bubbles in the methylcellulose. The junction between immersion fluid and tear film can not be identified. There may be little difference in their refractive indices and no sharp interface between the two layers.
00:14 to 00:23	Optical section through the surface of epithelium. The optical section is tangential to the surface. Borders of cells and bright nuclei are clear. Cells are approximately 40 µm in diameter.
00:23 to 00:41	The optical section is retracted to focus on the tip of the objective, cutting through the periphery of the front of the lens. The surface of the objective is curved to match the radius of the eye. Peripheral bright rings are seen where

	the optical section cuts through the edge of the lens.
00:41 to 00:49	The optical section is advanced through immersion fluid and then epithelium, down to the subepithelial nerve plexus. Faint cell borders of deep epithelial cells can be detected, but are less clear than at the surface, presumably because there is little difference in refractive index at cell junctions.
00:49 to 01:07	Subepithelial nerve plexus. The plane of focus is at the junction of the epithelium and stroma. The microscope is moved up and down, and optical section advanced and withdrawn, to show the thin layer of dense nerves. A sample image of the plexus is shown in figure 3.5. Nerve fibres measured 5-8 µm in diameter. Single axons are less than 1 µm wide and therefore these are probably bundles of axons (Zander and Weddell 1951).

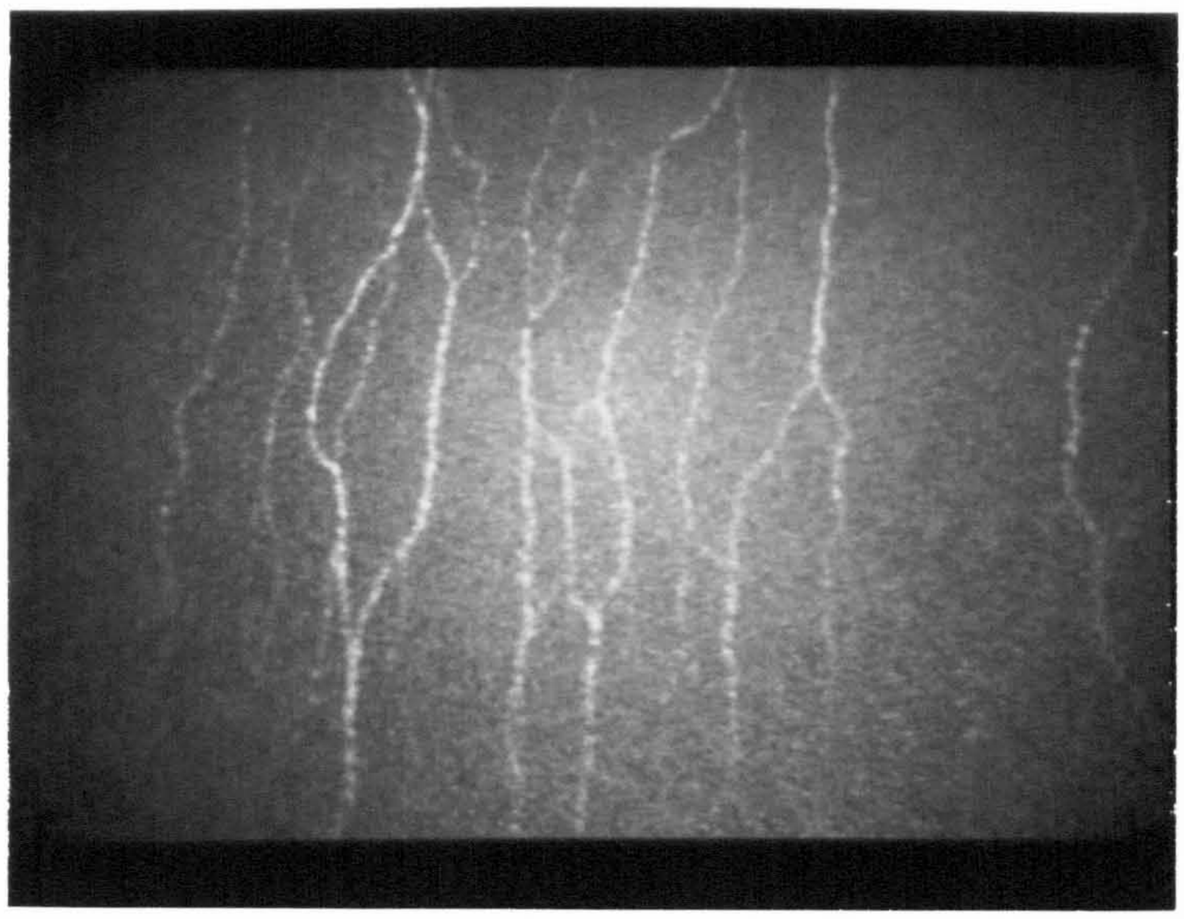


Figure 3.5
Tangential optical section through the subepithelial nerve plexus in a normal cornea.

01:00	Here the optical section makes a slight angle with the tangent to the eye surface and thus crosses through deep epithelium into stroma. Nerves pass between stroma and epithelium.
01:07 to 01:52	The optical section is being advanced through the stroma at 20 µm/sec. Density of kerato-cytes is greatest in superficial stroma and de-creases towards endothelium.
01:29, 01:32, 01:35	Stromal nerves. Diameter approximately 12 µm. Occasionally Schwann cells were seen adjacent to stromal nerve fibres. An example is shown in figure 3.6

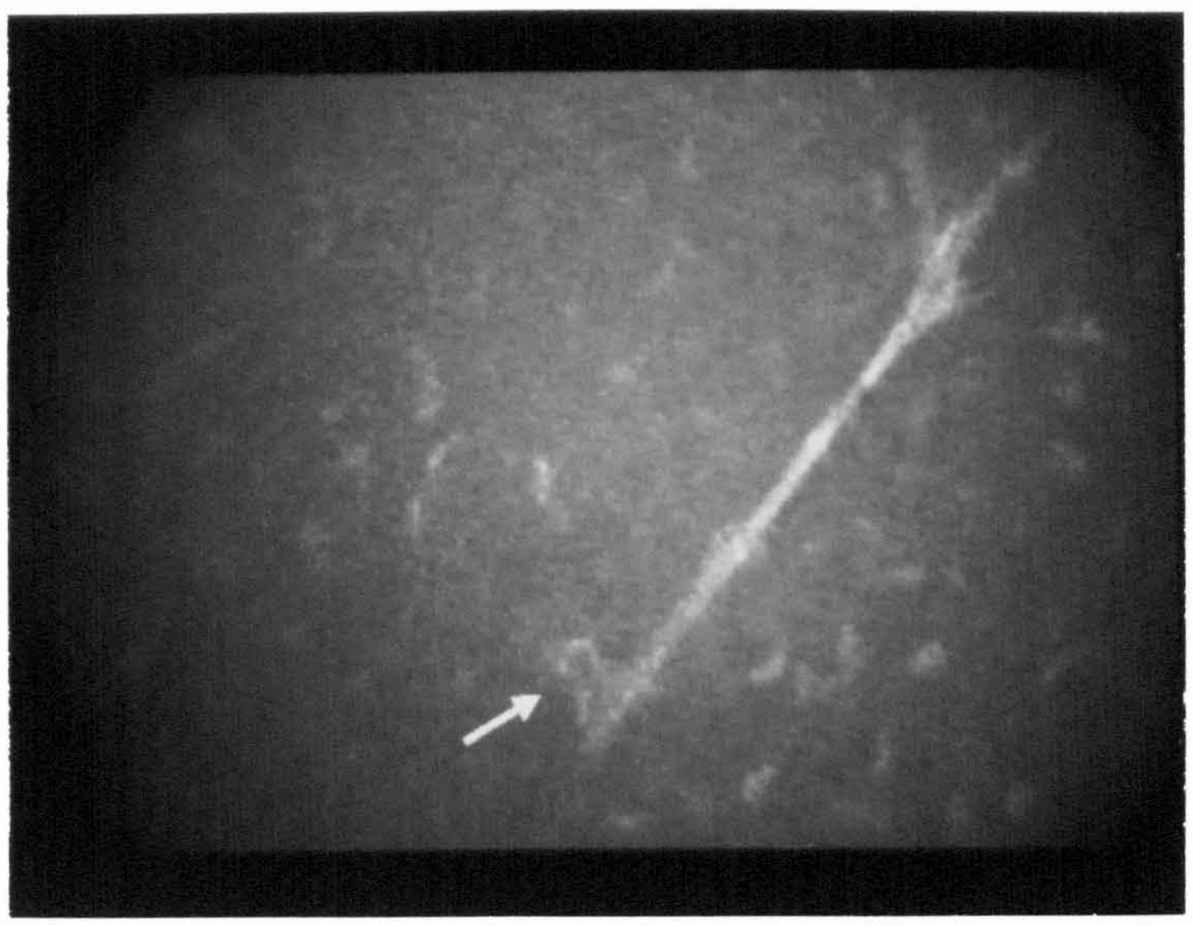


Figure 3.6
Optical section through stroma of healthy cornea showing stromal nerve fibre with adjacent Schwann cell (arrow).

01:45 to 01:58	Just superficial to Descemet's membrane, keratocytes density increases. Cells become more rod shaped and in places are arranged in parallel rows.
01:58 to 02:20	The optical section has been moved past the endothelium, showing a ring of cells where it cuts through the cell layer. Adjustments are made to bring the endothelium into the centre of the field of view.

3.3.2 Oblique optical sections

02:20 to 02:30	The microscope is rotated to make an angle of 20-30° to the eye surface (figure 3.3).
02:30 to 03:00	The optical section passes obliquely through epithelium and stroma. The front surface of the epithelium is to the right, Bowman's membrane and the sub-epithelial nerve plexus to the left. Further to the left are stromal keratocytes.

CHAPTER 4

4 MEASUREMENT OF EPITHELIAL THICKNESS USING OBLIQUE OPTICAL SECTIONS

4.1 Introduction

4.2 Contact lenses for calibration

4.3 Method of measurement from oblique optical sections

4.4 Tests of accuracy

- 4.4.1 Curvature of eye surface
- 4.4.2 Image distortion
- 4.4.3 Model of eye surface

4.5 Measurements in humans

- 4.5.1 Oblique optical sections
- 4.5.2 Tangential optical sections

4.6 Images from eyes without contact lenses

4.7 Discussion

4.8 Conclusions

4.1 Introduction

In earlier work, the author used confocal microscopy to measure thickness of tear film and epithelium in several species (Prydal 1991, Prydal and Campbell 1992). Freshly sacrificed animals were examined. Tissues were immobile and thus the separation between surfaces could be measured using the stage micrometer of the microscope.

However this method is not suitable for accurate measurements in conscious humans. Involuntary eye and head movements, as well as instability of the instrument introduce unknown errors. These are difficult to quantify.

An alternative method of measurement is described in this chapter. Thickness of corneal epithelium was determined from single fields of video recordings with optical sections oblique to the eye surface. A soft contact lens of known thickness was worn by subjects and used for calibration. Optical sections passed through full thickness of contact lens and epithelium. The ratio of the separation of surfaces in images was used to determine epithelial thickness. Measurements of were made in the centre and at different positions across the cornea in healthy subjects.

Models of the eye surface were used to test the assumptions made in using this technique and determine the conditions that gave sufficiently accurate results. The identity of structures in oblique optical sections was investigated using axial scans through the cornea. Images were tangential to the eye surface.

BIBL. LONDIN. UNIV.

4.2 Contact lenses for calibration

Contact lenses were specially manufactured by Contact Lens Precision Laboratories (Cambridge, UK). They were of hydroxymethylmethacrylate, water content 43%, refractive index 1.45 and diameter 14 mm. The central 12 mm was of constant radial thickness, nominally 60 μm. The manufacturing process was limited to tolerances of ±5%.

Thickness was measured after their use. Lenses were cut normal to the surface, mounted between two saline soaked sponges to maintain full hydration and the edge viewed using a standard microscope at x400 magnification and calibrated eye-piece graticule with markings corresponding to a spacing of 1.7μm.

The same contact lens was used for all subjects. It was sterilised in 0.3% hydrogen peroxide. Thickness at 10 positions across the central 12 mm zone with parallel sides was 58.3 ± 0.5 μm (Mean ± 95% confidence interval).

A second lens used in tests of the method measured 51.2 ± 3.9 μm.

4.3 Method of measurement from oblique optical sections

Images of oblique optical sections through the cornea showed the surface of the contact lens, the interface between contact lens and epithelium, and the surface of the stroma.

Figure 4.1 is a scale diagram showing an optical section through the eye surface

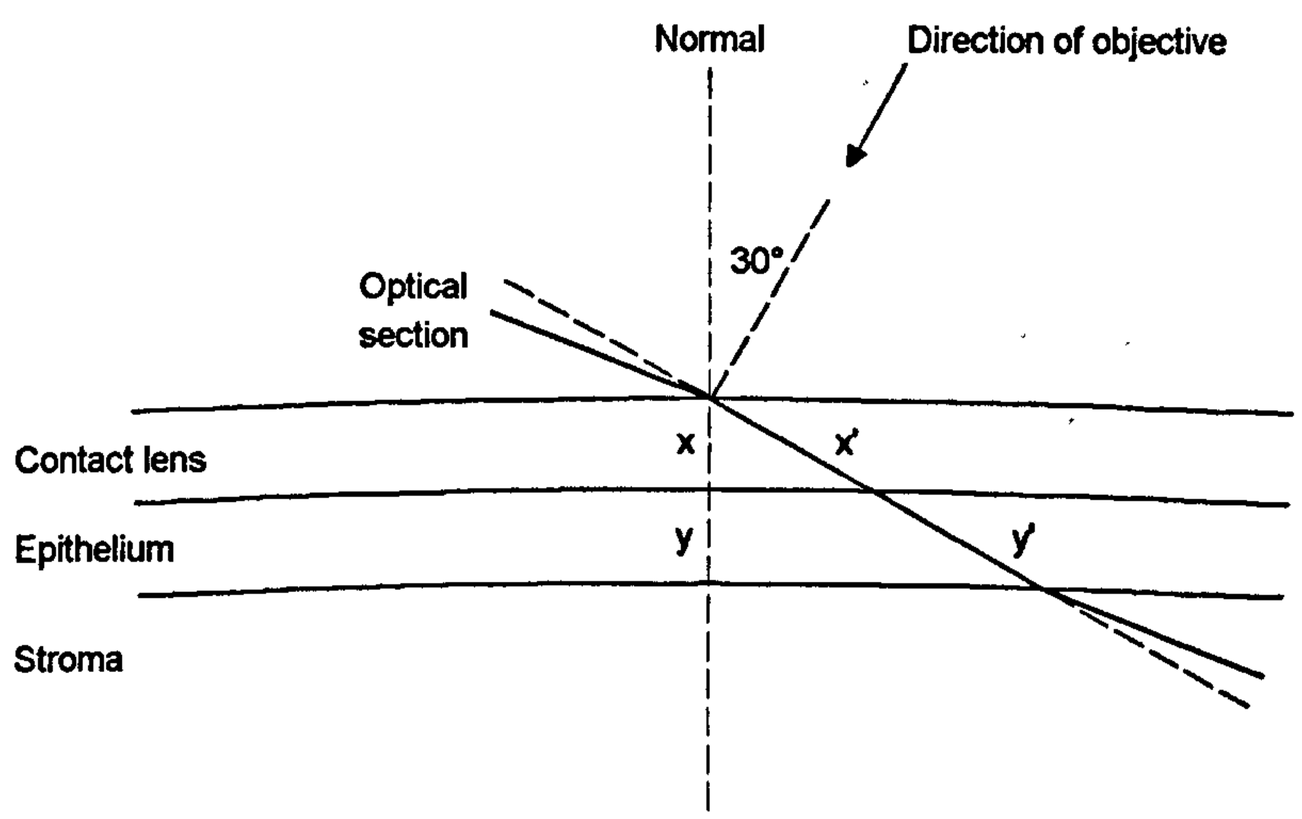


Figure 4.1
Diagram of optics showing oblique optical section through contact lens, epithelium and superficial stroma. Objective at angle of 30° to normal. Optical section assumed to be flat, and contact lens and epithelium to be of same refractive index. Distances x' and y' determined from images and radial epithelial thickness, y, calculated from the ratio: x/y=x'/y' using known value of x, radial thickness of the contact lens.

The optical section is shown as flat and the contact lens and epithelium are assumed to be of the same refractive index and thickness. The ratio of the thickness of the contact lens in oblique sections (x', figure 4.1) to that of the epithelium (y') was taken to be equal to the ratio of the radial thicknesses of the two layers (x/y):

$$\frac{x}{y} = \frac{x'}{y'}$$ (See figure 4.1)

where
- x = radial thickness of contact lens
- y = radial thickness of epithelium
- x' = apparent thickness of contact lens in optical section at oblique angle through the contact lens and epithelium.
- y' = apparent thickness of epithelium in same image

Images were computer analysed to measure the distances x' and y'. Contact lens thickness, x, was measured by the independent method described in section 4.2. Epithelial thickness, y, was calculated from the equation.

4.4 Tests of accuracy

4.4.1 Curvature of corneal surface

It was assumed in calculations that the contact lens and epithelium were flat parallel layers. Errors introduced due to the curvature of the eye surface were estimated using accurate drawings such as that in figure 4.1. These were drawn at a scale of 300:1. The radius of the cornea was taken to be 7.5 mm and the thickness of the epithelium and contact lens to be 50 µm each. Thus the stromal surface was of radius 225 cm, the outer surface of the epithelium 225.15 cm and external contact lens surface 225.30 cm. Optical sections were drawn for ten angles of incidence of the microscope - from 14° to 90°. The ratio of the distance between intersections of the optical section with each surface (x'/y' in figure 4.1) were measured from drawings. This was used to determine the error in the estimation of epithelial thickness at each angle.

Figure 4.2 shows the error in measurement plotted against angle of incidence. At an angle of 20°, epithelial thickness would be overestimated by about 7%. At 30°, the overestimate was 1%.

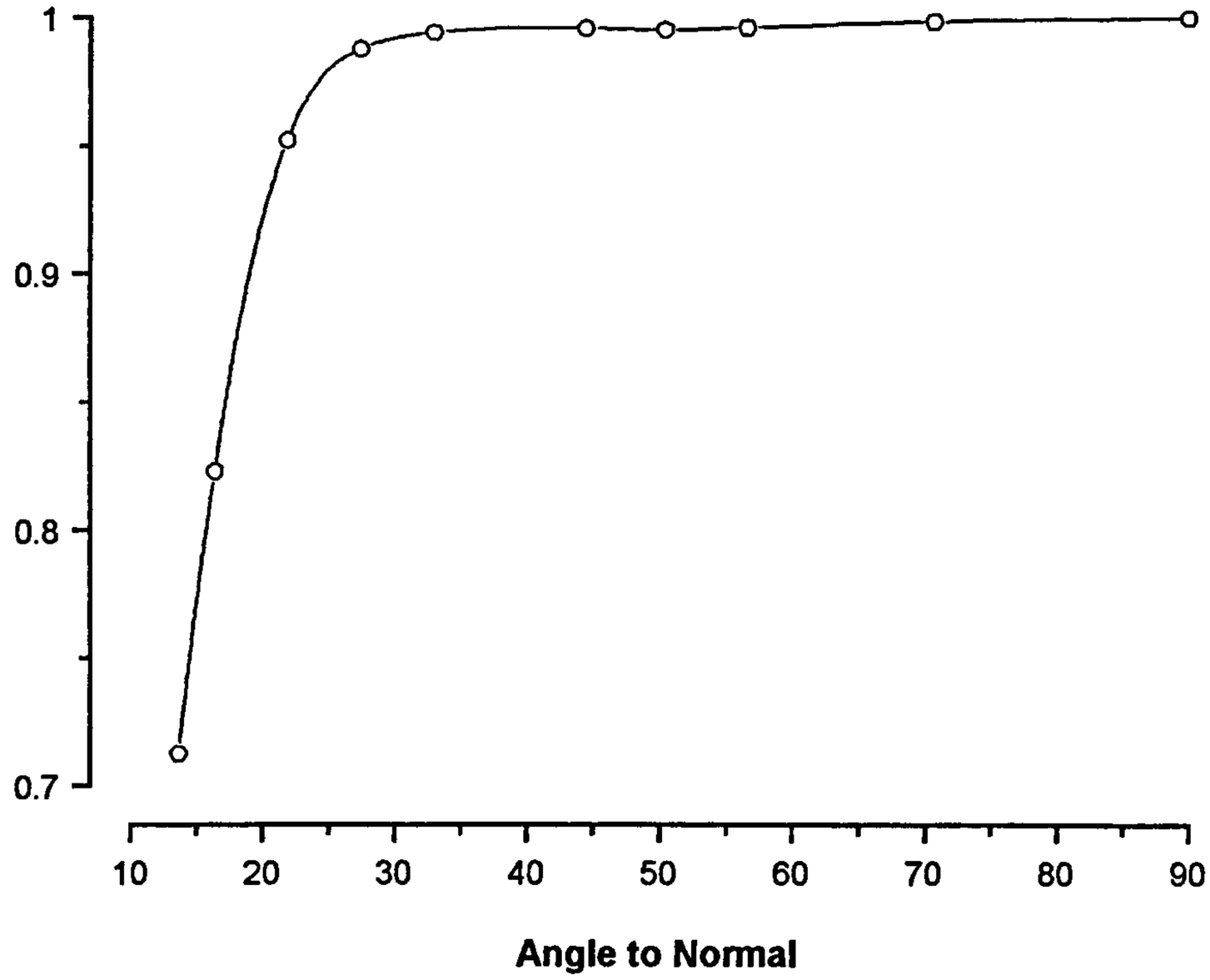


Figure 4.2

Error in estimation of epithelial thickness resulting from assumption that contact lens and epithelium are flat parallel layers. The ratio x'/y' is plotted against the angle of the objective to normal. Radius of curvature of stromal surface taken to be 7.5 mm. Contact lens and epithelium each taken to be 50μm thick and thus the ratio x'/y' would be 1.0 if the surfaces were flat.

The angle of optical sections to the eye surface in each digitised video image was determined from the thickness of the optical section through the lens (x', figure 4.1) and its known radial thickness (x, figure 4.1). Radius of curvature was taken as 7.5 mm. The curvature of subjects' corneas was not measured. If it was as much as 1mm different from the value used, the error in calculation of angle would have been less than 0.1°. Those images in which the angle was less than 20° were excluded as they would have resulted in an overestimate of more than 7%. The maximum angle in images was about 30°. Results would have been more accurate had the microscope been orientated at larger angles of inci-

dence. This was not possible as images were then less clear, probably because less light was reflected back to the objective at the increased angle to the reflecting surfaces.

Optical sections are curved with the apex towards the objective and radius similar to that of the cornea*. In the above considerations, the optical section was assumed to be flat. The additional error introduced by its curvature with radius 7.5mm was estimated. However it was too small to be detected in the scale drawings.

4.4.2 Image distortion

Confocal images of a calibration crystal (Agar Scientific Ltd., Stanstead, UK) marked with regular squares at periodicity 9.9 µm showed pin-cushion distortion, but it was restricted to the edge of images. Within the central region of 640 by 384 pixels there was no significant distortion. Therefore measurements were only made from this region. At the edge of images, the separation of two points was approximately 2.5% greater than that in the centre.

4.3.3 Model of eye surface.

The method was tested by imaging oblique sections through two soft contact lenses in contact with each other. They were supported on a hard contact lens. The ratio of the apparent thickness of the two soft lenses was determined from images to be 0.8 ± 0.1. The actual ratio was 0.9,

---

* Personal communication, J. Hill, Tandem Scanning Corporation, Reston, Virginia, USA.

determined from the thickness of each lens as measured by the independent technique described in section 4.2. The pair of soft lenses were then turned over so that the rear surface was now at the front. The ratio was then 1.1 ± 0.03 (actual ratio 1.1).

These results indicated that the method was valid.

4.5 Measurements in normal humans

4.5.1 Oblique optical sections

METHOD

Four normal subjects, two male and two female, aged 32 to 72 years were examined. Eyes were anaesthetised with two drops of 0.4% Oxybuprocaine Hydrochloride (Benoxinate) and the contact lens inserted. The microscope was orientated at an angle of approximately 30° to the centre of the cornea and brought close to the eye. Methylcellulose was applied to the objective before contact was made with the eye. Remote focusing controls were used to advance the optical section until images were cross sections through lens and epithelium. This was near to the end of its range, 1.0 - 1.5 mm from the objective tip.

In subsequent analysis, video recordings were carefully reviewed, in places 1 frame at a time. Clear images were selected and single fields digitised. A sample is shown in figure 4.3. Surfaces of the contact lens, epithelium and stroma appeared as straight parallel bright bands. If these were not vertical, images were rotated a few degrees as this simplified the image analysis process.

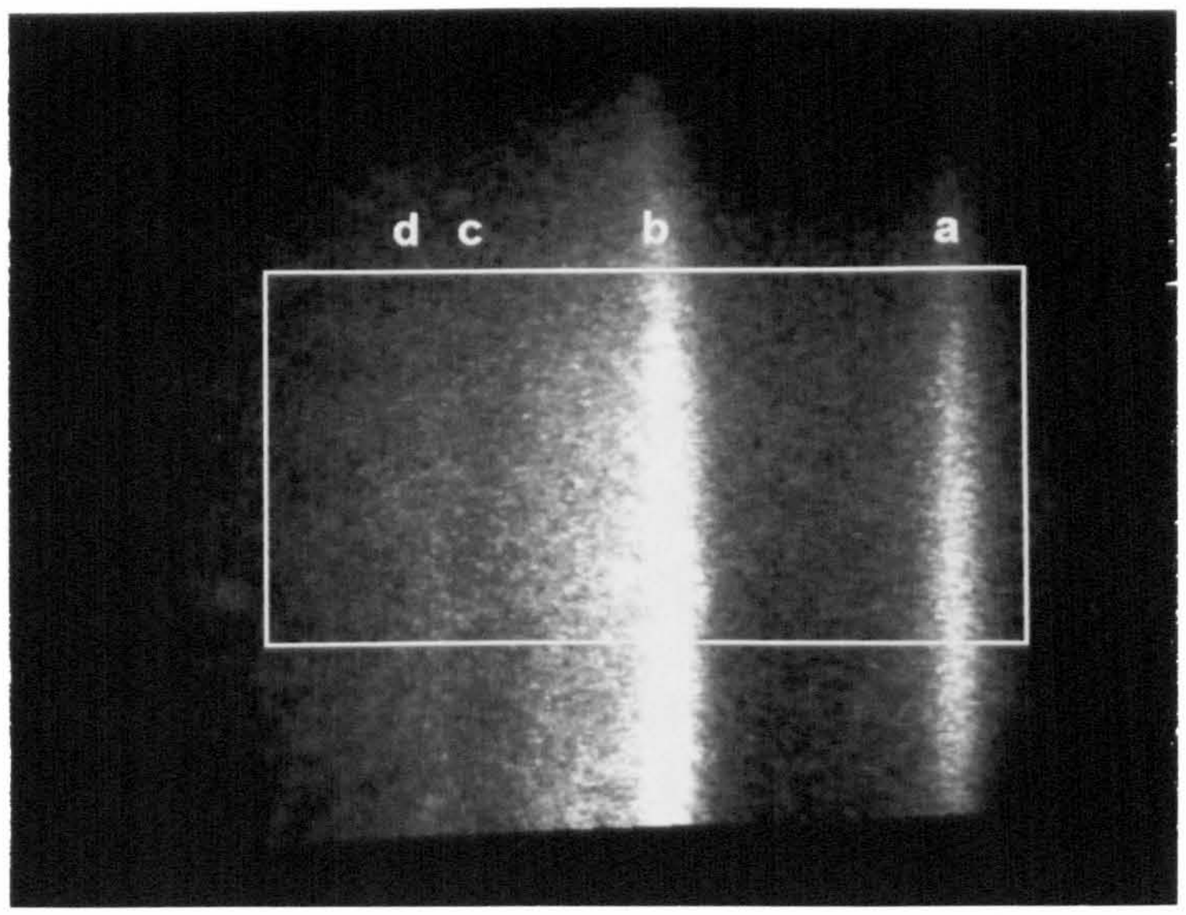


Figure 4.3
Confocal optical section through the eye surface.
(a) External surface of contact lens
(b) surface of epithelium
(c) dark band reflected from near stromal surface
(d) lighter band reflected from near stromal surface.
The section marked is that used for determining separation of surfaces.

Images were brighter at the centre and dimmer towards the edge. A flatter profile was obtained by subtracting a background image. One such image was used for all subjects. It was made by advancing the plane of focus to image oblique sections through stroma. Fifty such images were digitised, averaged and then filtered until featureless and smooth in profile.

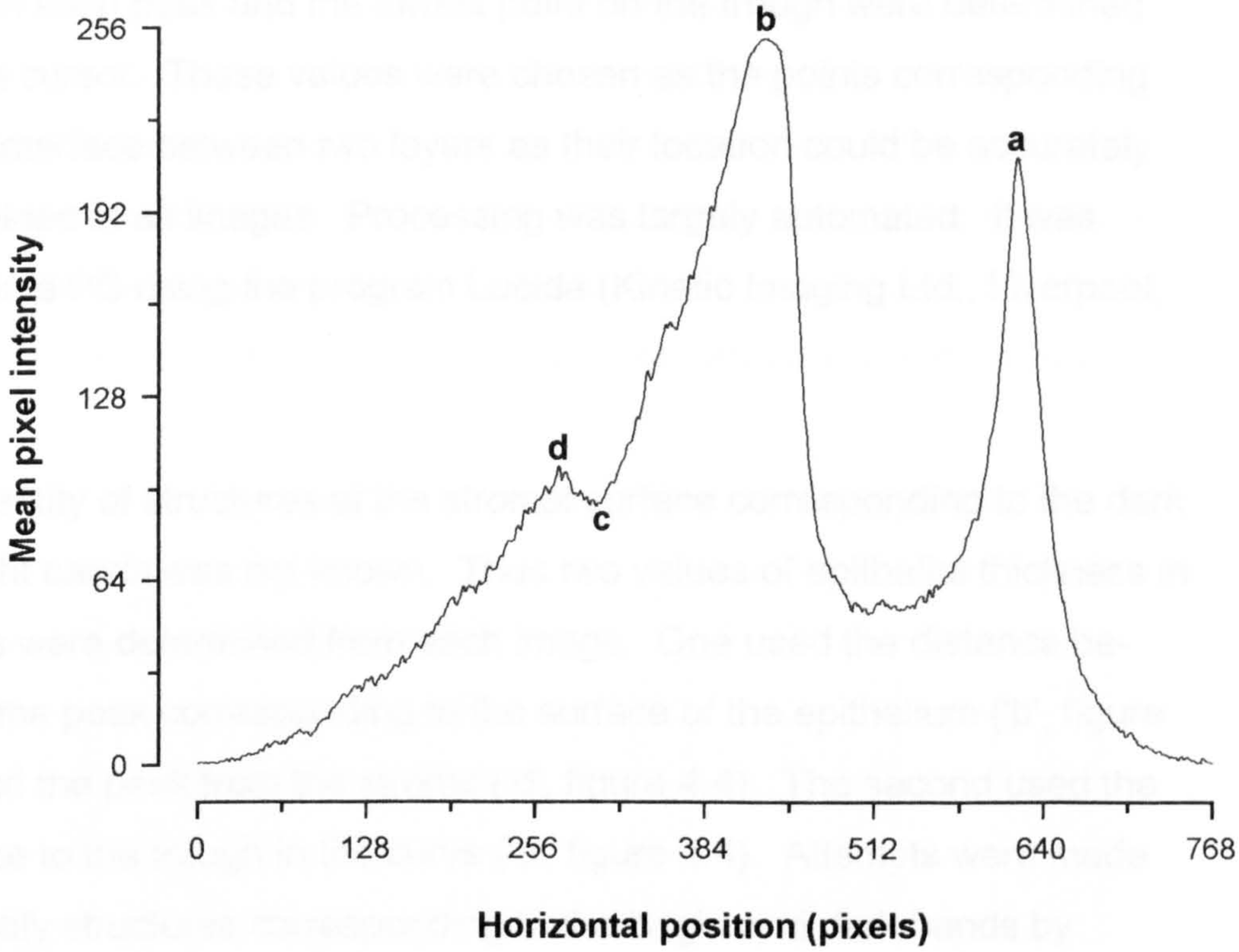


Figure 4.4
Mean pixel intensity in each column of the image in figure 4.3 plotted against horizontal position across image.
a: Front surface of contact lens
b: Interface between contact lens and epithelium
c: Dark band at stromal surface
d: Bright band at stromal surface
Letters correspond to structures marked in figure 4.3.

Five images from each subject were analysed. The background was subtracted and, if necessary, brightness and contrast adjusted to identify structures. An area of approximately 512 by 256 pixels was selected from as close as possible to the centre of images. Values in each column of the selected area were averaged and these results plotted. Figure 4.4 is a sample plot of the values determined from the image in figure 4.3. This showed peaks in brightness corresponding to the front surface of the contact lens ('a' figure 4.4), the interface between contact lens and epithelium ('b' figure 4.4) and the stroma ('d' figure 4.4). A dark band at the stromal surface gave a trough in the curve ('c' figure 4.4). This dark band

could be clearly identified in all images. The co-ordinates of the highest point on each peak and the lowest point on the trough were determined using a cursor. These values were chosen as the points corresponding to the interface between two layers as their location could be accurately determined in all images. Processing was largely automated. It was done on a PC using the program Lucida (Kinetic Imaging Ltd., Liverpool, UK).

The identity of structures at the stromal surface corresponding to the dark and light bands was not known. Thus two values of epithelial thickness in images were determined from each image. One used the distance between the peak corresponding to the surface of the epithelium ('b', figure 4.4) and the peak from the stroma ('d', figure 4.4). The second used the distance to the trough in the curve ('c', figure 4.4). Attempts were made to identify structures corresponding to the bright and dark bands by scanning through the cornea with optical sections tangential to the eye surface. This is described in section 4.5.2. Information was also available from images of oblique optical sections through eyes without contact lenses (section 4.6).

RESULTS

Results in the four subjects are plotted in figure 4.5. Thickness measured from epithelial surface to the dark band ('c' figure 4.4) ranged from 38.2 ± 2.5 to 52.9 ± 2.7 μm. That measured to the peak ('d' figure 4.4) ranged from 45.6 ± 4.1 to 60.4 ± 2.0 μm. The significance of these two measurements is reviewed below. Variation in thickness across the central 5 mm of the cornea is shown in figure 4.6. There was no significant difference in this area.

A layer of fluid between the contact lens and epithelium, 10-15 µm thick, was occasionally seen. This is consistent with earlier work (Prydal and Dilly 1994). During the first minute after contact between objective and eye, the thickness of fluid between lens and epithelium was found to reduce to less than the minimum that could be detected. Alignment of the microscope in the present experiments took about 1 minute. Further measurements of fluid thickness between contact lens and eye are given in chapter 8.

Figure 4.5

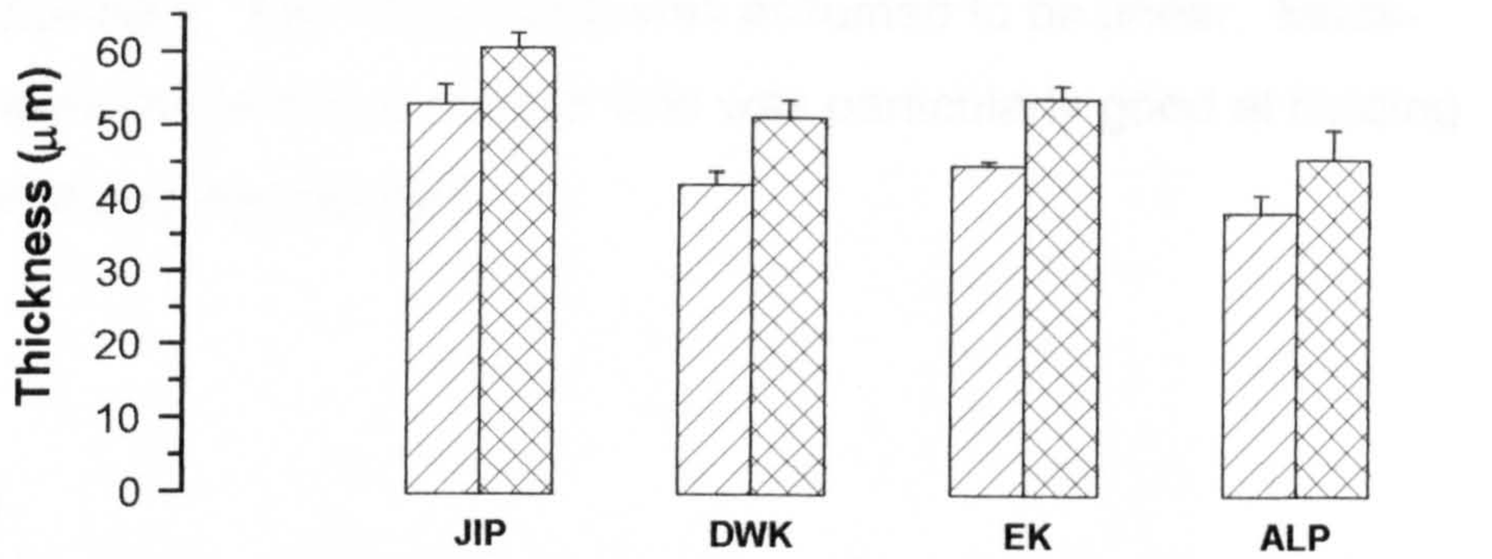


Figure 4.6

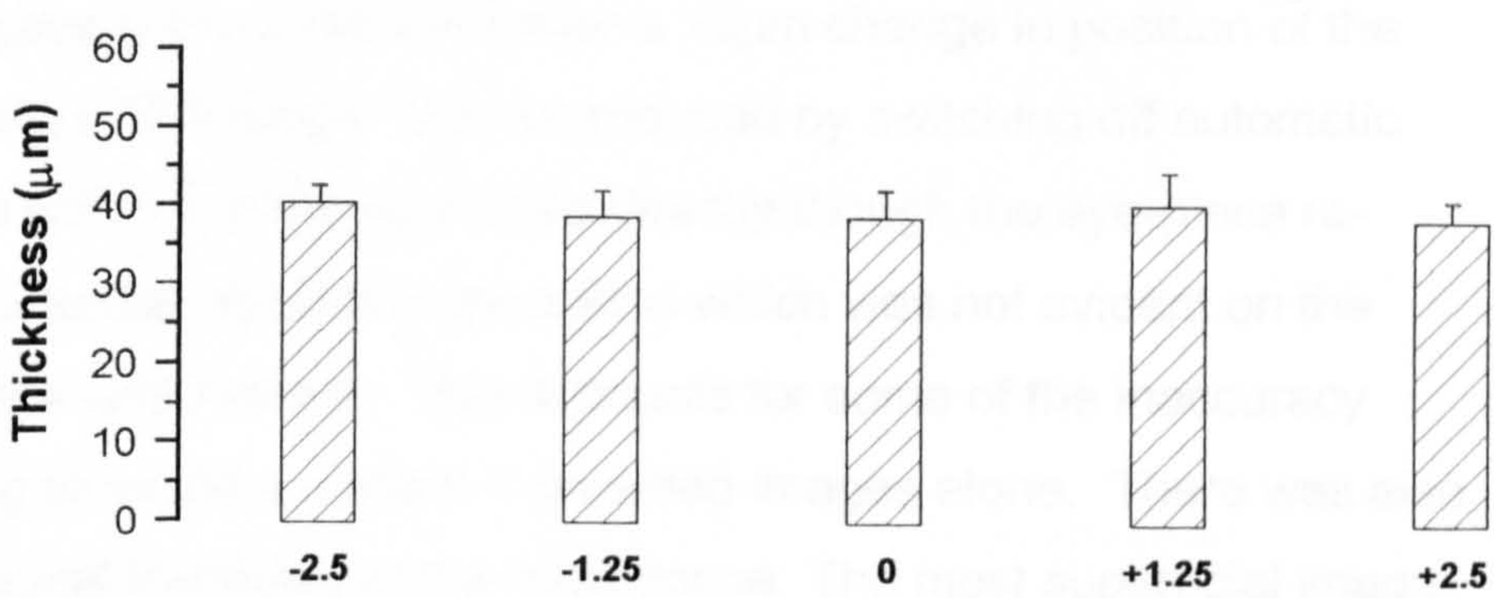


Figure 4.5
Mean epithelial thickness in 4 subjects. Two values were calculated for each subject (see text). Error bars are +95% confidence limits.

Figure 4.6
Epithelial thickness at 5 positions across the cornea: Centre (0), two positions below centre (-1.25 and -2.5 mm) and two positions above centre (+1.25 and +2.5 mm). Error bars are +95% confidence limits. The smaller of the two measured values are plotted.

4.5.2 Tangential optical sections

METHOD

Attempts were made to correlate measurements of epithelial thickness with those made by scanning through the cornea with optical sections tangential to surfaces.

Measurements of thickness were made from the change in position of the focal plane when focusing from a superficial layer to a deeper one. This was done with the contact lens in the eye. It was used to calibrate the axial displacement. The relationship was assumed to be linear. Measurements were made in one subject who was particularly good at holding a stable head and eye position.

RESULTS

Surfaces gave bright reflections over a 15µm change in position of the plane of focus. The range could be reduced by switching off automatic gain of the camera. Viewing images directly though the eye-piece revealed substantial chromatic aberration which was not evident on the monochrome video screen. This accounts for some of the inaccuracy when trying to locate a surface from video images alone. There was also the mechanical instability of the microscope. The most superficial image showing bright reflections from a surface was taken as the location of the surface. The separation between epithelial surface and the sub-epithelial nerve plexus was 39.3 µm and the depth to the first visible keratocytes 47.6 µm. Thickness measured using oblique optical sections in the same subject were 41.8 ± 1.9 µm to the dark band at the stromal surface and 51.0 ± 2.5 µm to the bright reflection from stroma. The significance of these results is discussed in section 4.7

4.6 Oblique optical sections without contact lenses

Sub-epithelial nerves could occasionally be seen in oblique sections with a contact lens in the eye. They were seen more clearly in images of eyes without lenses and were located within the dark band, often close to the external surface of the bright reflection (Fig. 4.7).

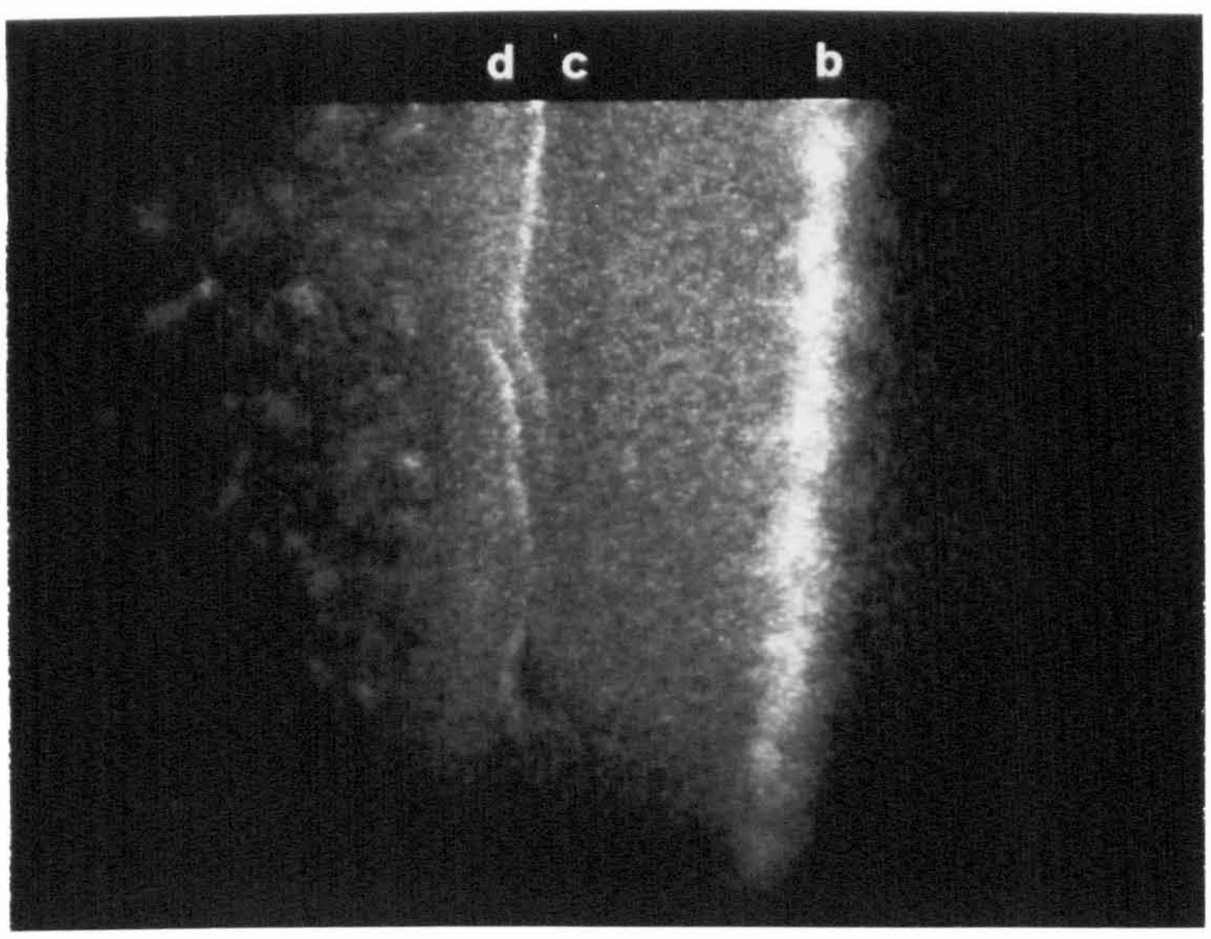


Figure 4.7
Confocal optical section through epithelium and superficial stroma without contact lens.
(b) Surface of epithelium,
(c) Dark band in reflection at stromal surface
(d) Lighter band at stromal surface
Subepithelial nerves are mostly within the dark band at the stromal surface

4.7 Discussion

In the earlier work of Wolff (1968), Calmettes et al. (1956) and Ehlers(1970), measurements of epithelial thickness were made by examination of histological specimens. Results in man varied from 30 to 100 µm. Using high frequency ultrasound, Reinstein et al (1994). measured epithelium to be 41 to 54 µm in conscious humans subjects.

Measurements here by confocal microscopy are comparable with these values. In our initial study we used confocal microscopy to measure epithelial thickness in nine animal species (Prydal and Campbell 1992). In the present work values measured in man were similar to that found in rabbit, rat, and two species of fish, but larger than measurements in gerbil, pigeon, duck and two species of frog.

Ehlers(1970) reported the epithelium to be thicker at the edge of the cornea. Results by confocal microscopy did not indicate any significant variation over the central 5mm of the cornea. More peripheral measurements were not made.

Wilson (1980) measured epithelial thickness in human subjects using a modification of the pachymetry technique developed by Maurice for measurement of corneal thickness (Maurice and Giardini 1950). It gave results of 55 to 67 µm. Values obtained by confocal microscopy ranged from 38 to 60 µm, which is up to 29 µm smaller. The difference may result from measurements by pachymetry including the thickness of the precorneal tear film.

Oblique confocal optical sections through epithelium show a dark band superficial to a bright reflection from stroma. Attempts were made to identify the structure of these regions by scanning through the cornea with optical sections tangential to the eye surface. This method can give

accurate results with stable immobile tissues and with direct visualisation of images (Prydal 1991, Prydal and Campbell 1992). However, the technique was less accurate for examination of conscious human subjects because of involuntary head and eye movements and some mechanical instability. The automatic gain of the video system made localisation of surfaces less precise. Such errors are difficult to quantify. However, results of axial scans seemed to indicate that the dark band corresponded to the layer of dense sup-epithelial nerves and that the bright reflection was from superficial keratocytes within the stroma.

Images of eyes without contact lenses showed the subepithelial nerve plexus to be largely within the dark band at the stromal surface, close to the surface of the brighter reflection (figure 4.7). Rózsa and Beuerman (1982) examined the neural structure of rabbit cornea. Dense plexuses of nerves were found both deep and superficial to the basal lamina of epithelial cells. Thus this level, corresponding to the dark band in our images, better defines the interface between epithelium and stroma.

No correction was made for the difference between the refractive index of epithelium and that of the contact lens used to calibrate images. Estimates of epithelial refractive index were reviewed by Clarke and Carney (1971). They varied widely. Fischer (1928) used two different techniques and found values of about 1.54 and 1.41. Tagawa (1928) also found values of about 1.41 for rabbit corneal epithelium. Patel (1992) found similar values using an Abbe refractometer to measure refractive index in conscious human subjects. However, there may have been mucus and tear fluid between the instrument and the epithelial surface. The contact lenses used in the present work had a refractive index of 1.45, which is within the range found for epithelium. If the refractive index of epithelium was as low as 1.4, the calculated results would be overestimates by less than 2 μm.

4.8 Conclusions

Measurement of thickness in conscious subjects using oblique optical sections through the cornea are probably more accurate than those using axial scans. Use of single fields of video recordings exclude inaccuracies from subject movement or instability of the instrument.

CHAPTER 5

5 DENSITY SIZE AND ORIENTATION OF KERATOCYTES

5.1 Introduction

5.2 Examination of subjects

5.3 Digitising of images

5.4 Density and size of cells

5.4.1 Problems in analysis of images

5.4.2 Procedure for image analysis

OUTLINE

DETAILS

a) Contrast enhancement

b) Subtraction of background

c) Thresholding

d) Removal of noise

e) Final stages

5.4.2 Results

5.5 Orientation of cells

5.5.1 Image analysis

5.5.2 Results

5.6 Discussion

5.7 Conclusions

5.1 Introduction

Measurements of the density, size and orientation of keratocytes in normal cornea are described in this chapter.

Optical sections through the stroma showed detailed structure of keratocytes. It provided the opportunity to examine a functioning cornea at magnification not available before. The structures revealed were not fixed or stained or disturbed in any way.

Video recordings of scans though the cornea in one subject could give up to 15,000 different confocal images. Imaging of such large amounts of information has not been possible in the past. New techniques were required to extract usable data. The author developed methods of digital image analysis to quantify characteristics of cells. It involved several complex sequences. Such processing has only recently become practical with the availability of sufficiently powerful computers and adequate storage capacities. Analysis of images from each subject took about 12 hours on a 486PC.

The combination of in-vivo confocal microscopy and image analysis enabled, for the first time, quantification of ongoing physiological and pathological processes in conscious humans. Measurements of changes during wound healing are presented in the next chapter.

5.2 Examination of subjects

Four subjects, two male, two female, aged 23 to 39 years were examined. After contact between objective and eye, the focal plane was advanced and the position of the microscope adjusted until images of superficial epithelium were circular. Optical sections were then tangential to the cell surface. The plane of focus was advanced into the most superficial layer of keratocytes and then in steps of 50 µm (25 µm in one of the subjects). Pauses for about 5 seconds were recorded at each level. The depth displayed on the focusing control unit was recorded on the audio track of the video. When the endothelial surface was reached fine adjustments were made to obtain images of the layer of keratocytes just superficial to Descemet's membrane.

In one subject, images of endothelium were not tangential to its surface. The microscope was repositioned and recordings made while moving in outward steps. Only this portion of the recording was used for analysis.

5.3 Digitising of images

Ten fields at each level were digitised for all subjects giving a total of 100-200 images per subject. The only criteria used in selecting images were that they should not be blurred or show stromal nerves. The presence of nerves complicated computer analysis and made measurements unreliable.

5.4 Density and size of cells

5.4.1 Problems in analysis of images

A sample image is shown in figure 5.1. Keratocytes appeared as bright objects against a dimmer background. Our early attempts at processing used thresholding of grey scale images with 256 levels of intensity to produce binary images with 2 levels. Pixels with values greater than the threshold level were set to 1 and those with smaller values to 0.

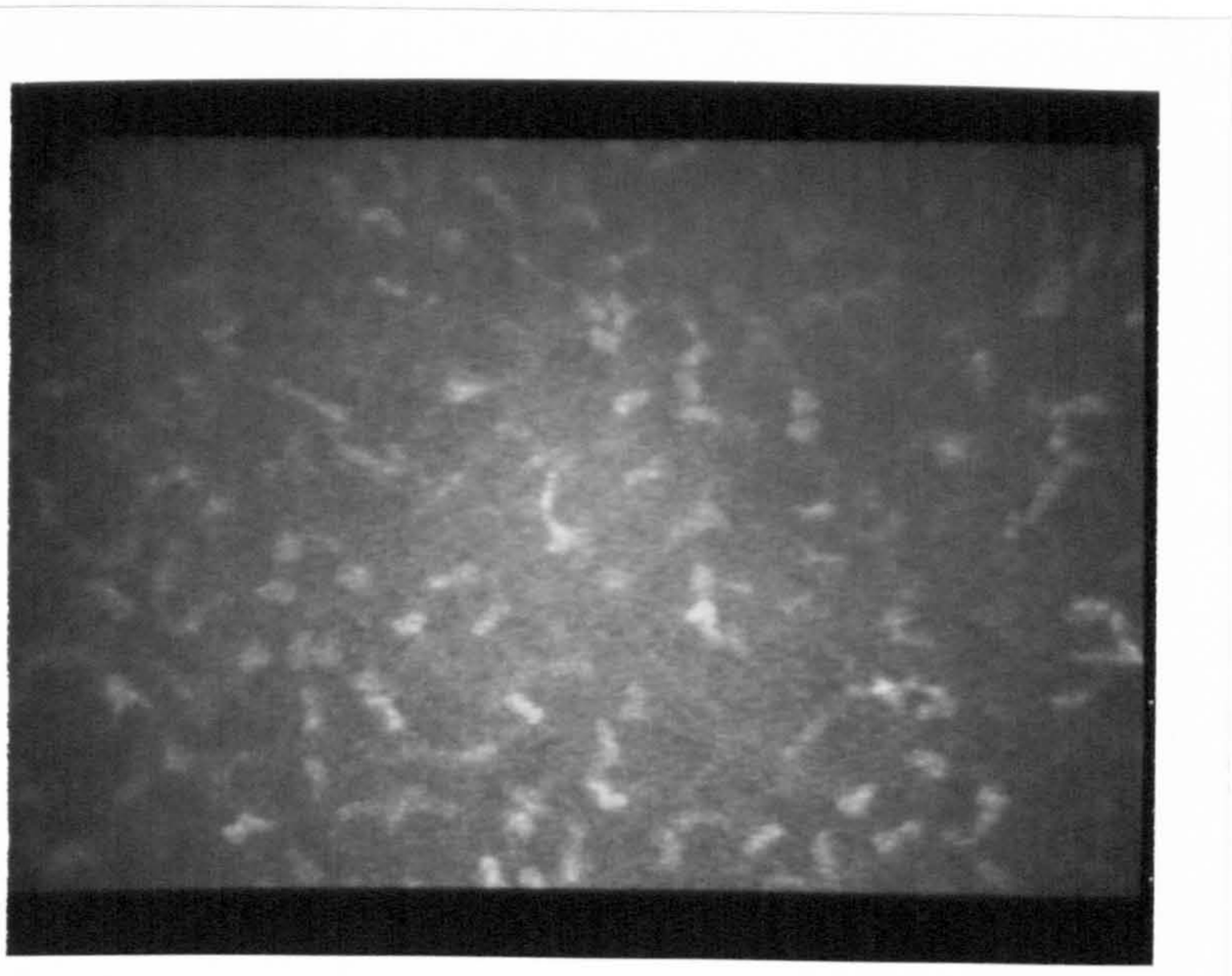


Figure 5.1
Grey scale confocal image of keratocytes in superficial stroma. Full size image 768 by 512 pixels.

However, images were brighter in the centre than at the edge and thus a suitable threshold level in the centre was not appropriate for the entire image, and could incorrectly portray the size and shape of cells. Variations in brightness were due in part to the camera. Controls to counteract this were not fully effective. Also the illumination was brighter in the cen-

tre. It was possible to adjust a condenser lens to produce more even illumination, but this reduced image contrast.

Even within small sections of images where background intensity was nearly constant, careful manual setting of an appropriate threshold level was necessary to select cell shapes. Several other small bright areas were included in the resultant binary image. It was presumed that these bright spots were not from cells and were considered to be 'noise'.

5.4.2 Procedure for image analysis

Several approaches were used to overcome these problems. A outline of the procedure is given below followed by a detailed description.

OUTLINE

a) Contrast was enhanced. This made the range of brightness levels the same in all images, from 0 to 255 (arbitrary units).

b) There was less variation in background intensity across small areas of the image. Small sections from the centre of images were processed. Images of the background were computed and then subtracted from the recorded image. This resulted in images with more uniform background. They contained cell shapes, but also noise.

c) A threshold brightness level was set at a point between 0 and 255. Pixels less than the threshold where set to zero, those greater to a value 1. This gave a binary image.

d) Binary images contained cell shapes, but also other small bright spots which were assumed to be 'noise' (not cell structure). This 'noise' was removed from images. Groups of pixels which were too small to be cells, or were of a different shape from cells, were removed. This gave images in which the background was at value zero and cell structures at value 1.

e) Such images could then be processed to give information about cell structure. The total area of an image occupied by cells was determined by summing the value of all pixels in the image. Methods of measuring other characteristics of cell structure are given below.

DETAILS

a) Contrast enhancement

First contrast was enhanced by the process of 'normalisation' (Gonzalez and Wintz 1983b). A new value for each pixel of an image was determined using the equation given in chapter 2, section 2.5.

b) Subtraction of background

Processing was done using only the central region of images, 256 by 256 pixels, as within this area there was less variation in background intensity. Further flattening was achieved by subtracting an image of background alone. It was found necessary to use a background image specific to each subject. Such images were made by averaging all digitised images from a subject. This gave a featureless image without structural detail. However, averaging revealed streaks caused by the scanning holes in the disk. These were removed by a standard image averaging process in which each pixel is replaced by the average of itself and the surrounding eight pixels(Gonzalez and Wintz 1983a). This filter was performed 15 times and resulted in background images of smooth profile, slightly brighter in the centre than at the edge.

c) Thresholding of images

A suitable threshold level was then determined. The same level could not be used for all images and therefore the relationship between the appropriate threshold level and various parameters of the image were investigated.

Eleven images from each of 3 subjects were processed as described above. The best threshold level for each was then chosen 'by eye'. Mean intensity in the image, minimum and maximum frequencies of pixel values, the value at the most frequent intensity and the standard deviation of pixel values were determined for each image. The selected

threshold level was correlated with each of these parameters. The highest correlation was found to be with the calculated mean intensity. Results are plotted in figure 5.2.

Linear regression analysis gave:

$$T = (0.481 \times M) - 0.216$$

where T = Estimated threshold

M = Mean of all pixel intensities in image

At a typical mean intensity (M=22, T=10), the 95% confidence interval was ±1. This equation was used to determine the threshold level in the automated image analysis process.

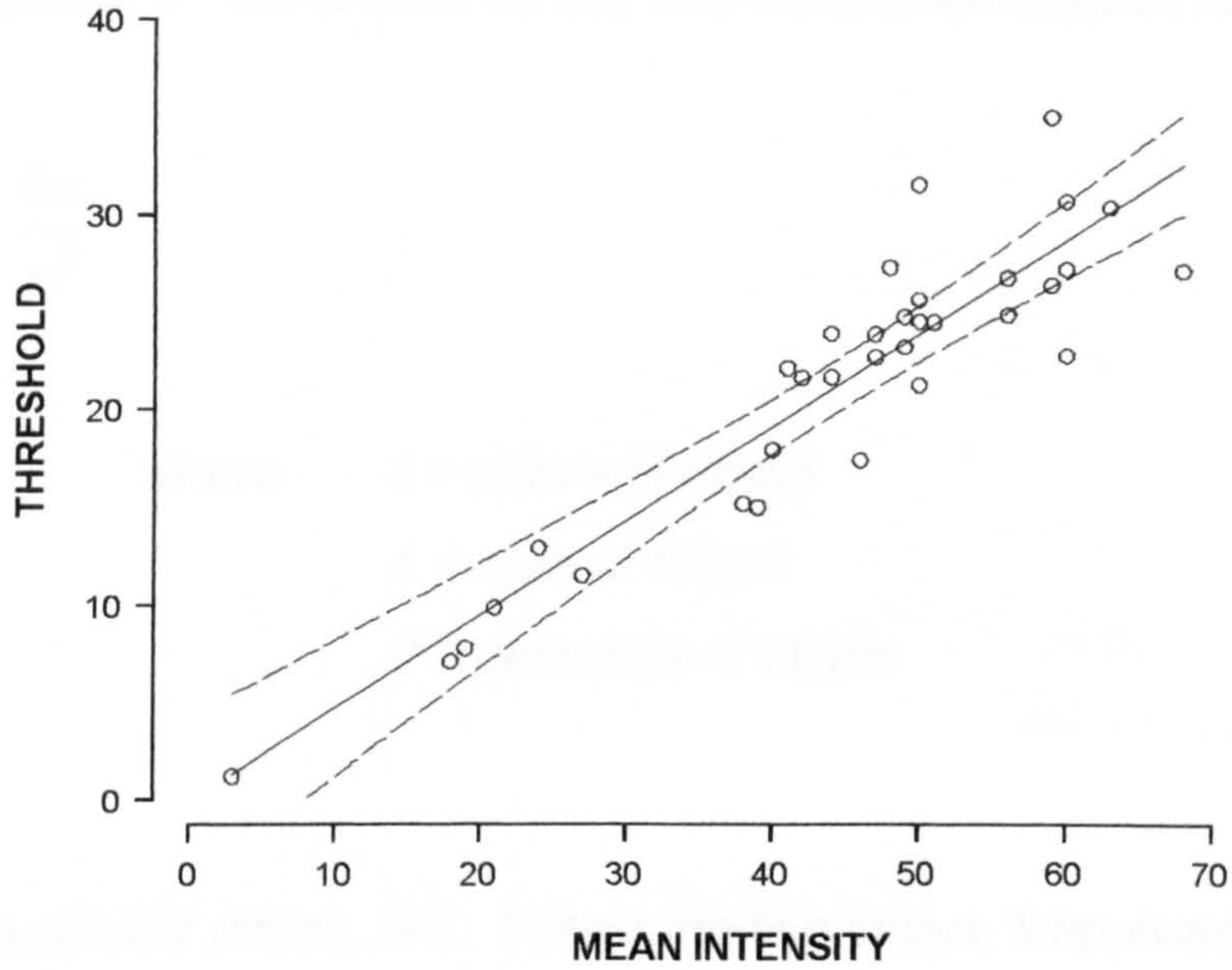


Figure 5.2
Correlation of threshold values against mean intensity of image. Best threshold level determined 'by eye' plotted against mean intensity. Units of intensity were arbitrary, range 0-255. Linear regression line shown, constant -0.216, co-efficient 0.481, correlation co-efficient 0.92. Dashed lines are 95% confidence limits.

d) Removal of noise

Binary images included all cells, but there were also random small areas which did not seem to be related to cellular structure. These were removed from images by two processes.

The first excluded those objects which were smaller than 50 pixels in area, approximately 15 μm^2. Cells were much larger than this, 100-200 μm^2, and small changes in this cut off did not seem to give substantially different results.

The second process filtered out objects that were circular in shape. Keratocytes tended to be elongated, sometimes 'U' shaped, but rarely cir-

cular. Thus noise was also removed by excluding circular objects. The parameter 'S', as defined below, was measured for each object in images:

$$S = \frac{4a}{p^2}$$

where S = shape of object

A = area of object

P = perimeter of object

For a circular object, S=1. For a long thin object, S approaches zero. Various cut off levels were tested and 0.5 found to be suitable.

The combination of these two filters removed noise from images.

e) Final stages

Any holes within objects were filled with pixels of value 1. These were usually small, 1-3 pixels.

Analysis of binary images gave the percentage of the area of images occupied by cells and the number of cells per image. Thus mean cell size and density of cells per mm^2 could be calculated.

Processing of results from each subject was automated using the macro languages in 'Ludica' and 'Windows 3.1'. It ran unattended.

5.4.2 Results

A sample image of 768 by 512 pixels is shown in figure 5.1. The optical section was through stroma immediately deep to Bowman's membrane. The central region of 256 by 256 pixels used in analysis is shown in figure 5.3a and the processed binary image in figure 5.3b. Optical sections just superficial to Descemet's membrane are shown in figure 5.4a (grey scale image) and 5.4b (binary image). They are from the same subject as those in figure 5.3a and 5.3b

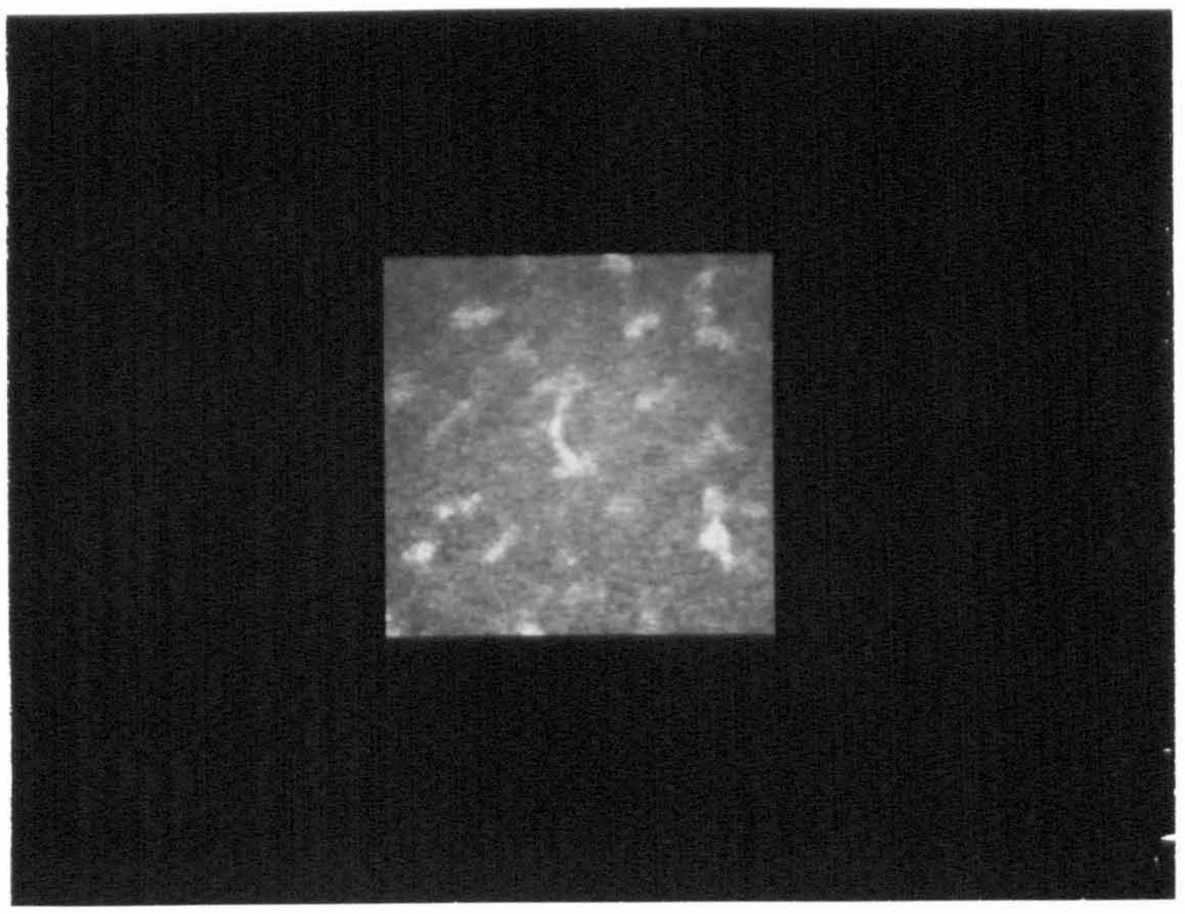


Figure 5.3a

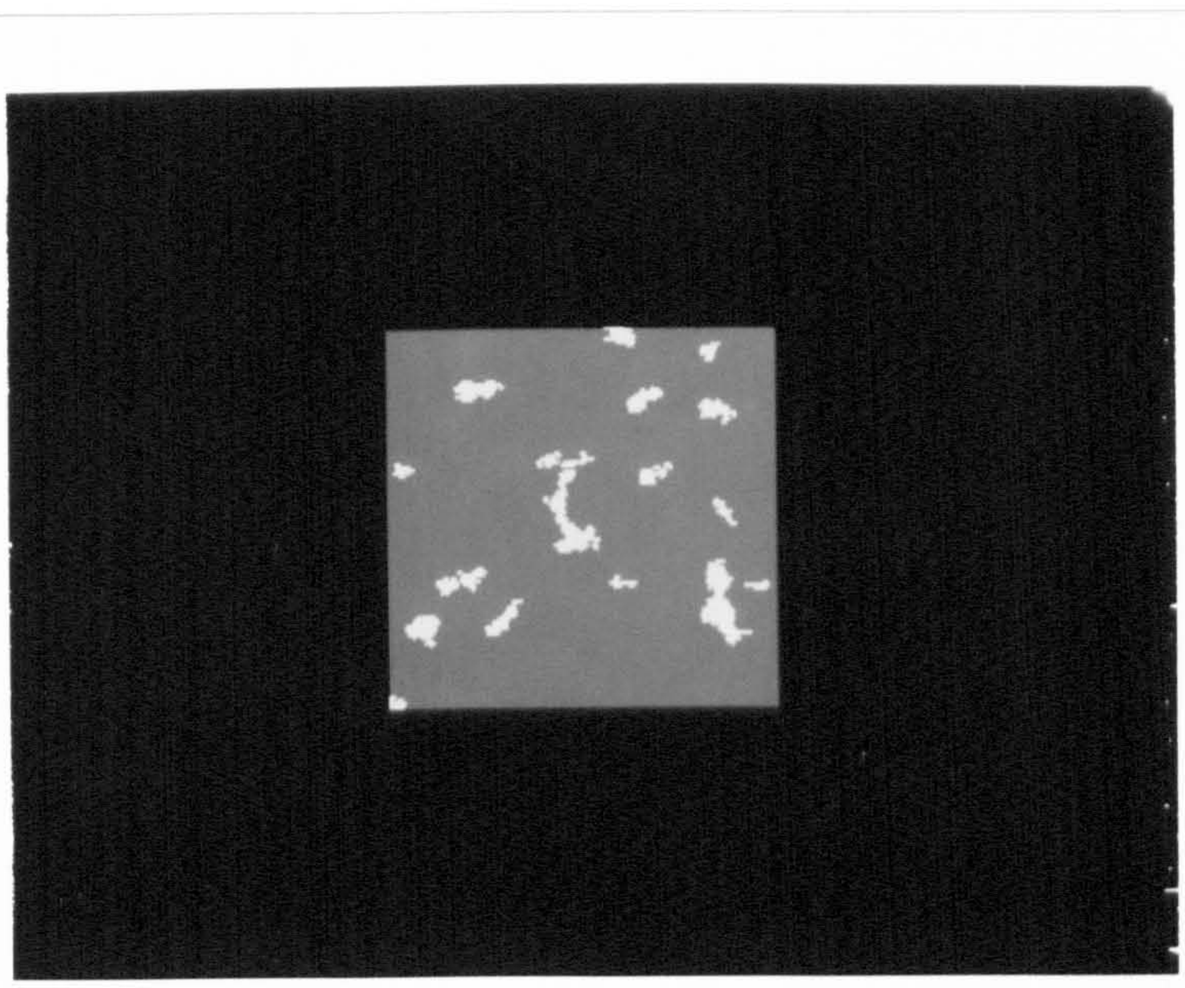


Figure 5.3b

Images before and after processing. The central region of images 256 x 256 pixels (210 x 210 μm) were processed. (a) Grey scale image. Section through superficial stroma. The full sized image is shown in Fig. 5.1. (b) Binary image, result of processing image 5.3a. Grey areas are of value 0, white of value 1.

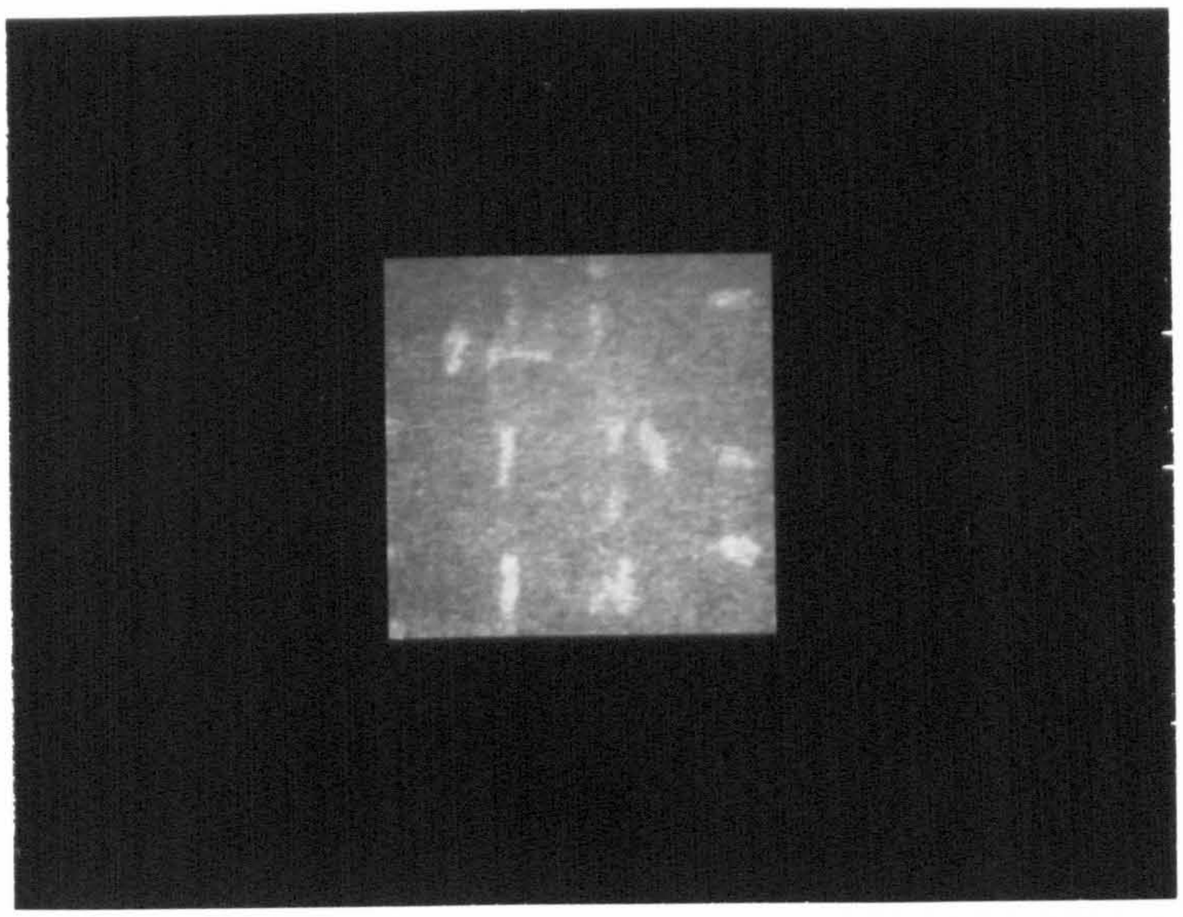


Figure 5.4a

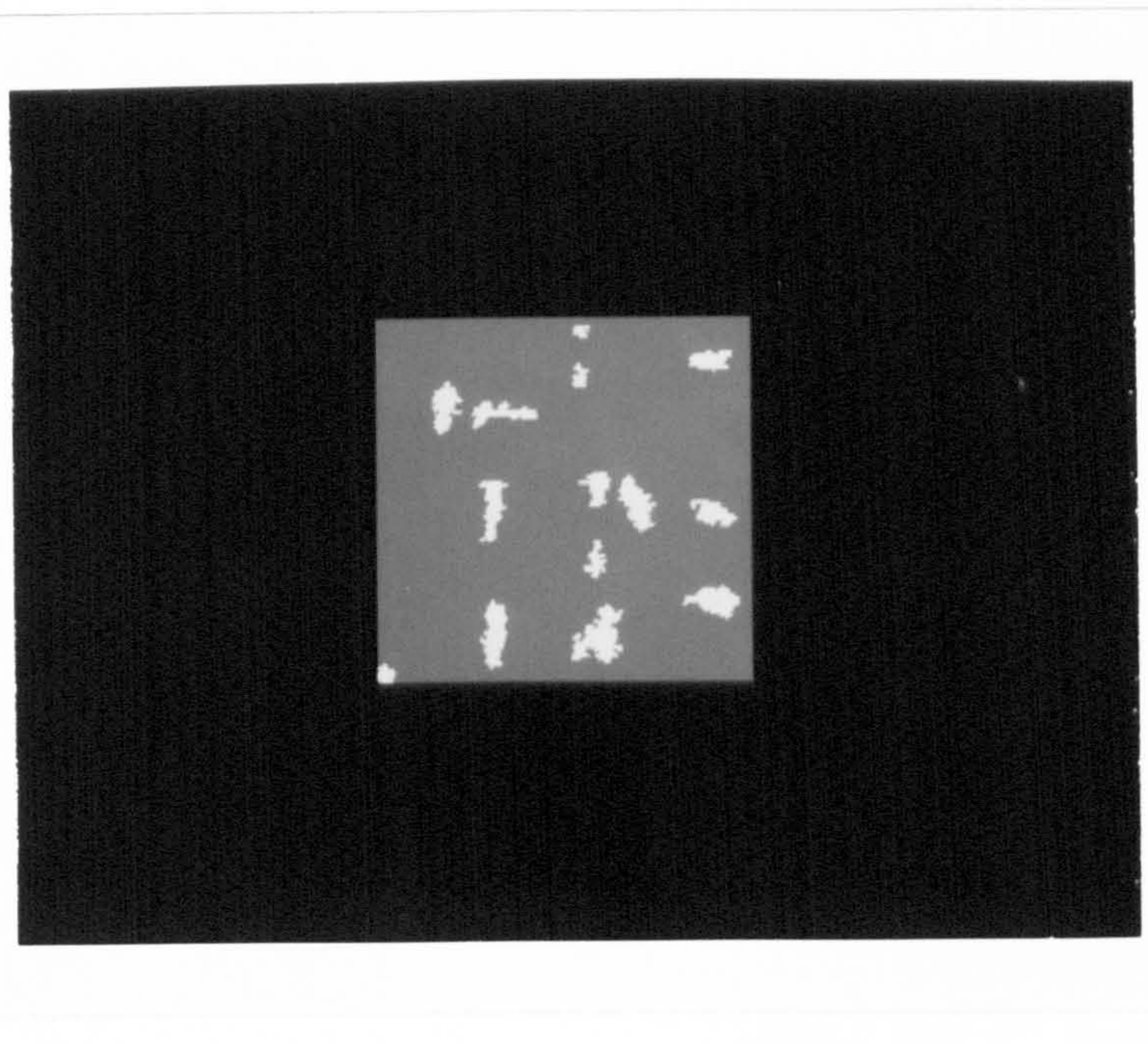


Figure 5.4b

Images before and after processing. (a) Grey scale image. Section 25 μm superficial to Descemet's membrane. From same subject as images in Fig. 5.3. (b) Binary image after processing of image shown in 5.4a. Grey areas are of value 0, white of value 1.

Density of cells in each subject is plotted against depth from the epithelial surface in figure 5.5. The percentage of image area occupied by keratocytes is shown in figure 5.6.

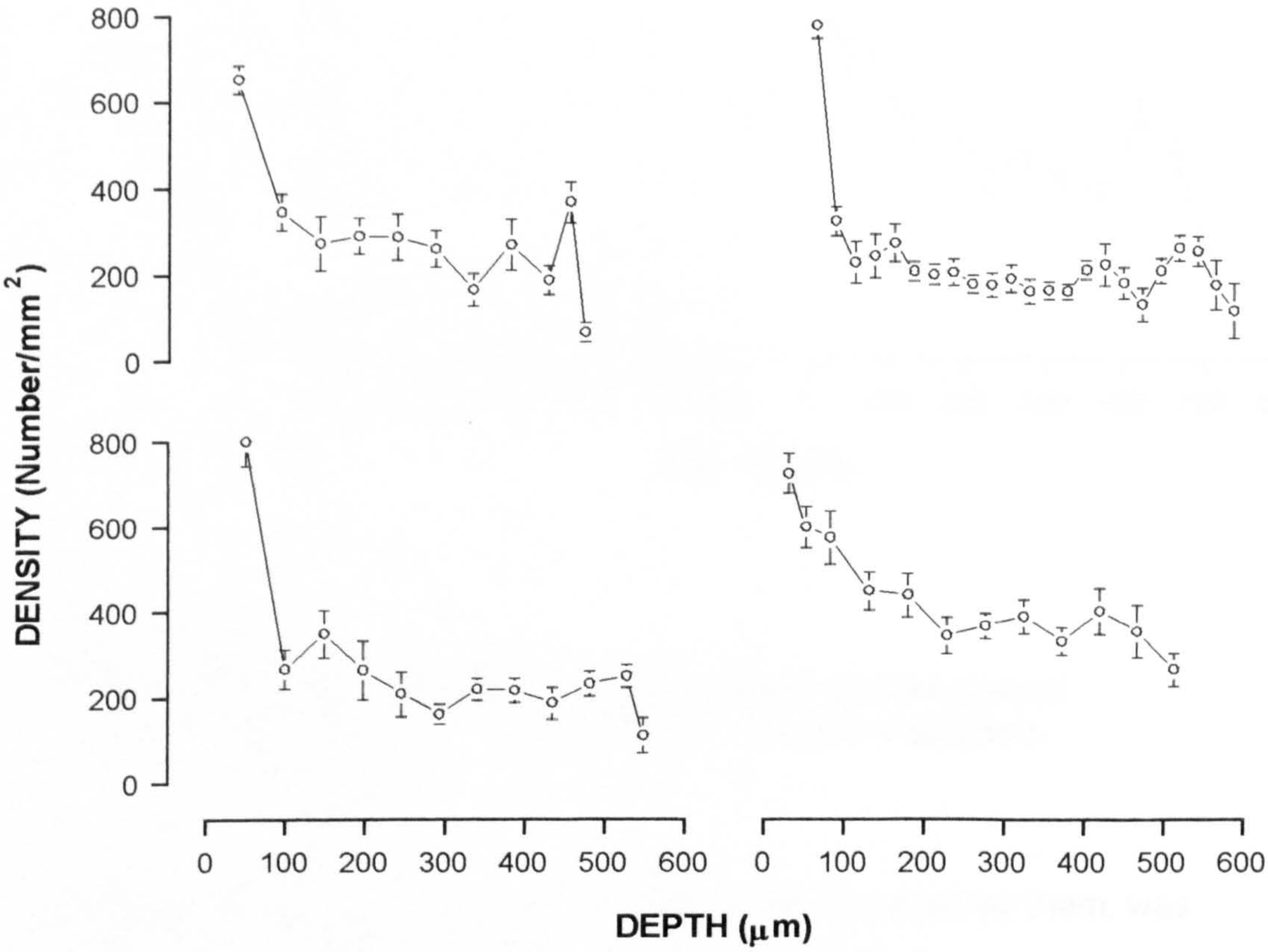


Figure 5.5
Density of cells (number / mm^2) plotted against depth of image from epithelial surface in each of 4 subjects.

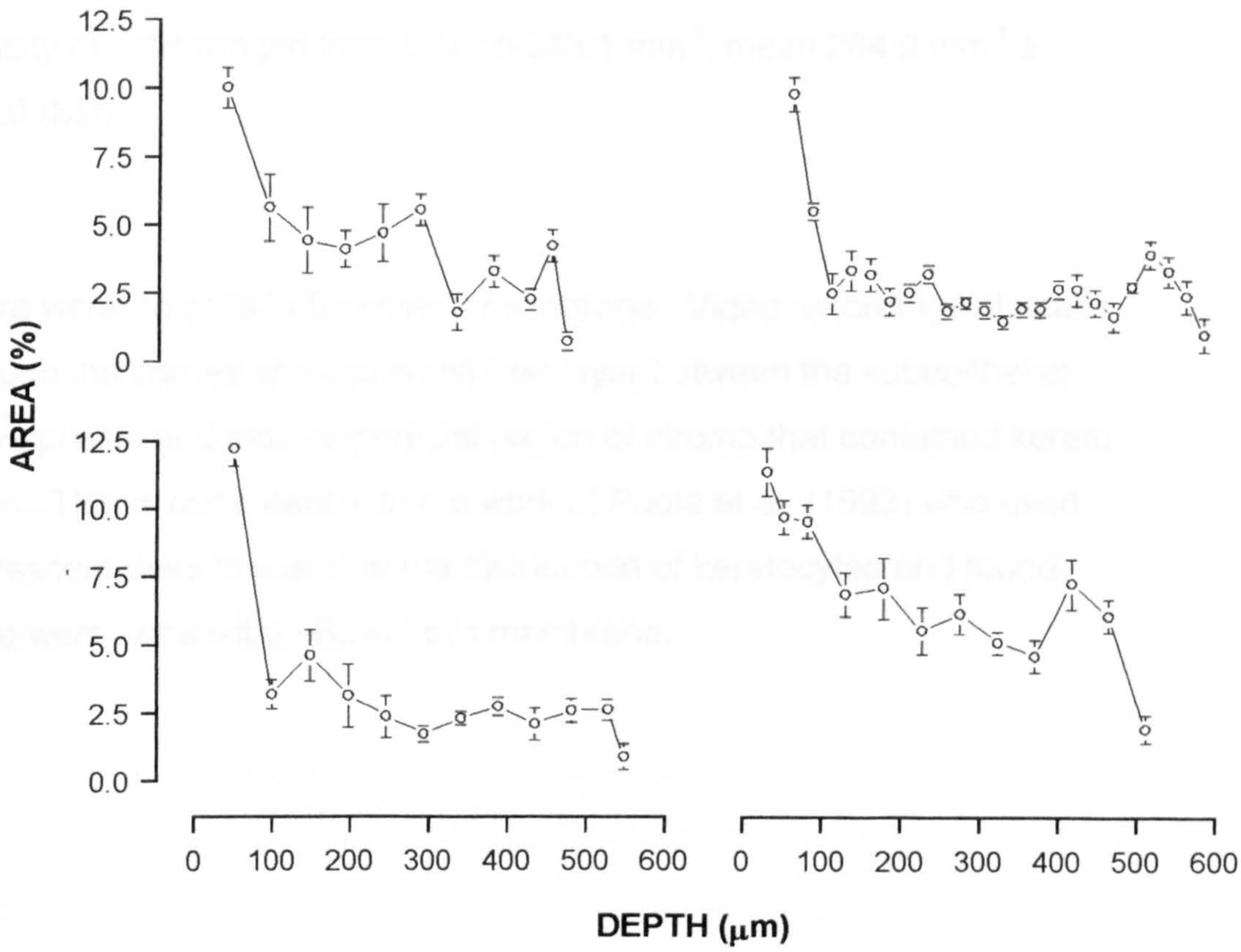


Figure 5.6
Percentage area of images occupied by cells plotted against depth of image from epithelial surface in each of 4 subjects.

Both the density of cells, and the percentage area occupied by them, was greatest near the stromal surface and reduced sharply towards posterior cornea. Approximately 50 μm from the endothelium where there was an increase in cellularity. The decrease in values deep to this region may have been because optical sections passed into Descemet's membrane. Both plots (figures 5.5 and 5.6) show a similar pattern through the whole stroma. Thus changes in area seem to be largely a result of changes in density, the size of cells remaining approximately constant. This was supported by plots of cell size against depth which did not show a consistent trend. Cells in superficial regions were not of a significantly different size to those in mid or deep stroma. The size of cells varied in area from

77.7 to 210.6 μm^2, mean 151.1 μm^2 ± 29.8 (standard deviation,SD). Density of cells ranged from 59.0 to 848.1 mm^{-2}, mean 264.9 mm^{-2} ± 152.0 (SD).

There were no cells in Bowman's membrane. Video recordings of scans through the cornea showed a cell free layer between the subepithelial nerve plexus and most superficial region of stroma that contained keratocytes. This is consistent with the work of Poole et al. (1993) who used fluorescent dyes to examine the distribution of keratocytes and found there were none within Bowman's membrane.

5.5 Orientation of cells

5.5.1 Image analysis

Keratocytes seemed to be randomly arranged in some images and aligned in rows in others. This was examined by doing 2 dimensional Fourier transforms of images using the program MDIFFT (Kinetic Imaging, Liverpool, UK). Images with randomly arranged cells gave a circular transform, while those with cells orientated in columns gave oval ones. This process was not automated and was only applied to a few selected images.

5.5.2 Results

It was apparent from reviewing video recordings that cells just superficial to Descemet's membrane were often more rod shaped than those elsewhere in the cornea and were sometimes arranged in parallel columns. However, careful selection of images was required to demonstrate this. The direction of orientation could be determined from Fourier transforms. Figure 5.4a and 5.4b are examples of sections through deep stroma with cells arranged in parallel rows. In some subjects it was possible to find such images in deep stroma, but it was not possible to find images showing orientation in more superficial layers.

Figure 5.7a is a two dimensional Fourier transform of the image shown in figure 5.3a, where the optical section was just under Bowman's membrane. The central vertical line is an artefact caused by edges of the image. The transform is otherwise circular, indicating no orientation. Fig-

ure 5.7b is the transform of an image just superficial to Descemet's membrane (figure 5.4a). It is oval in shape with the long axis horizontal. This indicates that cells were not randomly arranged, but tended to be orientated in parallel rows. The rows in figure 5.4a are vertical, orthogonal to the long axis of the Fourier transform in figure 5.7b.

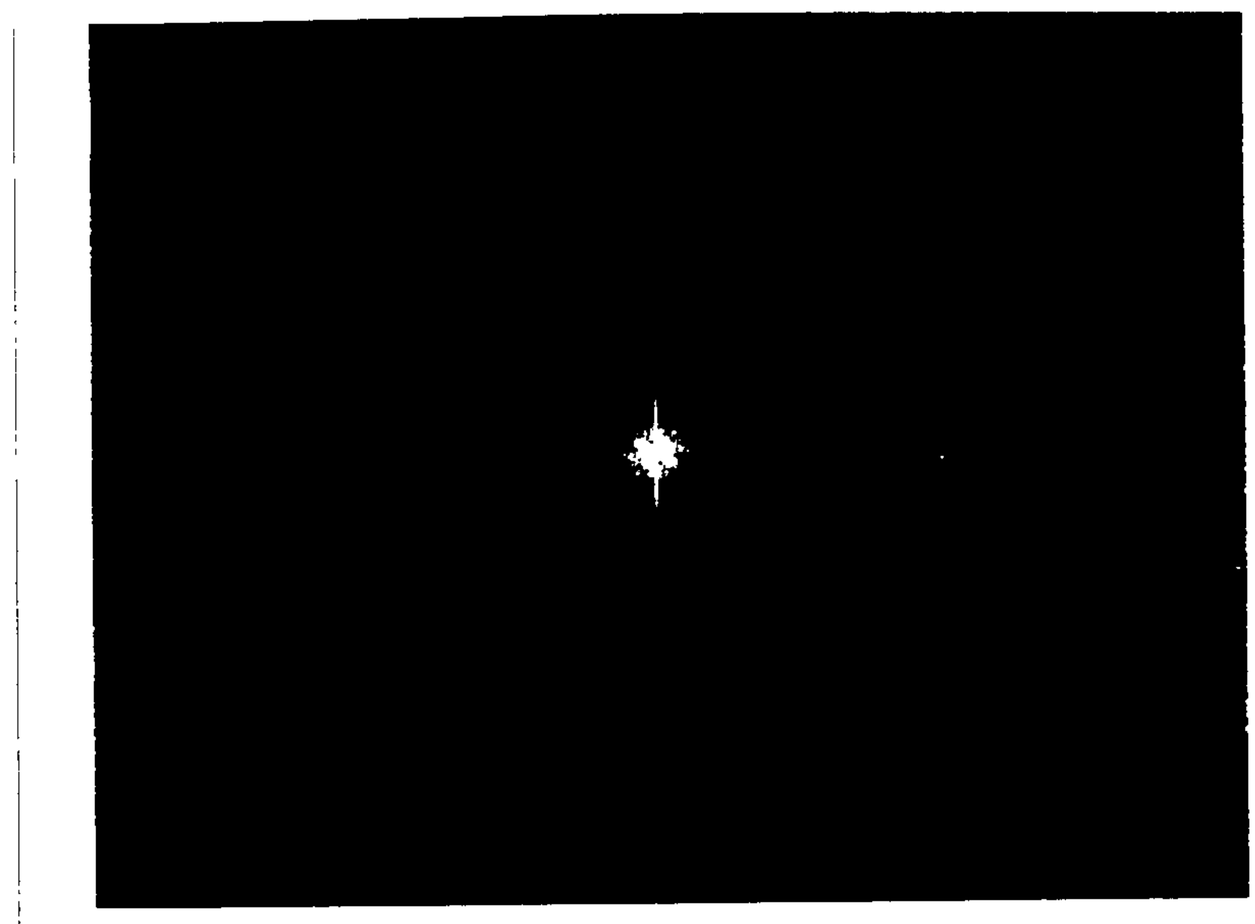


Figure 5.7a
Two dimensional Fourier transform of optical section just deep to Bowman's membrane (Fig 5.3a).

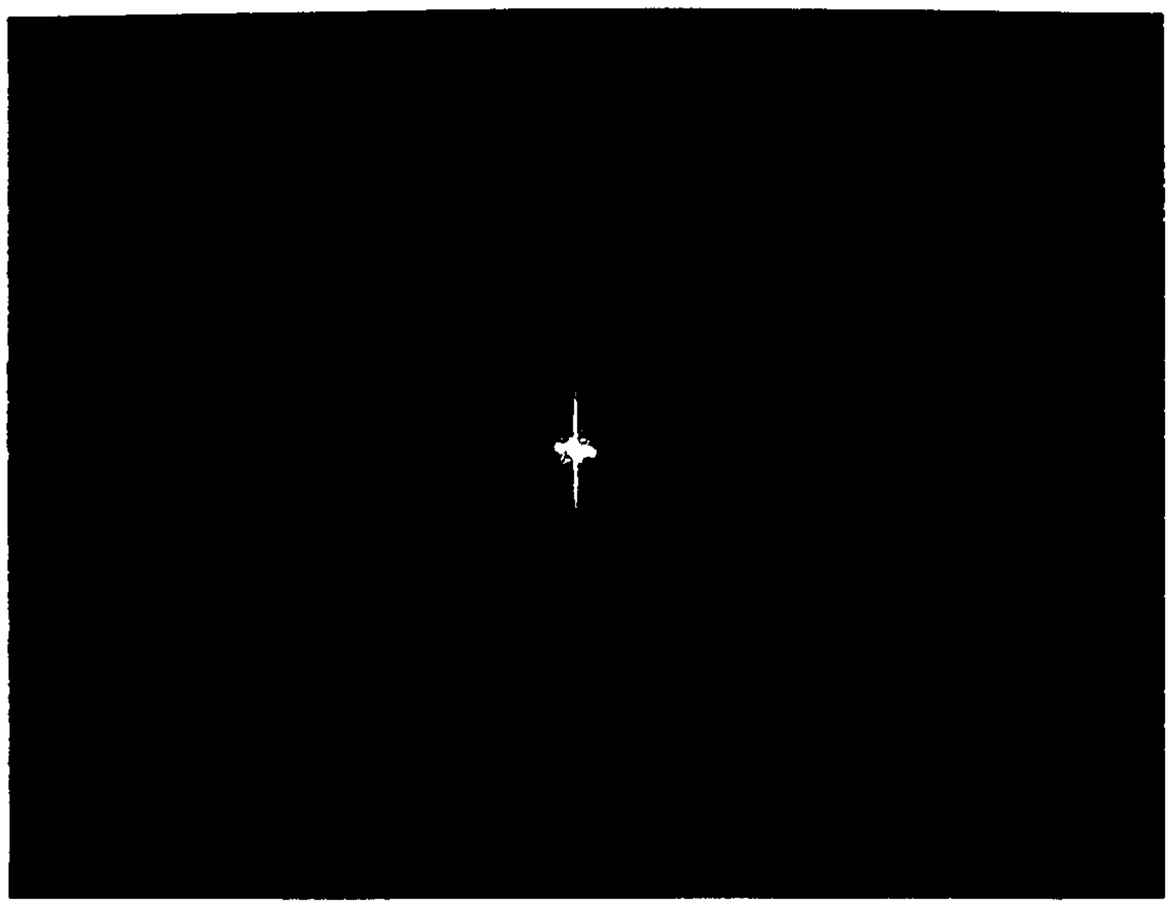


Figure 5.7b
Two dimensional Fourier transform of optical section just superficial to Descemet's membrane (Fig 5.4a).

5.6 Discussion

The methods used give measurements of cell density, the area of images occupied by keratocytes and cell size. Processing involved selection of various parameters to enable quantification. Objects smaller than 15 μm^2 were excluded. However, the minimum size of cell in all subjects was much larger, 78 μm^2. Thus it seems unlikely that this cut off excluded any keratocytes. Filtering of objects which were close to circular in shape may have excluded some cells, but was necessary to remove noise from images. Also, the threshold level was determined by linear regression analysis (section 5.4.2c). Thus the results presented are based on fixed criteria. Close comparison of binary and grey scale images showed that processed images gave a good representation of cells in the original image. Changes in measurements through the stroma were as anticipated from reviewing video recordings.

The present results are consistent with earlier work using histological and biochemical techniques in isolated tissues. Møller-Pedersen et al. (1994) determined the density of keratocytes in human post-mortem corneas using conventional microscopy and found a good correlation with measurements of tissue DNA content. Cell density measured 100 to 350 mm^{-2}. It did not vary with the length of time tissue was stored in culture medium and this was taken by them to indicate that measurements were similar to those in living tissue. In the work presented here, values up to 800 mm^{-2} were measured in superficial optical sections, but deep to this layer cell density was close to the range found by Møller-Pedersen.

Poole et al. (1993), using fluorescent dyes in pig and steer cornea, found a high concentration of cells in a narrow band deep to Bowman's membrane, little variation through most of the stroma, and increased density immediately superficial to Descemet's membrane. In this region they reported cells to be larger and more irregularly shaped, but did not report

cells to be orientated in rows. Boettcher et al. (1994) found in rabbit that cell density decreased from superficial to deep layers of stroma, with an increase just before the endothelium.

CHAPTER 6

6 WOUND HEALING

6.1 Introduction

Reaction of tissue to injury

Earlier studies of wound healing in animals

Advances enabling studies in humans

Refractive surgery by excimer laser

6.2 Methods

6.2.1 Patients

Details

Refractive errors

6.2.2 Treatment

Procedure for excimer surgery

6.2.3 Examination

Observations by confocal microscopy

6.2.4 Image analysis

Structures quantified

Selection of images

Subtraction of background

Formation of binary images

6.3 Results

Sample images

Changes in density and size of cells

Deposition of acellular material

6.4 Discussion

Possible causes of increased cellularity

Nature of subepithelial deposits

Changes in corneal transparency

and visual function

6.1 Introduction

Methods for analysis of images in normal cornea have been described in chapter 5. These techniques were also used to study reactions to injury. Results are presented in this chapter.

Earlier studies of corneal wound healing were done by sacrificing animals at intervals following the injury. Katakami et al. (1991) examined keratocyte activity after epikeratophakia in rabbits using conventional histological methods with sectioned and fixed specimens. Laser scanning confocal microscopy was used by Ichijima et al. (1993) to study healing following trauma to the endothelium, as well as the whole cornea, but again this work was done in isolated tissue. Measurements by confocal microscopy after radial keratotomy in rabbit and cat eyes were made by Jester et al. (1992).

Confocal microscopy, in combination with the latest video and computer methodology, made it possible for the author to examine ongoing healing processes in living human eyes. Changes in stromal structure were examined after excimer laser photokeratectomy.

Argon fluoride excimer lasers are used to remove discs of superficial stroma from the centre of the cornea. The thickness removed can be precisely controlled and there seems to be little damage to adjacent tissue (Marshall et al. 1985, Marshall et al. 1986). It changes the curvature of the external corneal surface and thus can be used to reduce refractive errors. However, the residual refractive error can not be accurately predicted (Gartry et al. 1992a). Also some corneal transparency may be lost, although this usually lessens within 6 months of treatment (Lohmann et al. 1991a, Lohmann et al. 1991b, Gartry et al. 1992b, Lohmann et al. 1992, Hanna et al 1992).

In our study, an advantage of using healing after excimer surgery was that all patients had the same corneal wound. Density and size of keratocytes was measured in superficial stroma of central cornea. Within 2 weeks of treatment, a brightly reflecting layer of apparently acellular scar tissue developed between epithelium and superficial stromal keratocytes. The density of this layer was also quantified. Observations were made at regular intervals for 6 months.

6.2 Methods

6.2.1 Patients

Professor Marshall (St. Thomas' Hospital) was studying a group of ten patients undergoing treatment with excimer laser. He kindly enabled additional examination of the patients by confocal microscopy. The laser surgery and measurements of refractive errors were done by members of his research group. All other work presented here was done by the author alone.

Most subjects examined by confocal microscopy found that the procedure caused little if any discomfort. The small amount of immersion fluid that remained in the eye sometimes resulted in a mild sensation of stickiness with slight blurring of vision. Some found the light caused discomfort. The nature of the procedure and frequency of appointments was explained in full to patients and consent obtained. However there was a significant non-attendance drop out rate. This may have been because patients first underwent several other procedures by members of the research group, requiring several hours attendance at the hospital.

Sufficiently frequent results were obtained in four subjects. They were aged 23-29 years. Two were male, two female. Pre-operative refractive errors ranged from -5 to -8 dioptres (D) spherical with cylindrical errors of less than 1.75 D. Refraction and visual acuity of each subject is given in table 6.1 (see section 6.3).

6.2.2 Treatment

Excimer photorefractive keratectomy was done using an 'Omnimed' laser (Summit Technology, Waltham, Massachusetts, USA). Wavelength was 193 nm and beam pulse rate 10 Hz, giving energy exposure of 180 mJ/cm^2. Eyes were anaesthetised with 1% Amethocaine, epithelium removed with a scalpel blade and the stromal surface dried with a swab. Treatments to correct for -6.00 D were applied over an area 6mm in diameter. Patients were prescribed antibiotic drops. Steroids were not given.

6.2.3 Examination

Patients were examined before treatment and afterwards at 2, 4, 7, 14, and 28 days, and then 2, 3 and 6 months. The plane of focus was advanced into stroma. Up to 30 seconds of recordings were made with the optical section in the most superficial layer of keratocytes. Images of the acellular structure between epithelium and keratocytes were also recorded.

6.2.4 Image analysis

The image processing techniques described in chapter 5, section 5.4.2, were used to analyse images of keratocytes and scar tissue. The methods gave the percentage of image area occupied by cells or scar tissue. This was taken as a measure of density. The number of cells per image was also determined.

In each of the four subjects, at each examination, ten video fields of optical sections through the most superficial stromal keratocytes from the four subjects at each examination were digitised for analysis. In addition, five fields showing acellular scar tissue were digitised.

The procedure of image analysis was as described in chapter 5. Two background images were made for each subject - from recordings made before and after treatment. As was done for normal eyes, the best threshold was determined by first processing a set of sample images. This gave equations relating threshold to mean intensity of images. Three such equations were determined: (a) for images of keratocytes before treatment. This had already been determined in normal eyes (Chapter 5). (b) for images of keratocytes after treatment, and (c) for images of subepithelial scarring. For each, 15-39 sample images from all 4 subjects were processed. Linear regression determined the equation relating threshold to mean intensity. This was used in the automated analysis process.

The best threshold level, as determined by eye, plotted against mean intensity of sample images is shown in figure 6.1 for each of the 3 sets of images, with linear regression lines and their 95% confidence limits. Equations and correlation coefficients are given in the figure legend.

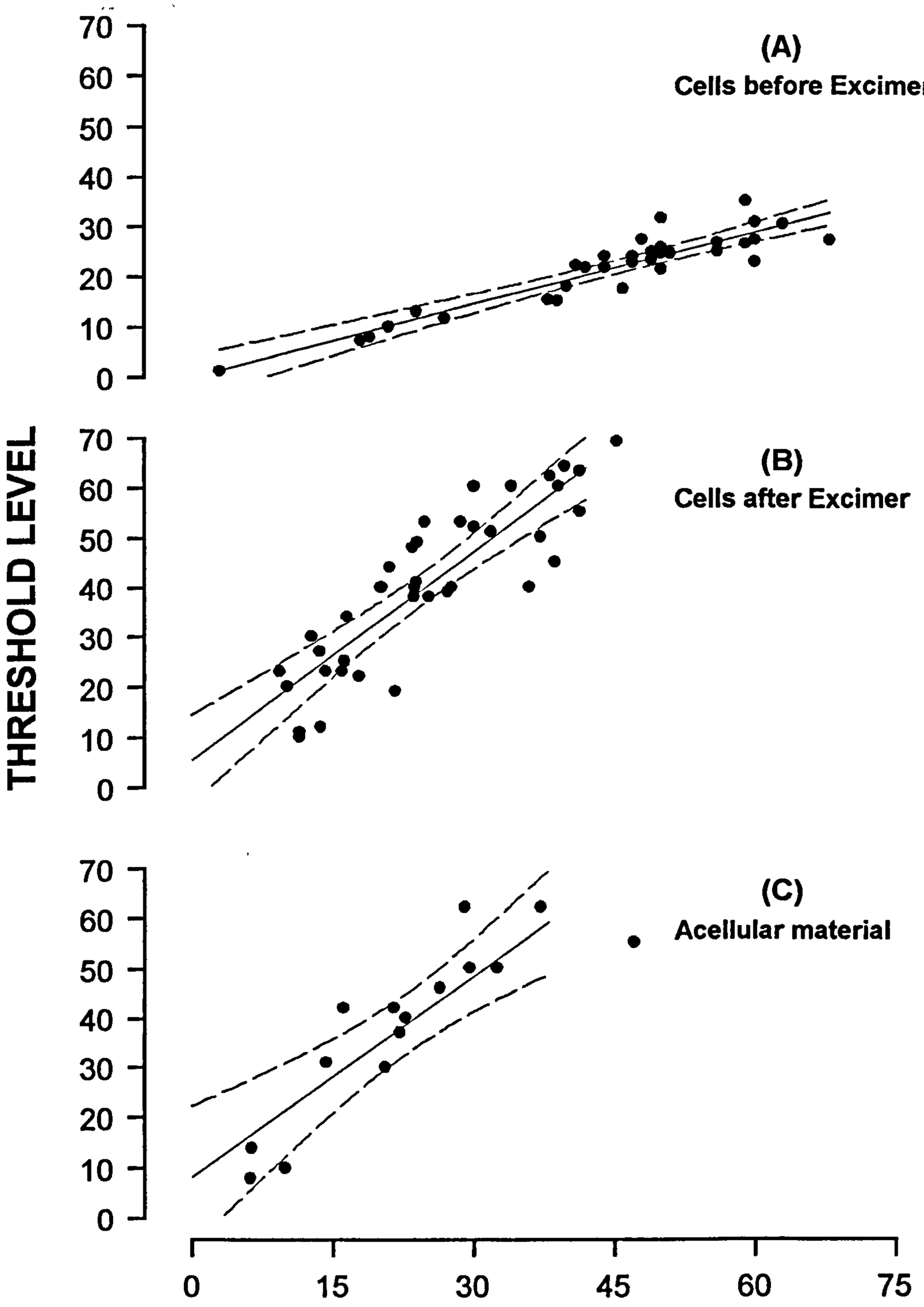


Figure 6.1 (Legend on next page)

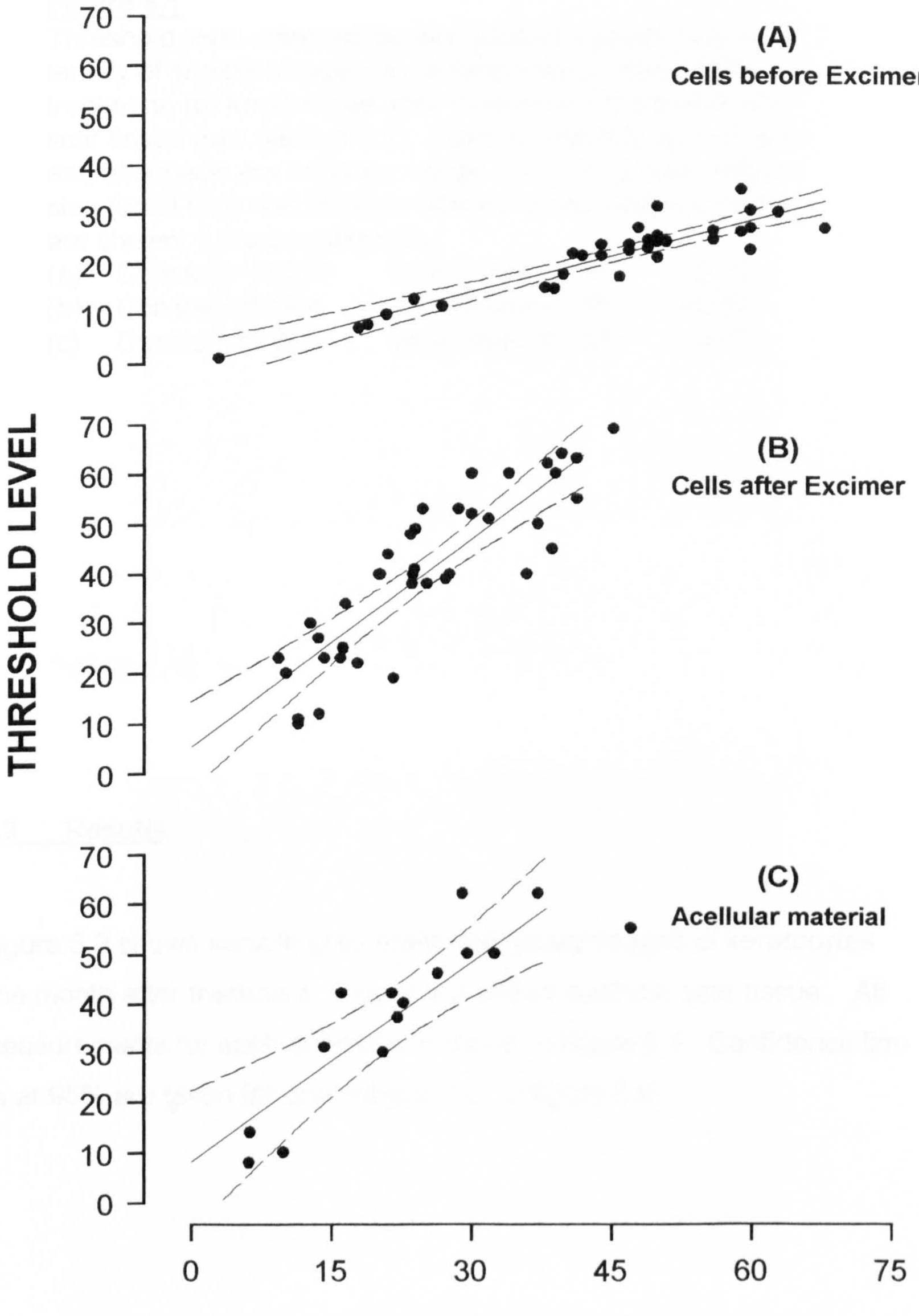


Figure 6.1 (Legend on next page)

Figure 6.1
Threshold level selected 'by eye' plotted against mean intensity of sample images (a) of keratocytes before laser treatment, (b) keratocytes after treatment, (c) subepithelial scar tissue (see section 6.1). Units of intensity on ordinates and abscissas are arbitrary, range 0 to 255. Linear regression (solid line) and 95% confidence limits (dashed lines) are shown. Linear regression:

(a)	Constant=-0.216	co-efficient=0.481	r=0.92
(b)	Constant=5.504	co-efficient=1.383	r=0.87.
(c)	Constant=8.302	co-efficient=1.330	r=0.88.

6.3 Results

Figure 6.2 shows sample grey scale and binary images of keratocytes one month after treatment. Figure 6.3 shows acellular scar tissue.. All measurements for each subject are shown in figure 6.4. Confidence limits at 95% are given for one subject, LC, in figure 6.5.

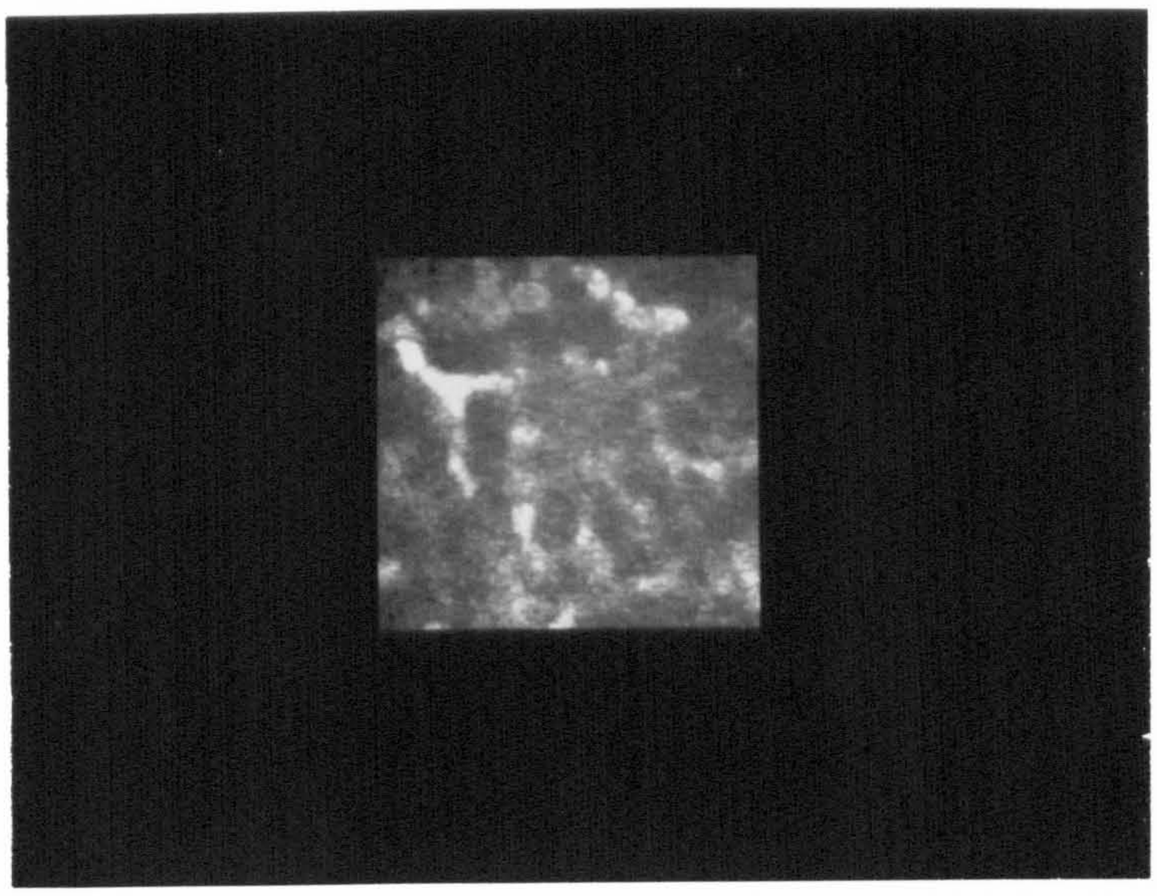


Figure 6.2a

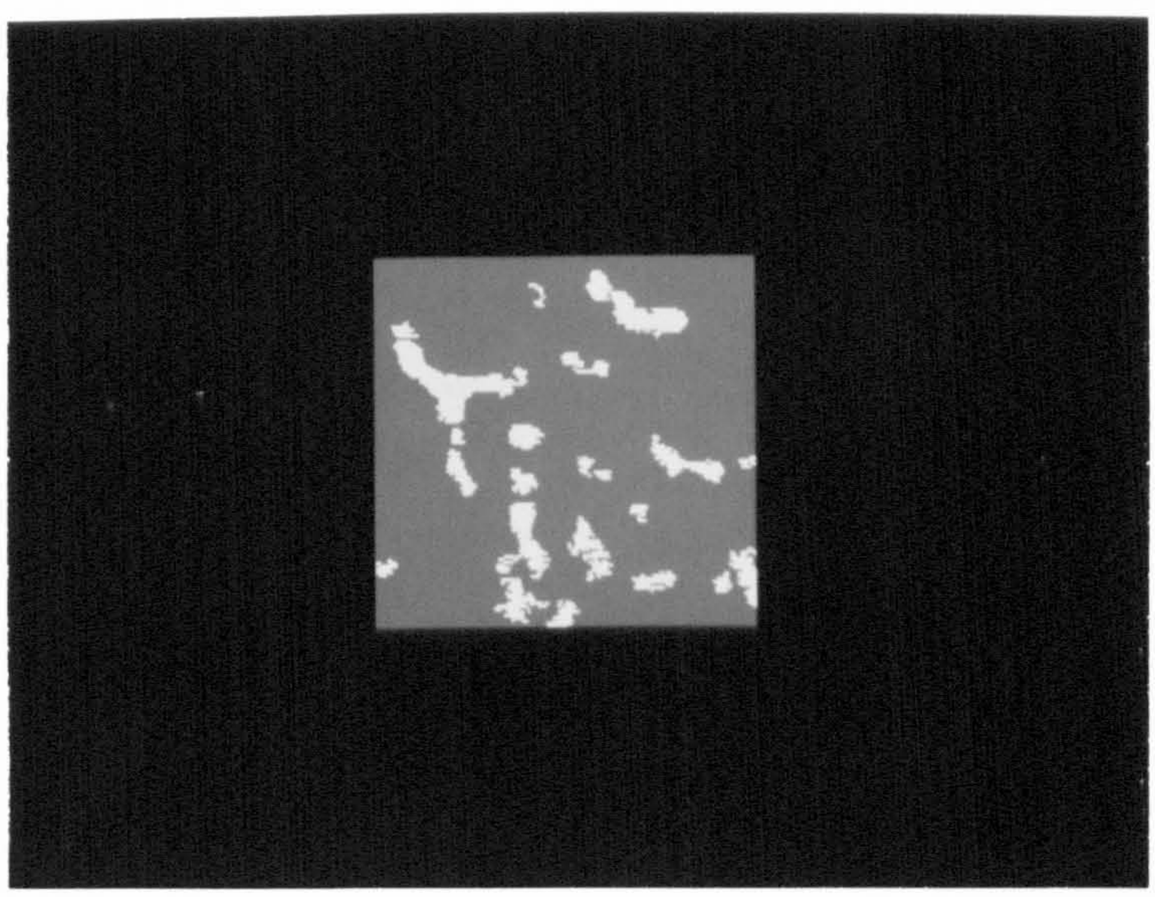


Figure 6.2b

Grey scale and binary images of keratocytes in superficial stroma at one month after laser treatment. Images are 210 x 210 μm, the central region 256 by 256 pixels from full image, size 768 by 512 pixels. In binary images grey areas are of value 0, white of value 1.

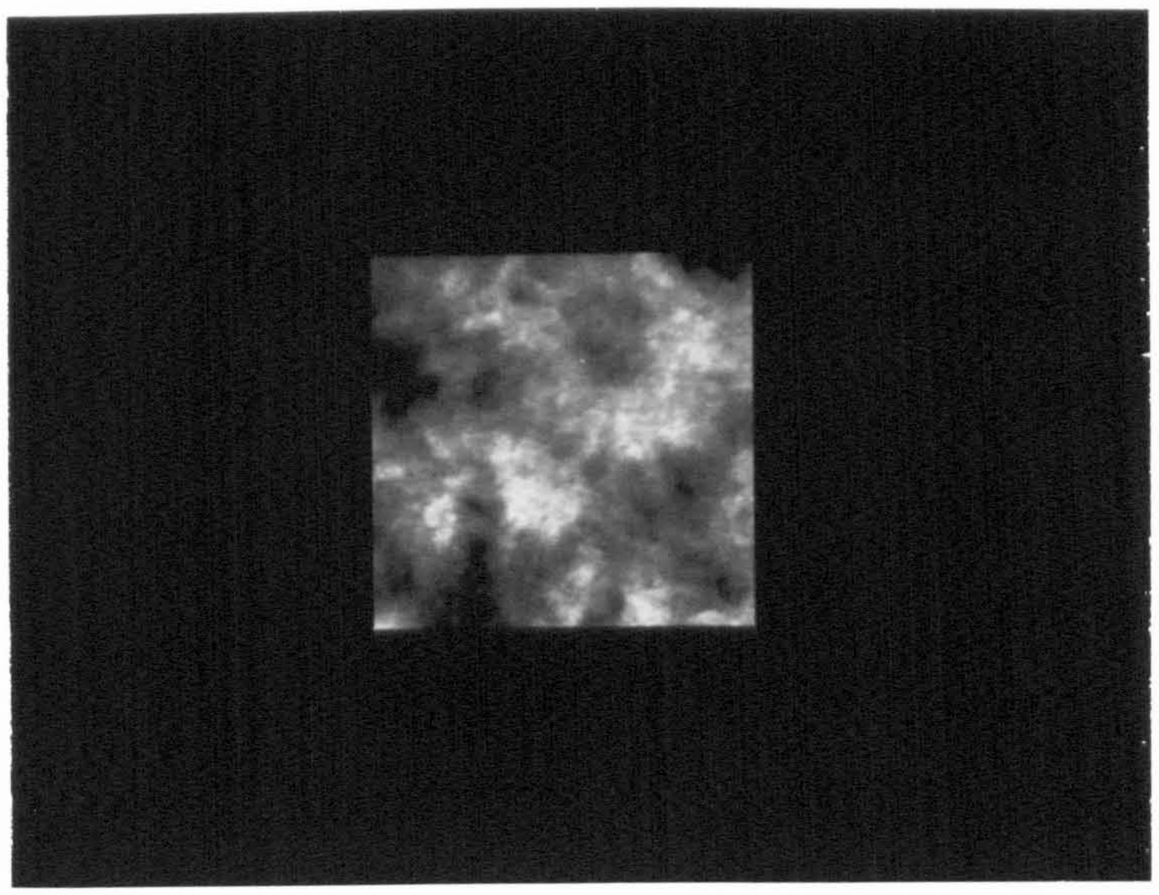


Figure 6.3a

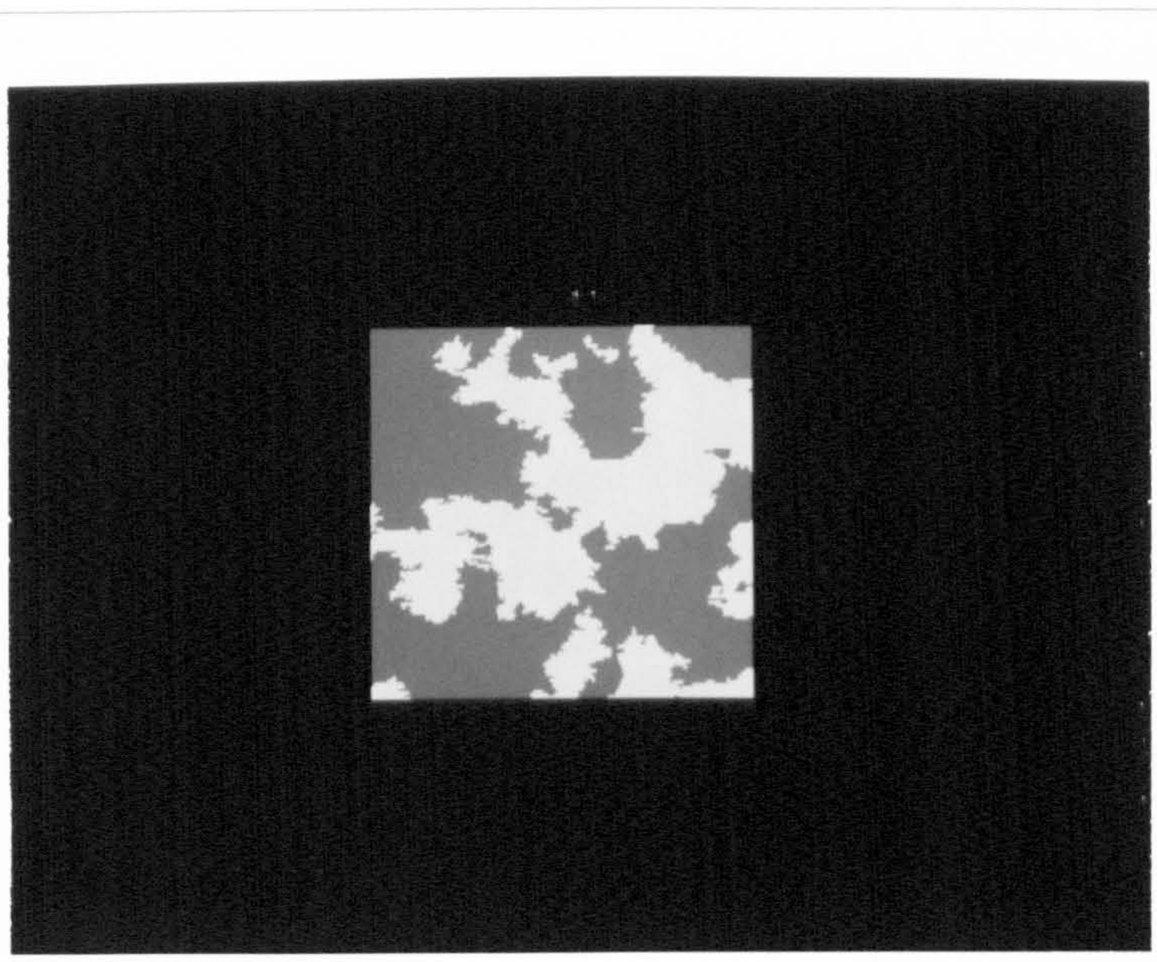


Figure 6.3b

Grey scale and binary images of subepithelial scarring one month after treatment. The full sized grey scale image is shown in figure 7.1.

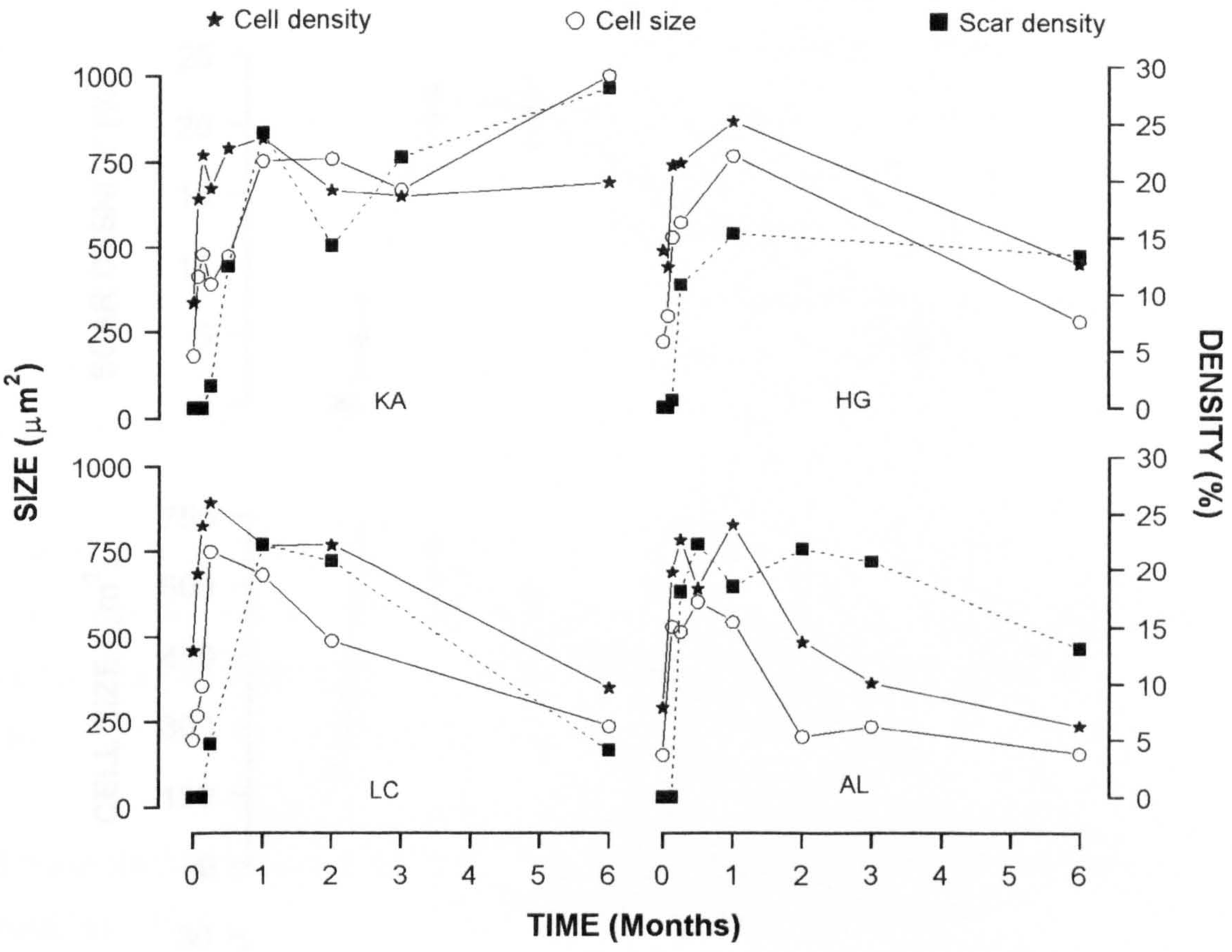


Figure 6.4
Results for each subject after photokeratectomy are plotted against time in months after the treatment. Size of cells (open circles, left ordinate), cell density (solid stars, right ordinate) and density scar tissue (solid squares, right ordinate) are plotted. Time zero is before treatment.

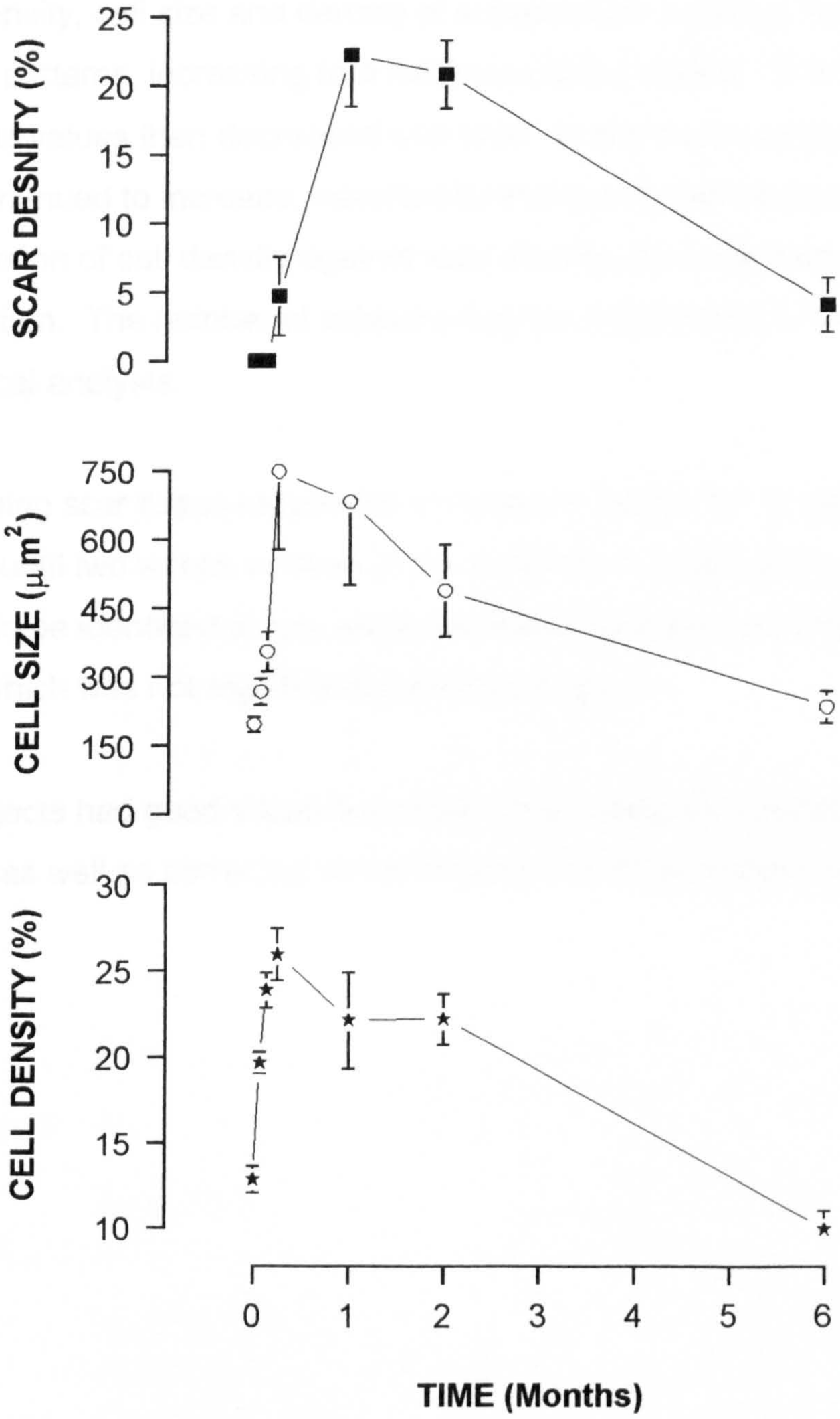


Figure 6.5
Results in subject LC as plotted in figure 6.4 to show error bars, ±95% confidence limits. Cell density, cell size and density of scar tissue are plotted against time after treatment.

Cell density, cell size and density of subepithelial scarring followed similar patterns, increasing to a maximum at 2-4 weeks. In three of the subjects values then decreased with time. In the fourth subject, KA, scarring continued to increase, matched by increasing cell density and size. Regression of cell density against scar density did not show a significant correlation. The number of subjects may be insufficient for meaningful statistical analysis.

Increasing scar tissue lagged the increase in cellularity. It was not apparent until two weeks in three of the subjects. In the fourth some deposits could be identified at one week, but these covered only 2% of image area, which was not significantly different to zero.

All subjects had good visual outcomes. Pre- and post-operative refractive errors, as well as corrected visual acuities are given in table 6.1.

TABLE 6.1

Refractive errors in each subject before and 6 months after excimer laser treatment

Before laser

Subject	Refractive Error	Spherical Equivalent	Corrected visual acuity
KA	-4.75/-0.25 x 180°	-4.875	6/9
HG	-5.00/-1.50 x 90°	-5.75	6/6
LC	-8.00	-8.00	6/5
AL	-6.00/-1.00 x 160°	-6.50	6/6

After laser

Subject	Refractive Error	Spherical Equivalent	Corrected visual acuity
KA	-0.75/-0.25 x 90°	-0.875	6/6
HG	-0.50/-1.00 x 10°	0	6/6
LC	-1.25/-0.25 x 180°	-1.375	6/6
AL	-0.50/-1.00 x 160°	-1.00	6/6

6.4 Discussion

Changes in the density and size of cells, as well as the alterations in acellular structure, have been quantified in conscious human subjects after treatment with excimer laser. Increased size of cells may have resulted from an increase in their volume, or changes in internal cell structure, which made more of the cell visible by confocal microscopy. Migration of cells, and cell division, may also have contributed to the measured increased cellularity.

A highly reflective layer of tissue developed between epithelium and stroma. It was first evident at about 2 weeks after treatment. No cellular detail was visible. It may have been disordered collagenous material or deposits of glycosaminoglycan matrix. Rabbit cornea has been examined by conventional histological methods after exposure to Excimer laser (Goodman et al. 1989). A layer of superficial disordered collagen fibres was identified. However, there is evidence that this layer may be of a different composition in man. Tissue removed from human eyes has been found to be composed largely of extra cellular matrix (Lohmann et al. 1994). The time course of increases in cellular and scar tissue seemed closely correlated. Keratocytes function to maintain the collagen fibres and extra cellular matrix of corneal stroma and presumably produced the layer of abnormal tissue at the stromal surface.

We found the greatest change in corneal structure to be at 1-2 months after laser treatment, followed by a gradual return to preoperative values. This matches closely the reported changes in visual, objective measurements of reduced corneal transparency and subjective assessments of corneal haze (Lohmann et al. 1991a, Lohmann et al. 1991b). Lohmann et al. found that the maximum increase in light scattering was at 2 months. Contrast sensitivity at 5% was reduced at 1 month, returning to within the normal range by 3-4 months. Results presented here seem to indicate

that changes in transparency and visual performance are a result of increased corneal cellularity as well as the formation of scar tissue. However, other structural changes, beyond the resolution of the current confocal microscope, may also contribute to changes in transparency. Vacuoles between collagen lamellae, 0.5-1 μm across, have been identified in histological sections of monkey cornea (Marshall et al. 1988).

The number of patients completing this study was insufficient for meaningful statistical analysis. However, no more were available in the time period. More work is necessary to investigate differences in the healing process in those subjects who develop severe scarring, or whose refraction regresses following refractive laser surgery.

CHAPTER 7

7 NERVE REGENERATION AFTER EXCIMER LASER

7.1 Introduction

Aim: To study regeneration of subepithelial nerves

Neuronal damage by excimer laser

Neuroanatomy of cornea

Studies of nerve growth in animals

Work presented here

7.2 Method

7.2.1 Patients

7.2.2 Laser treatment

7.2.3 Microscopy

7.3 Results

Subepithelial nerves before and after excimer laser

Changes in structure of stromal nerves

7.4 Discussion

Difference between our results and those of others

Changes in corneal sensation

7.1 Introduction

Removal of superficial layers of the cornea by excimer laser destroys all epithelial and subepithelial nerves within the treated area (Trabucchi et al. 1994). Some superficial stromal nerves are also damaged. The aim of work described in this chapter was to examine their regeneration.

There have been many studies of corneal neuroanatomy. Zander and Weddell (1951) examined 173 animals of 7 vertebrate species, including human, by light microscopy. Rózsa and Beuerman (1982) and Beuerman et al. (1982) also used light microscopy to examine rabbits. Electron microscopy was used by Whitear (1960) in mice and by Matsuda (1967) in rabbit and man. There seems to be little species variation. The cornea is innervated by about 20 nerve trunks which enter peripheral stroma. Branches form a subepithelial plexus, both superficial and deep to the epithelial basement lamina (Róza and Beuerman 1982). From here branches pass forward to terminate in more superficial epithelial layers.

Trabucchi et al. (1994) and Pallikaris et al.(1990) examined growth of subepithelial nerves after excimer laser ablation in animal eyes. Regeneration was complete by one month. In the present observations, neural structure was examined in the centre of the cornea of 19 human eyes up to 2.5 years after laser treatment. The patients were taking part in a large ongoing study by Professor Marshall. Observations by the author of neuronal structure were made at the same time as those of changes in keratocyte morphology (chapter 6). Examination of keratocyte structure took 5 to 10 minutes. Imaging of nerve fibres was limited to central cornea to avoid lengthening examinations. Approximately a further 10 minutes would have been required to examine neural structure at several positions across the cornea.

Results differed substantially from those of earlier work in animals. The subepithelial plexus did not seem to regenerate in any of the patients.

7.2 Method

7.2.1 Patients

Nineteen eyes of 12 patients treated with excimer laser were examined. Ages varied from 23 to 59 years, mean 35.7. Five were male, 7 female. All were originally myopic, in the range -3.0 to -8.0 D (spherical equivalent).

7.2.2 Laser treatment

Laser surgery was done by members of Professor Marshall's research group. The method was as described in 6.2.2. Intended corrections of 3-6 dioptres were applied. Diameter of the treated zone was either 5 or 6mm.

7.2.3 Microscopy

The plane of focus was advanced to the epithelial/stromal interface and images recorded for up to 60 seconds with optical sections tangential to the stromal surface. The microscope was moved small distances verti-

cally and horizontally to examine an area approximately 1 x 1 mm. The plane of focus was then advanced through central stroma to the endothelium for observations of keratocyte structure (as described in chapter 6).

In some subjects, the microscope was also orientated at an angle of about 30° to the eye surface and oblique optical sections imaged through epithelium and superficial stroma.

Eight of the subjects were examined before Excimer treatment. Observations after treatment were at 1 to 30 months, mean 9, standard deviation 8.

7.3 Results

Before excimer treatment, a dense plexus of subepithelial nerves was seen just superficial to the stromal surface (figures 3.4 and 3.5). Occasional bright spots were seen superficial to the plexus. They were presumed to be radially orientated nerves passing into superficial epithelial layers. No other intra-epithelial fibres could be identified.

Images in patients who had been treated with excimer laser showed a layer of acellular scar tissue at the stromal surface. This was described in chapter 6.3. In 17 of 19 eyes no subepithelial nerves were seen, either superficial or deep to this layer, at any time after treatment. An optical section tangential to the layer is shown in figure 7.1 and oblique to it in figure 7.2. In two subjects, a single nerve fibre was found superficial to the acellular layer (figure 7.3). In one of these subject a single tortuous fibre was seen deep to it (figure 7.4).

There was no apparent change in the structure or density of stromal nerves, although this was not quantified. Only occasional images of stroma contained nerves. Extensive scanning of the cornea would have been necessary to make measurements of their density.

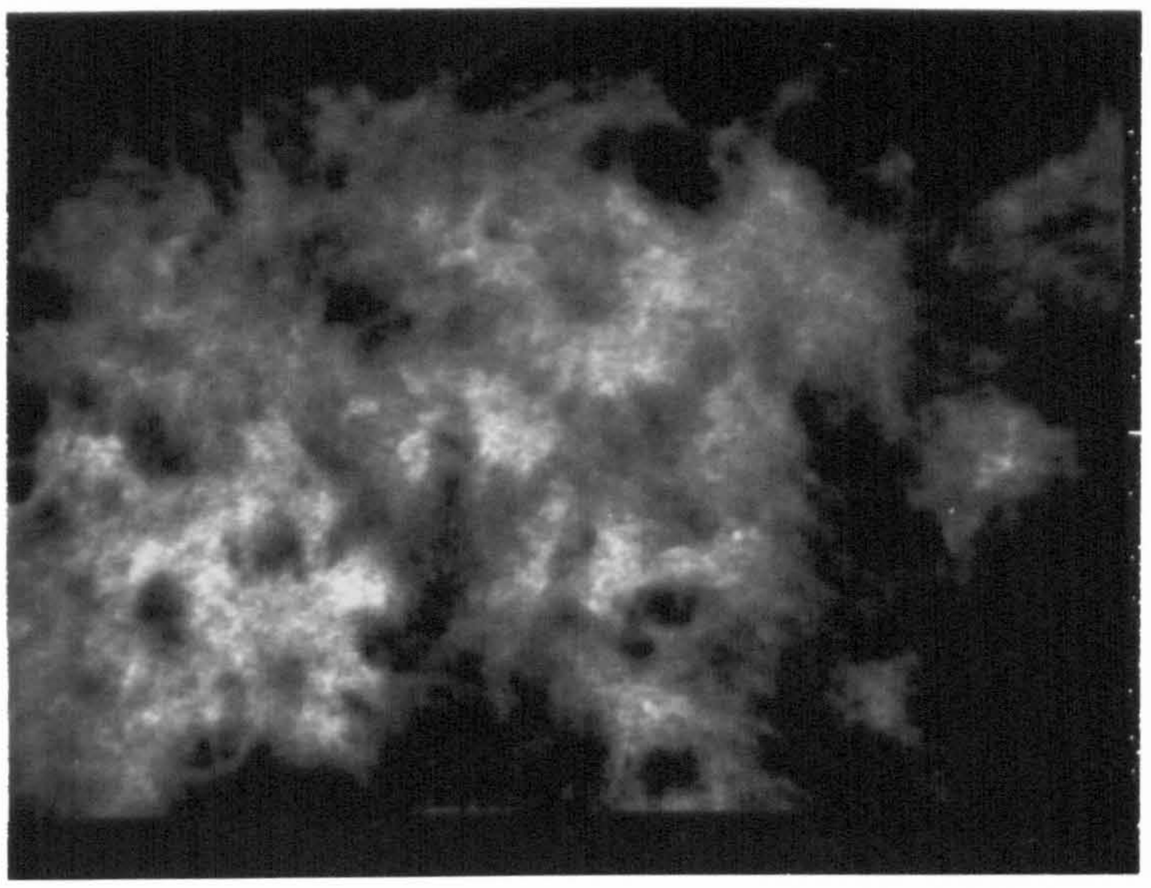


Figure 7.1
Optical section tangential to scar material 1 month after Excimer laser treatment.. No nerves were seen superficial to this layer.

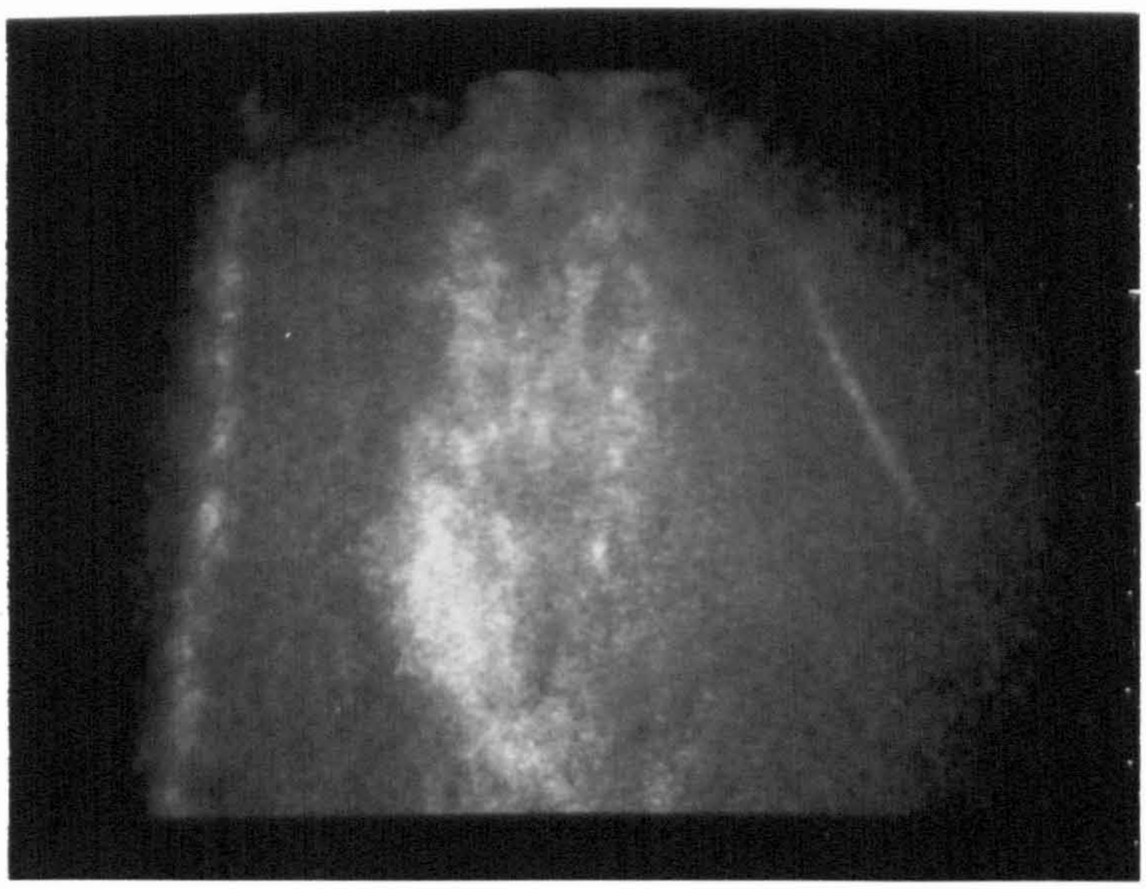


Figure 7.2
Structures shown in Fig 7.1 with optical section at oblique angle to eye surface.

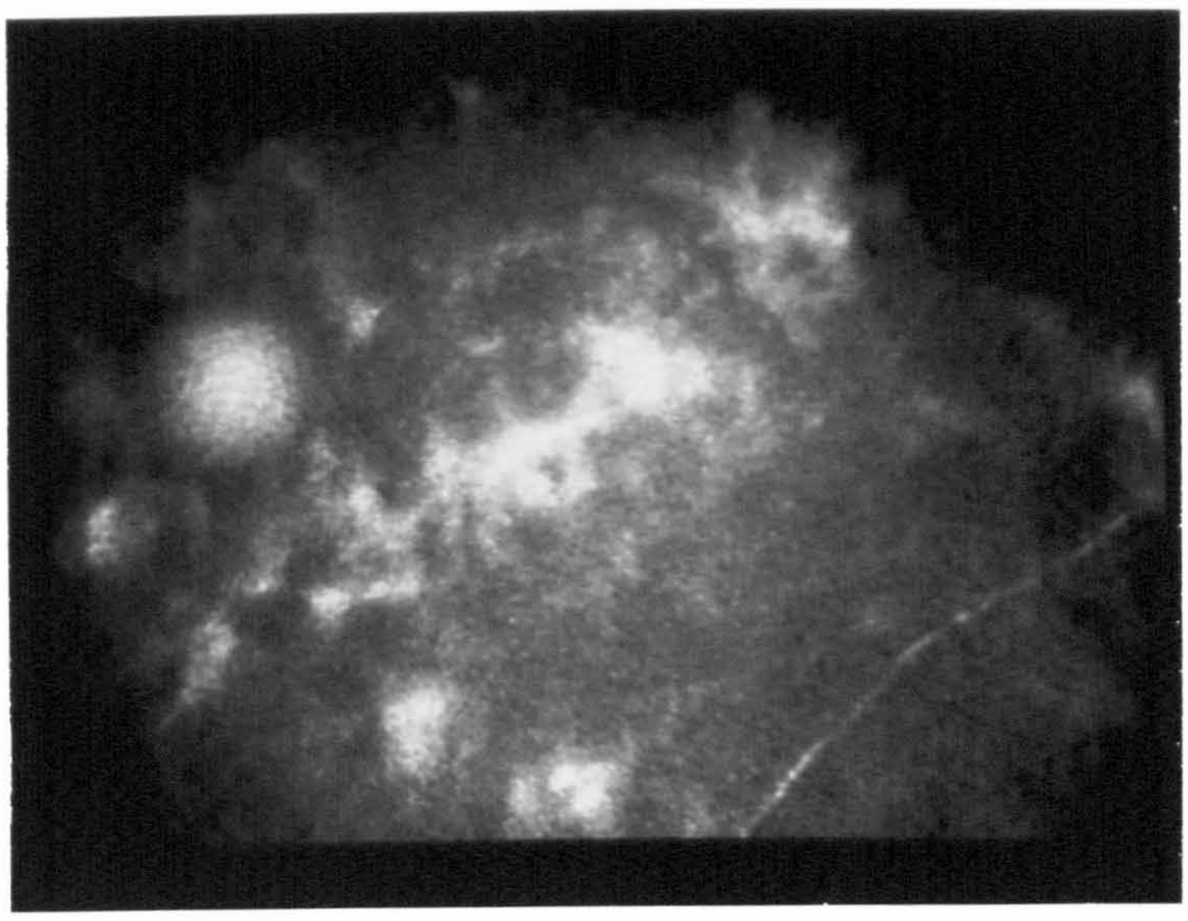


Figure 7.3
Single subepithelial nerve fibre as found in 2 of the 19 subjects examined.

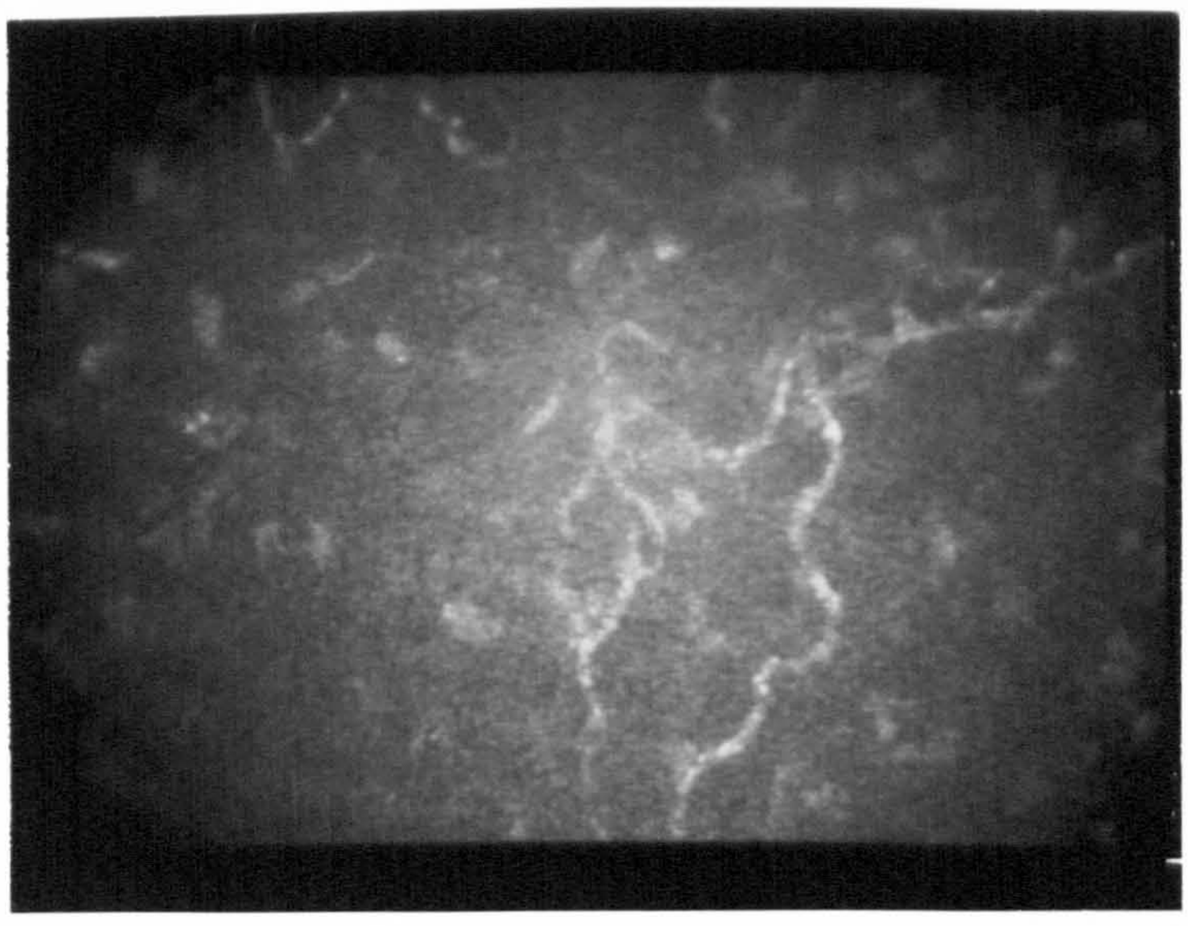


Figure 7.4
Tortuous nerve fibre in the superficial stroma as found in one subject following Excimer treatment.

7.4 Discussion

Almost no regeneration of subepithelial nerves was detected within the central cornea following excimer keratectomy in humans, even after 2.5 years. Trabucchi et al. (1994) examined rabbit corneas after excimer ablation to a depth of 100 µm. Sprouts from stromal nerves were identified within the first post-operative week. Regeneration of the subepithelial nerve plexus was complete by one month, extending throughout the treated area. The density and thickness of nerves was greater than that in untreated control animals.

Similar results are reported by Pallikaris et al. (1990), who also examined rabbit eyes and found re-innervation of the injured area by 1 month.

The different findings from those presented here may be a result of altered response in different species. However, there is little difference in normal neuroanatomy in the two species. Zander and Weddell (1951) found more loops of radially orientated fibres towards the corneal centre in man than in rabbit, but no other differences were reported.

Corneal sensation has been found to return to normal 6 months after excimer surgery, measured using a Cochet-Bonnet aesthesiometer (Lawrenson et al. 1995). If Lawrenson's observations are correct, a problem remains to explain how corneal sensation was normal when no nerves were seen by confocal microscopy. There may be a problem with the method of measurement, the Cochet-Bonnet aesthesiometer. It may not be appropriate because the minimum stimulus is above threshold. Thus it may not be sufficiently sensitive to detect reduced sensitivity.

It is also possible that the subepithelial plexus had regenerated, but could not be detected by confocal microscopy. The refractive index of new fibres may have been more closely matched to that of adjacent tissue.

Also it is possible that they were too thin to be resolved. However this is not consistent with the findings of Trabucchi et al. (1994) - that nerve fibre diameter was increased after laser ablation.

In the work reported here, the regeneration of fibres was only examined in the centre of the central 1mm^2 of the cornea. Nerves may have grown in from the edge of the ablated zone, but not reached the centre of the cornea. Sensation may have been carried by these fibres, or others outside the ablated area, detecting minute distortions of central epithelium or collagen fibres. Sensation may also have been detected by deeper undisturbed nerves in the stroma.

CHAPTER 8

8 THICKNESS OF TEAR FLUID BETWEEN SOFT CONTACT LENSES AND EPITHELIUM

8.1 Introduction

8.2 Author's earlier work

Measurement of tear film thickness without contact lenses

Measurement of tear layer on external surface of lenses

8.3 Measurements by confocal microscopy

8.3.1 Observations using immersion objectives

8.3.2 Observations using dry objectives

8.4 Discussion

8.1 Introduction

In earlier work the author measured thickness of tear fluid on the external surface of contact lenses (Prydal 1991). However, at that time measurement of the thickness of fluid between contact lens and eye was not possible. Such measurements may provide information about the physiology of cornea and tear film in contact lens wear. It may be helpful for assessment of different designs, their fitting, and for study of pathological changes in the cornea. Thickness of fluid may influence the comfort and duration of wear. Attempts were made to measure the thickness between soft contact lenses and epithelium using the new confocal microscope.

8.2 Author's earlier work

In work for the PhD (1987-1991, Prydal 1991) the author modified optical methods for measuring thickness of the tear film, without contact lenses, in humans and several animal species. This was a new application of the techniques. One method was laser interferometry, which could be used in both humans and animals. The other was confocal microscopy, but at that time it was not possible to make measurements in conscious human subjects. Results in animals by the two techniques were closely correlated in each eye and this provided evidence of the validity of both methods.

Thickness was found to be up to four times greater than earlier measurements (Prydal 1991, Prydal and Campbell 1992, Prydal et al. 1992). Also, tear film structure was found to be different from previous descriptions - there was evidence that the film was composed largely of mucus,

with little free aqueous fluid. It seemed possible that the mechanical and chemical techniques used in earlier studies disturbed film structure or were not sensitive to the full thickness of mucus in the tear film.

Thickness of tear fluid on the external surface of soft contact lenses was measured in man using interferometry. It was found to increase with adaptation to their wear. At that time it was not possible to examine the layer of tear fluid between lens and eye. Interferometry was not suitable for such measurements and confocal microscopy was then limited to use in immobile eyes.

8.3 Confocal microscopy for measurement of tear thickness under lenses

8.3.1 Observations using immersion objectives

In the present work, images of oblique cross sections through contact lens, tear layer and epithelium were recorded using the standard immersion objective. The coupling fluid was 2% methylcellulose. It was proposed to measure radial tear thickness using the ratio of thicknesses of layers in images. This technique was described in chapter 4 for measurement of epithelial thickness.

However, reproducible measurements were not obtained or possible. Often the back of the contact lens and the surface of epithelium could not be identified. Only occasionally could these layers be distinguished. Thicknesses of up to 40 μm were observed. A sample image is shown in figure 8.1. However, it is possible that immersion fluid mixed with tear fluid adding to the thickness under the lens so that such measurements were not considered valid.

Film thickness reduced to zero in about one minute. Fluid may have been squeezed out from under the lens by pressure exerted on the contact lens by the microscope objective.

No tear film was evident on the front surface of contact lenses. There may not have been fluid present, or it may have mixed with immersion fluid resulting in a gradual change in refractive index and no sharp interface to give an identifiable reflection.

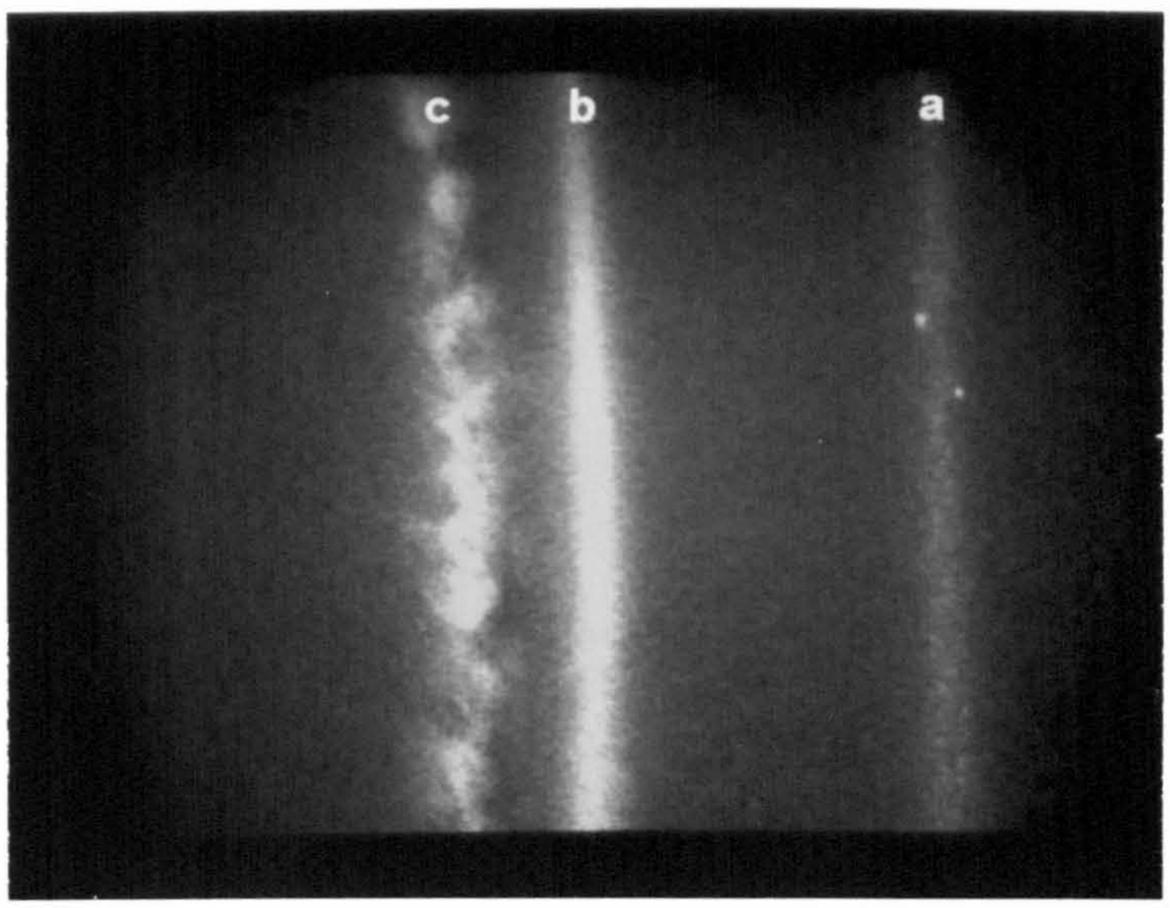


Figure 8.1
Oblique optical section through cornea.
(a) Outer surface of contact lens
(b) Inner surface of contact lens
(c) Surface of epithelium

8.3.2 Observations using dry objectives

It was clear that reliable measurements could only be made with a dry, non immersion, objective. Several lenses were tested, and those designed for use in metallurgy found to give the best images. These are intended for use in reflection microscopes and have appropriate anti-reflection coatings. Some images were recorded with a Nikon x10 metallurgy objective (M plan 10, NA 0.25). The surface of the contact lens and some structure in the cornea could be seen, but it was not possible to identify the inner surface of the lens and the external surface of epithelium. A sample image is shown in figure 8.2.

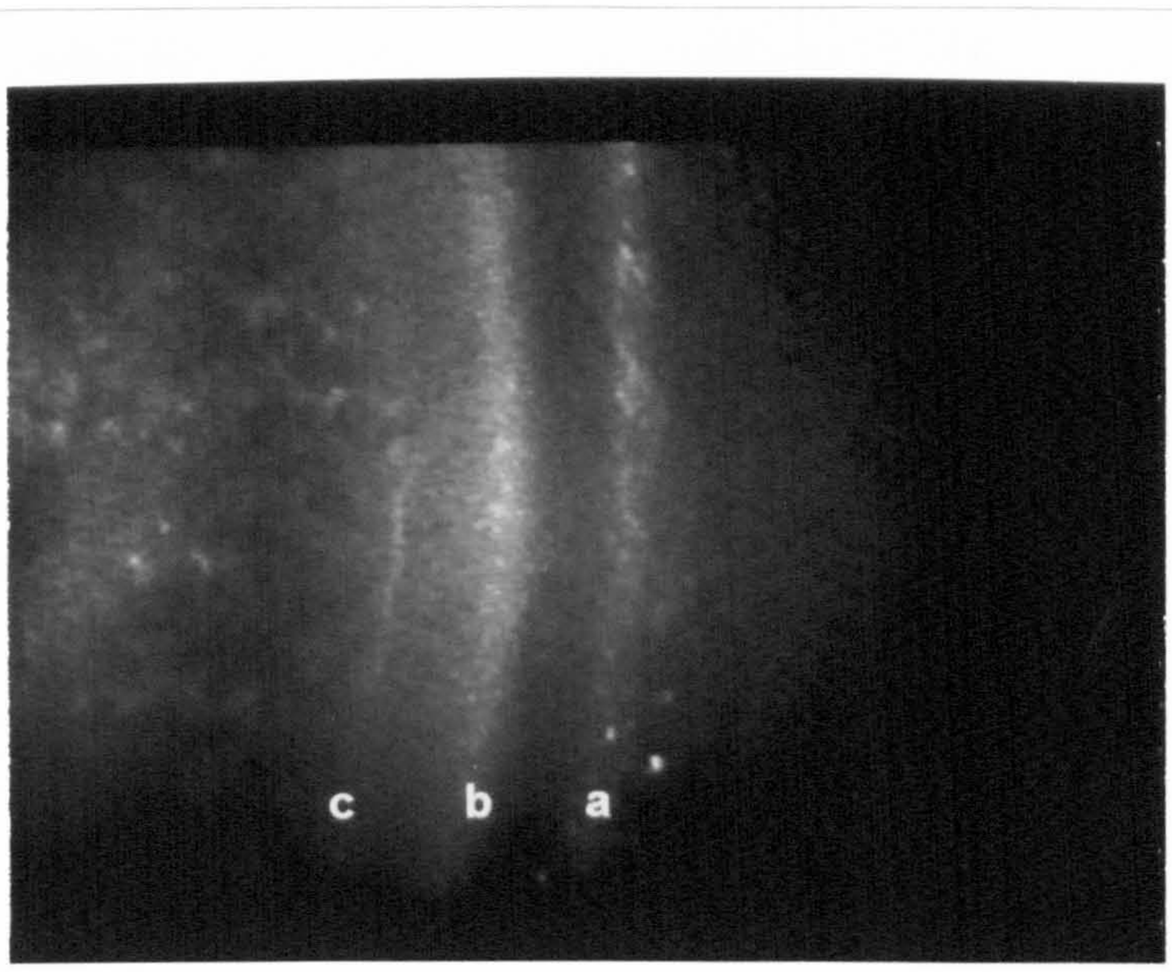


Figure 8.2
Non contact dry objective: Oblique optical section through contact lens and eye surface.
(a) Outer surface of contact lens
(b) Surface of epithelium
(c) Surface of stroma
Subepithelial nerves and stromal keratocytes can be identified.

8.4 Discussion

This issue remains unresolved. Further work is required to test other objectives, although it is possible that the imaging ability of the microscope is not limited by the objective alone. Bright reflections from the air/lens interface may obscure detail from deeper layers. When rapid scanning laser confocals and other new microscopes become available, higher resolution images may make reproducible measurements possible.

CHAPTER 9

9 CLINICAL APPLICATIONS

9.1 Introduction

9.2 Corneal abrasion

9.3 Infective keratitis

9.3.1 *Acanthamoeba*

9.3.2 *Herpes simplex*

9.3.3 *Herpes zoster* keratitis

9.3.4 Leprosy

9.4 Endothelial disease

9.5 Keratoconus

9.1 Introduction

The use of confocal microscopy as a part of the routine clinical examination of eyes has now become possible. The various technologies involved are sufficiently well developed. The procedure is straightforward. It causes little if any discomfort, and takes less than 5 minutes. Videos are the critical step and can be reviewed immediately afterwards. Special techniques for enhancement and analysis of images are only required for accurate measurement.

Confocal microscopy of a range of diseases is described in this chapter. The aim was to survey as many different conditions as was possible in the time available and to find those in which confocal microscopy may be useful as a clinical tool. Statistical data concerning any one condition was not sought.

9.2 Corneal abrasion

Healing of epithelial defects was examined in patients treated with excimer laser. Epithelium had been removed from the central 7 mm of cornea before the procedure. Five patients were examined at 2,4, and 7 days afterwards.

DAY 2

There was a large epithelial defect in the centre of the wound in all patients. Cells at the edge of the epithelial sheet appeared to be migrating into the wounded area. They were elongated in shape, about 100 x 20 µm (figure 9.1). Few nuclei could be seen. Groups of cells were aligned in parallel rows. One such group is shown in figure 9.1. Normal epithelial

cells (figure 3.2) are round and approximately 40 μm in diameter. They have bright central nuclei.

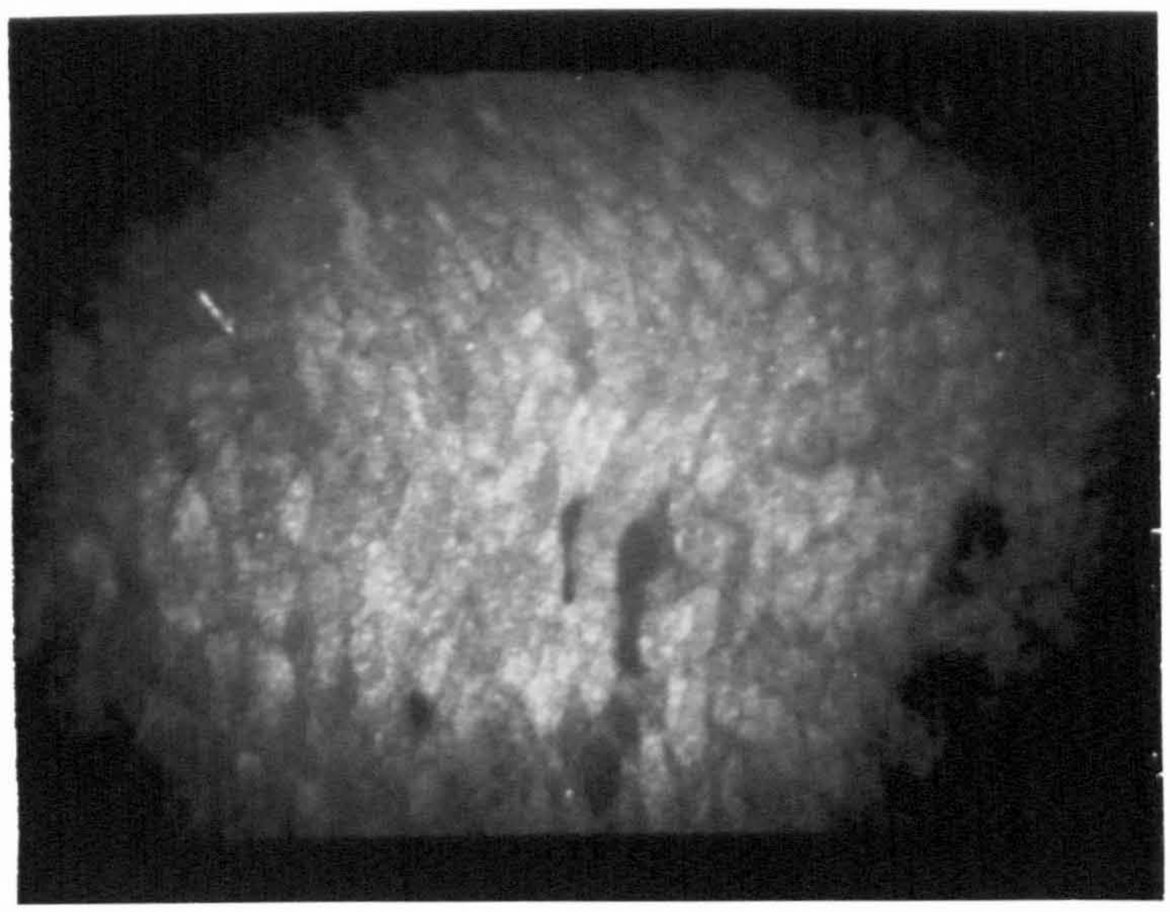


Figure 9.1
Epithelial cell surface 2 days after corneal abrasion showing elongated cells (Normal structure is shown in figure 3.2)

DAY 4.

The cell layer was continuous across the treated area in all patients, although less than normal thickness. Individual cells were of near normal dimensions.

DAY 7.

Epithelial structure appeared normal.

9.3 Infective keratitis

One application of confocal microscopy is for the diagnosis of corneal infections. It may provide immediate histological identification of organisms without the need for corneal biopsy, laboratory culture, and other procedures.

Patients with infections by *Acanthamoeba*, *Herpes simplex*, *Herpes zoster* and *Mycobacterium leprae* were examined.

Chew et al (1992) have used confocal microscopy to identify fungal organisms in cornea. No cases of fungal keratitis were available for examination during the period of this work.

9.3.1 *Acanthamoeba*

The incidence of keratitis due to infection by *Acanthamoeba* has recently increased. Ficker et al. (1989) established an association with the introduction of contact lens wear. Less rigorous cleaning methods have been considered important. Others have postulated that a more virulent strain of organism is responsible for the increase (Jones 1986).

The condition may be diagnosed using a slit-lamp. Characteristic changes are: epithelial defects, ring shaped stromal infiltrate and thickened stromal nerves. However, these signs often develop late in the disease. Early changes may be confused with bacterial, fungal or herpetic infection (Abbott and Elander 1990)

Prompt diagnosis is important, as corneal scarring is worse if treatment is delayed. Grafting may then be required to restore vision. Stromal biopsy and special laboratory culture techniques are often required to establish the diagnosis (Abbott and Elander 1990).

Other workers have used confocal microscopy to examine cases of *Acanthamoeba* keratitis. Winchester et al. (1995) examined 8 patients with the infection and was able to identify organisms in all cases.

In the present work, a 48 year old female patient with *Acanthamoeba* keratitis was examined two months after the start of symptoms. The diagnosis had been made using conventional histological techniques. She had worn disposable contact lenses.

Figure 9.2 shows an optical section through deep epithelium. Several *Acanthamoeba* were identified. The one in this image is marked with an arrow. It is approximately 35 µm in diameter, which is compatible with the known size of the organism, 15-45 µm (Winchester et al. 1995). Infiltration by smaller cells was seen. These were presumed to be leucocytes.

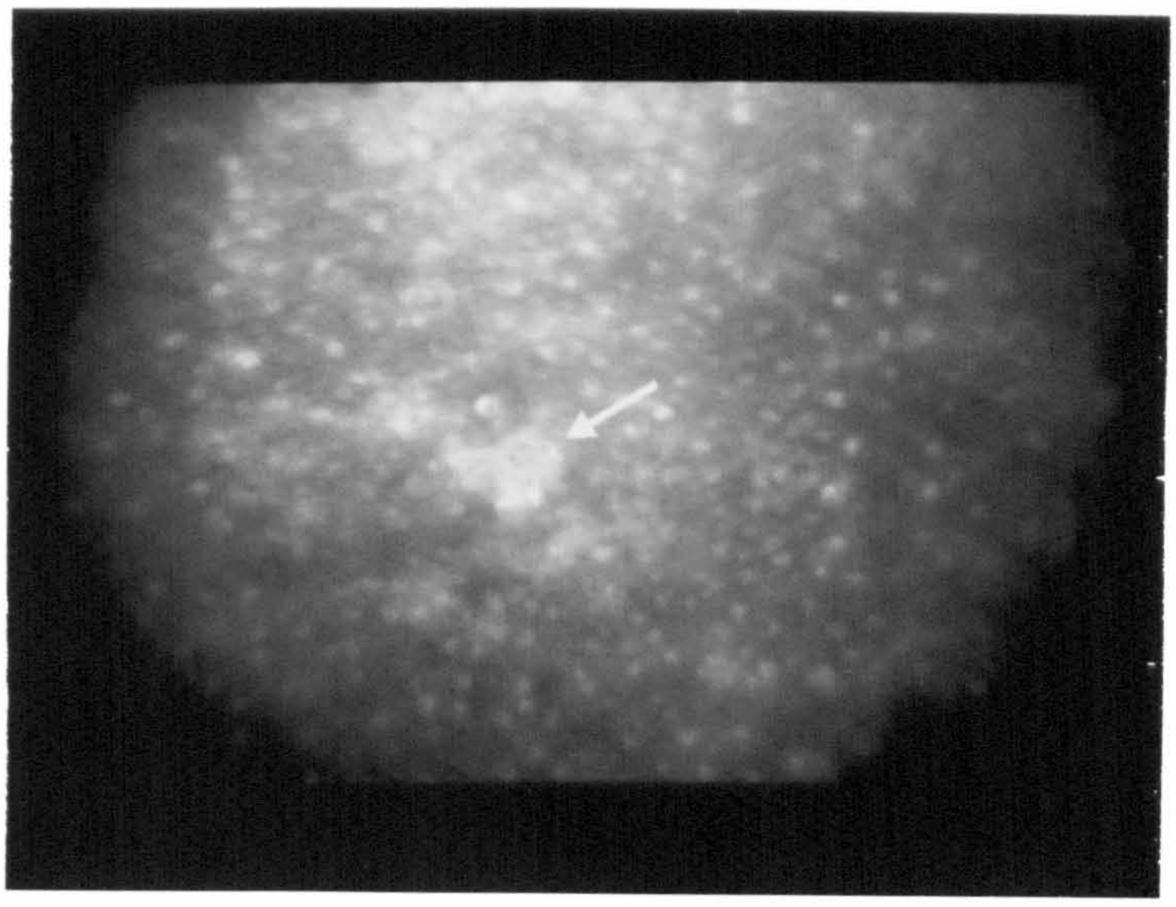


Figure 9.2
Optical section through deep epithelium in patient with *Acanthamoeba* keratitis. The organism (arrow) is about 35 µm in diameter.

Nerves in the stroma did not appear to be thickened (figure 9.3), but the density of keratocytes was increased along their length. It may be this that gives the impression of thickened nerves on slit-lamp examination.

Figure 9.3
Optical section through stroma in patient with *Acanthamoeba* keratitis showing nerve of normal diameter, approximately 8 μm.

The patient was re-examination 4 months later. Treatment had been completed. No active or encysted forms of the organism were seen.

9.3.2 *Herpes simplex*

Herpes simplex infection may result in dendritic ulceration of the cornea (O'Day and Jones 1990). This is a characteristic manifestation of the disease and can be diagnosed by slit-lamp examination. However, there are many other forms and it may be mistaken for various conditions. These include *Herpes zoster* keratitis and Thygeson's superficial punctate keratitis (O'Day and Jones 1990).

Two cases of *Herpes simplex* were examined, a 37 year old male and a 65 year old female. Both had suffered from recurrent disease for several years and had reduced corneal sensation when tested using a strand of cotton wool to stimulate the cornea. An image of the epithelial surface is shown in figure 9.4. Irregular clumps of enlarged cells were seen. Diameters measured up to 200 μm.

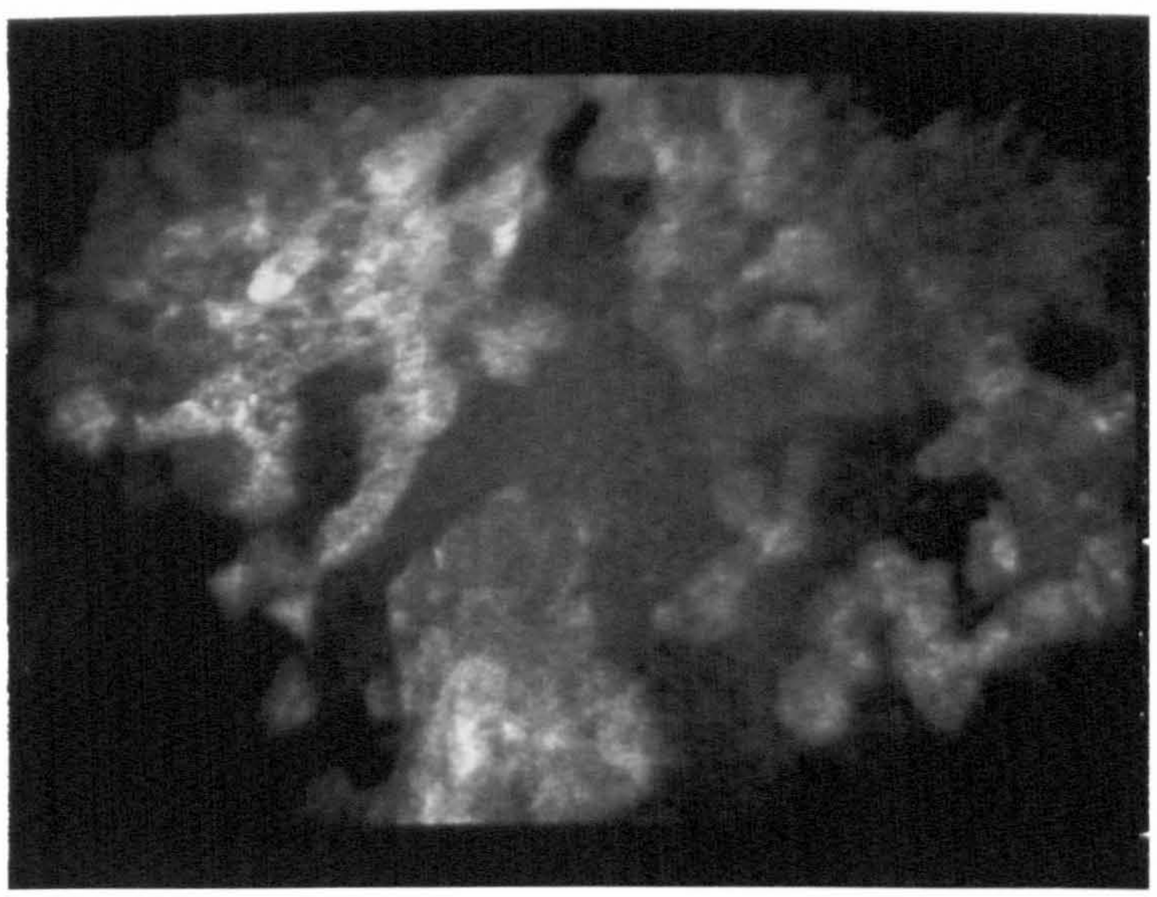


Figure 9.4
Optical section through surface of epithelium in patient with *Herpes simplex* keratitis

The subepithelial nerve plexus was broken up into isolated fragments of fibres. An optical section tangential to this layer is shown if figure 9.5 and oblique to it in figure 9.6. Only a few fragments of nerve fibres, 30-60 µm in length, could be identified. One of the patients was examined 3 months later. There was no evidence of regrowth of nerves.

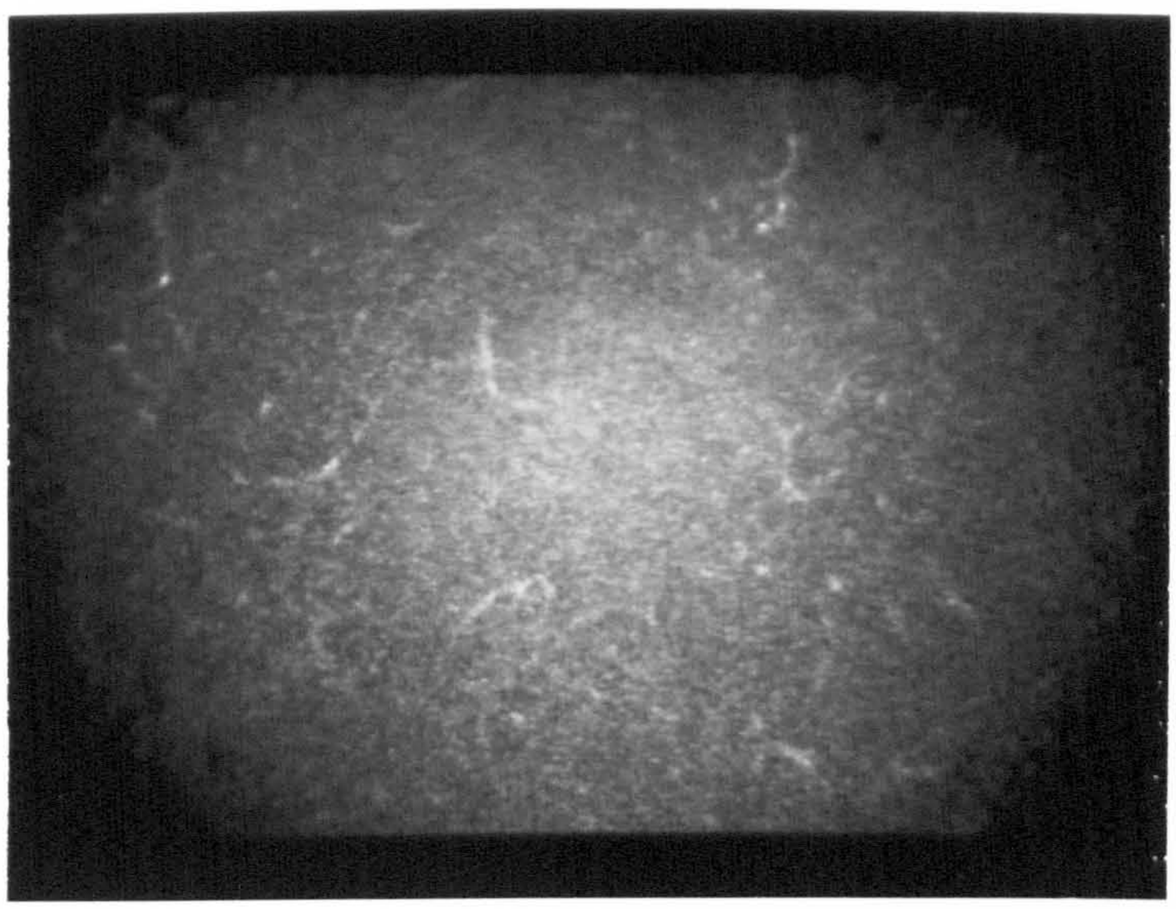


Figure 9.5
Optical section tangential to subepithelial nerve plexus in patient with *Herpes simplex* keratitis. Only small fragments of nerves remain.

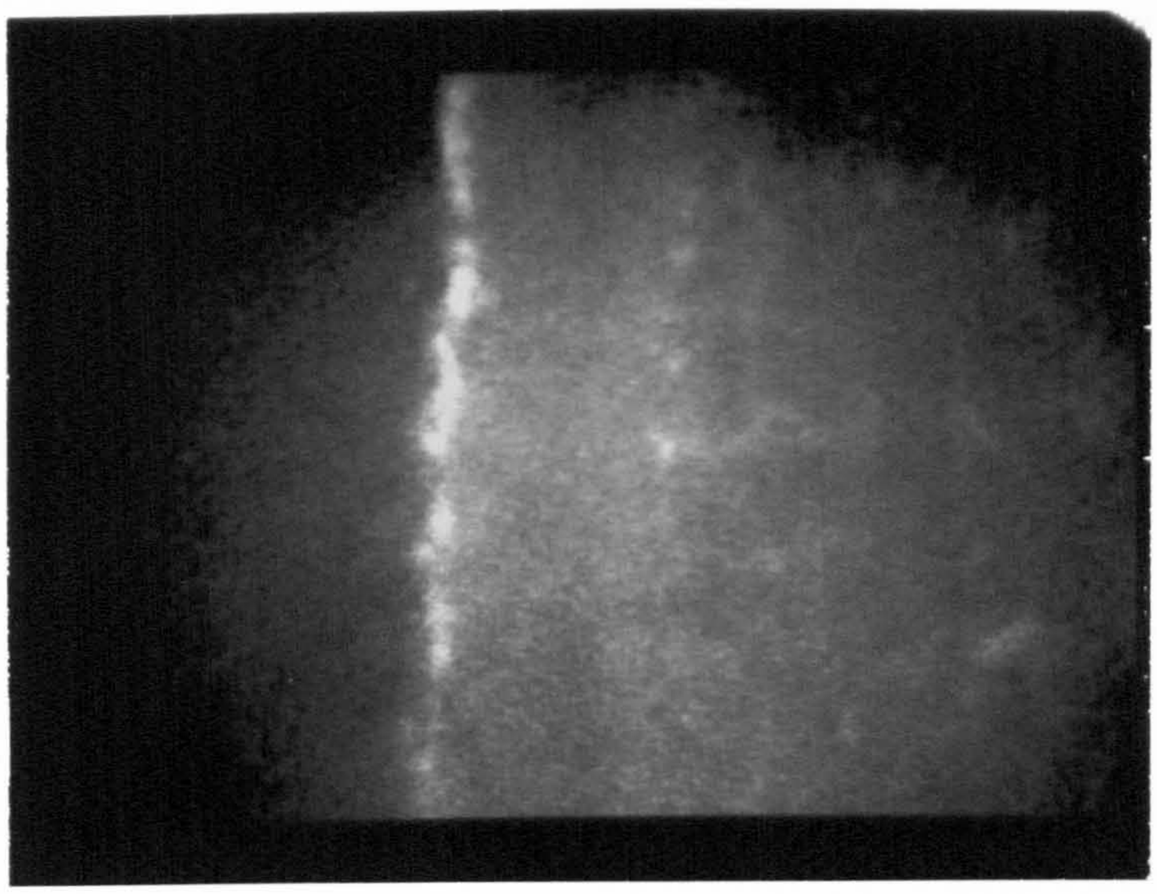


Figure 9.6
Optical section oblique to corneal surface in patient with *Herpes simplex* keratitis. No subepithelial nerves can be identified.

Similar appearances were seen in *Herpes zoster* keratitis (9.3.3) and it is possible that these changes are specific to infections by *Herpes* viruses.

9.3.3 *Herpes zoster* keratitis

Herpes zoster ophthalmicus may permanently reduced corneal sensation. Chronic epithelial defects with secondary bacterial infection are particularly common in those patients with anaesthetic corneas (deLuise and Wilson 1990).

A 67 year old lady was examined. She had suffered from the acute disease 14 years earlier. Diffuse stromal haze with vascularization of the stroma were seen using a slit-lamp. There was no sensation when cotton wool touched the cornea.

The nerve plexus imaged by confocal microscopy appeared similar to that shown in figure 9.5, with few remaining fragments of nerve fibres. Keratocytes in the stroma were densely packed and blood vessels containing moving cells could be clearly identified in deep cornea.

9.3.4 Leprosy

An 82 year old gentleman was examined who had suffered from lepromatous leprosy when young. There was marked corneal scarring. Schlaegel (1990) described transient thickening of corneal nerves in leprosy, resolving some weeks after the initial infection. Thickened nerves were not apparent in this patient using a slit-lamp, but by confocal microscopy, sub-epithelial nerve fibres appeared more than four times thicker than normal. A sample image is shown in figure 9.7. Scarring of the cornea in this case was severe. Deeper structures could not be imaged.

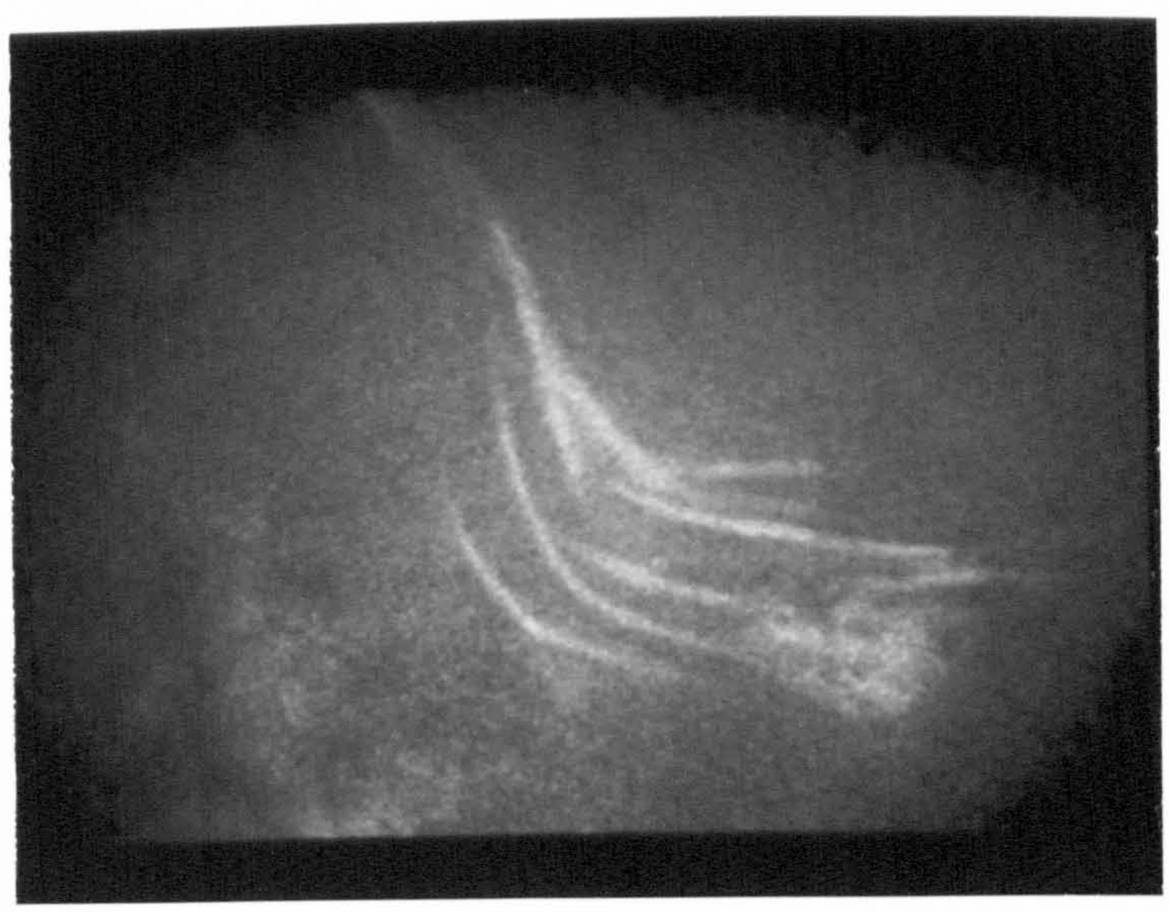


Figure 9.7
Thickened subepithelial nerve fibres in case of lepromatous leprosy.

9.4 Endothelial disease

Maurice, in 1963, described the specular microscope which is now used to examine the corneal endothelium. Imaging of the cell layer is made possible by elimination of some of the light scattered by superficial corneal layers. Illumination is via one half of the objective and observation via the other. However, it is less efficient than confocal microscopy at blocking light reflected from above and below the plane of focus. Imaging of the endothelium is not possible if the cornea is oedematous.

An advantage of confocal microscopy is that it can give clear images of endothelium despite corneal oedema. One of the endothelial functions is to maintain the dehydrated state of the stroma (Maurice and Giardini 1951). Oedema is common in diseases affecting the endothelium.

An example is presented here of a 46 year old lady with Irido-corneal-endothelial (ICE) syndrome, a rare disorder in which the endothelial monolayer is replaced by a sheet of abnormal cells (Kanski 1992a). In figure 9.8, the junction of normal and abnormal cells can be clearly identified. The overlying stroma was thickened and oedematous.

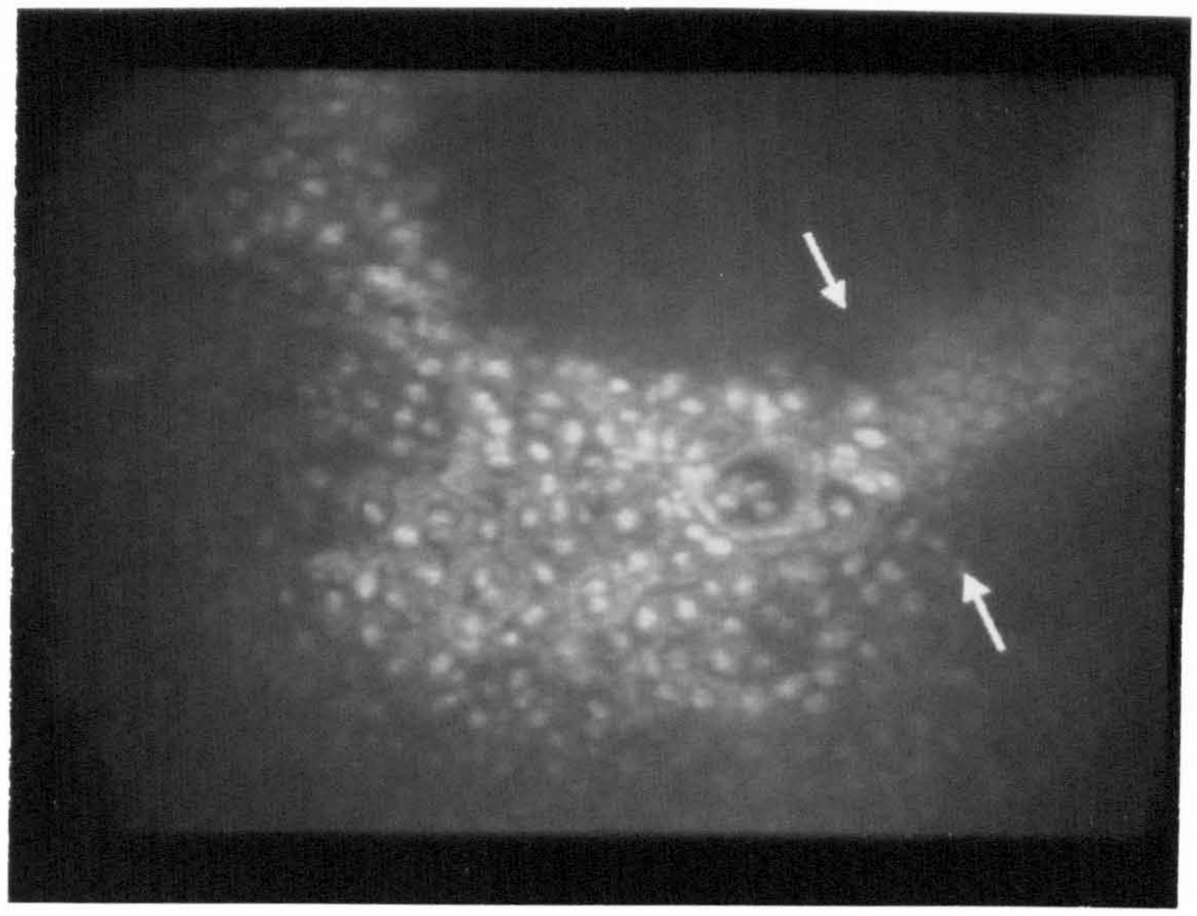


Figure 9.8
Junction of normal and abnormal cells in ICE syndrome (arrows). The overlying stroma and epithelium were hazy due to oedema.

9.5 Keratoconus

Several changes in the structure of the cornea have been described in keratoconus. There are abnormalities of the basal lamina with epithelial extensions into the stroma, thickening of the epithelium and areas of thinning of stroma (Lucas 1989). Corneal nerves are easily seen using a slit lamp and are presumed to be thickened (Kanski 1992b).

We examined two male patients with keratoconus (24 and 41 years old). Thickened stromal nerves were seen in both cases (figure 9.9). Fibre diameter measured 35-40 µm. No abnormalities of keratocytes adjacent to nerve fibres was observed. A normal stromal nerve, such as that in figure 3.6) measured about 12 µm across. No abnormalities of the epithelium, subepithelial nerve plexus, Bowman's membrane or keratocytes were observed.

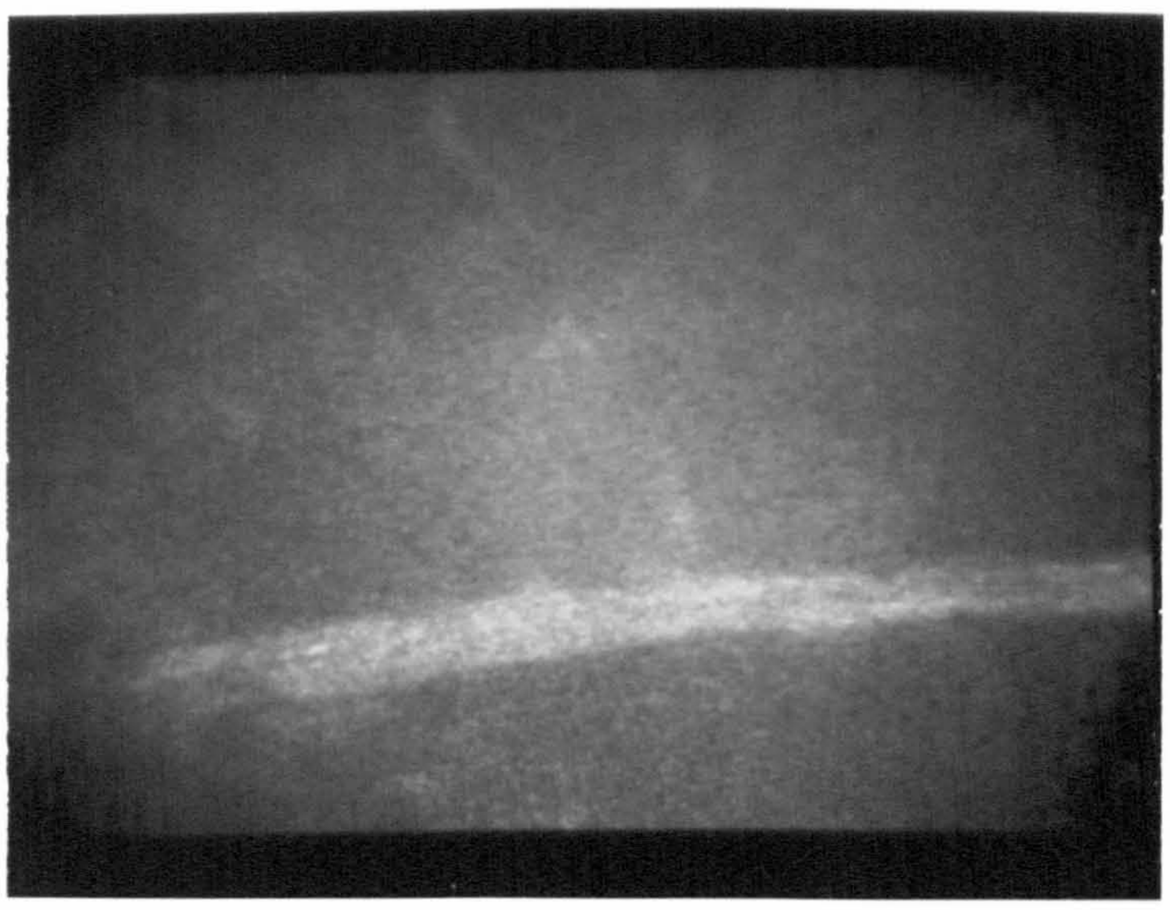


Figure 9.9
Thickened stromal nerve in case of keratoconus.

SUMMARY

The aims of the work reported in this thesis were:
(1) To use confocal microscopy to image internal corneal structure in conscious human subjects.
(2) To develop computerised methods for quantifying structures in images.
(3) To use the methodology to examine and make measurements in healthy eyes, during wound healing and in a variety of corneal diseases.

Confocal microscopy of normal cornea and methods for quantifying structure are reported in chapters 3, 4, and 5. Studies of tissue reaction to injury are described in chapters 6 and 7. Chapter 8 is concerned with the thickness of tear fluid between the eye surface and contact lenses, and chapter 9 with clinical applications of the techniques.

The work was made possible by very recent or ongoing advances in optical, video and computer methodologies. They enabled, for the first time, imaging and measurement of ongoing dynamic processes in undisturbed functioning corneal tissue in conscious human subjects. This is a significant advance in the methods available. Previously, microscopical structure in the cornea could only be seen using conventional histological techniques, which required complex methods of specimen preparation. Sectioning, fixation and staining of tissue was not required for confocal microscopy. As a result, sequential examinations and measurements could be made in the same subjects. This has not been possible before. The rapid advance in technology continues.

Confocal images are quite different from those by conventional light, fluorescence or electron microscopy - each of which require special procedures to prepare specimens and enable imaging of internal structure. Such preparation and processing of specimens may introduce artefacts. During confocal microscopy there was no physical or chemical manipulation of the tissue. Artefacts of this kind were eliminated. On the other hand, confocal imaging may have properties and limitations of its own. For instance the microscope objective used and methods of digital image processing may have introduced their own particular factors. This raises the question of how well the results represent actual corneal structure. However, this consideration is not new and applies equally to all techniques for imaging biological material. It is relevant to all forms of microscopy and different methods of staining.

The microscope objective used in the present work was of low magnification and numerical aperture. It was designed specifically for examining the cornea and its specifications enabled imaging of the full thickness of the tissue. Resolution of images was probably limited by the objective, in the plane of the image and at right angles to it. Collagen fibres in the stroma, fine cytoplasmic processes of keratocytes and the internal surface of contact lenses could not be resolved. Suitable objectives of higher magnification and numerical aperture may have enabled imaging of these and other structures. However, the lenses which are presently available would only have allowed imaging of superficial layers of the cornea and thus were not suitable for the work reported here. Also the higher magnification would have resulted in increased blurring in images due to eye movements, which are involuntary and continuous. Briefer exposure times would have been required to give clear images, but suitable equipment of sufficient sensitivity was not available.

Despite these various limitations, good quality images were obtained and enabled measurements to be made under specific and important clinical conditions: Epithelial thickness was measured to be 38 to 53 µm, with no variation across the central cornea. Density of keratocytes was greatest near the stromal surface, reducing towards posterior cornea, with increased cellularity just superficial to Descemet's membrane. After excimer laser photoablation, cell density, cell size and density of subepithelial scarring all increased to a maximum at 2-4 weeks. Almost no regeneration of subepithelial nerves was found up to 2.5 years after laser treatment. Clinical observations were made in infections by *Acanthamoeba*, and *Herpes simplex*, and in patients with *Herpes zoster*, Keratoconus, Leprosy, and Irido-corneal-endothelial syndrome.

REFERENCES

Abbott, R.L. and Elander, T.R. (1990) *Acanthamoeba* keratitis. In: Schwab, I.R. (Ed.) *Duane's clinical ophthalmology*, pp. 1-7. Philadelphia: Lippincott Company]

Beuerman, R.W. and Kupke, K. (1982) Neural regeneration following experimental wounds of the cornea in the rabbit. In: Hollyfield, J.G. (Ed.) *The structure of the eye*, pp. 319-330. Elsevier Noth Holland Inc.

Boettcher, K., Petroll, W.M., Jester, J.V. and Cavanagh, H.D. (1994) Determination of 3-dimensional keratocyte density in the rabbit cornea using laser confocal microscopy. *Invest. Ophthalmol. Vis. Sci.* **35**, 1355.

Bourne, W.M., McCarey, B.E. and Kaufman, H.E. (1980) Scanning mirror microscopy with optical sectioning characteristics: applications in ophthalmology. *Appl. Opt.* **19**, 1749-1757.

Boyde, A., Petran, M. and Hadravsky, M. (1983) Tandem scanning reflected light microscopy of internal features in whole bone and tooth samples. *J. Microsc.* **132**,1-7.

Boyde, A., Xiao, Q., Corle, T., Watson, T.F. and Kino, G.S. (1990) An evaluation of unilateral TSM for biological applications. *Scanning* **12**, 273-279.

Calmettes, L., Déodati, F., Planel, H. and Bec, P. (1956) Étude Histologique et Histochimique de L'épithélium Antérieur. *Arch. Ophthalmol. (Paris)* **16**, 481-506.

Cavanagh, H.D., Jester, J.V. and Essepian, J. (1990) Confocal microscopy of the living eye. *CLAO J.* **16**, 65-73.

Cavanagh, H.D., Petroll, W.M., Alizadeh, H., He, Y., McCulley, J.P. and Jester, J.V. (1993) Clinical and diagnostic use of *in vivo* confocal microscopy in patients with corneal disease. *Opthalmology* **100**, 1444-1454.

Chew, S., Beuerman, R.W., Assouline, M., Kaufman, H.E., Baron, B.A. and Hill, J.M. (1992) Early diagnosis of infectious keratitis with in vivo real time confocal microscopy. *CLAO J.* **18**, 197-201.

Clark, B.A.J. and Carney, L.G. (1971) Refractive Index and Reflectance of the Anterior Surface of the Cornea. *Am. J. Optom.* **48**, 337-346.

deLuise, V.P. and Wilson II, F.M. (1990) *Varicella* and *Herpes zoster Ophthalmicus*. In: Schwab, I.R. (Ed.) *Duane's clinical ophthalmology*, pp. 1-21. Philadelphia: Lippincott Company.

Dilly, P.N. (1988) Tandem scanning reflected light microscopy of the cornea. *Scanning* **10**, 153-156.

Egger, M.D., Gezari, W., Davidovits, P., Hadravsky, M. and Petran, M. (1969) Observation of nerve fibers in incident light. *Experientia.* **25**, 1225-1226.

Egger, M.D. and Petran, M. (1967) New reflected-light microscope for viewing unstained brain and ganglion cells. *Science.* **157,** 305-307.

Ehlers, N. (1965) The epithelial surface. *Acta Ophthalmol.* **Suppl. 181**, 35-54.

Ehlers, N. (1970) Some Comparative Studies on the Mammalian Corneal Epithelium. *Acta Ophthalmol.* **48**, 821-829.

Elkington, A.R. and Frank, H.F. (1984) Properties of light. In: *Clinical optics*, pp. 1-13. Oxford: Blackwell Scientific Publications.

Ficker, L., Hunter, P., Seal, D. and Wright, P. (1989) *Acanthamoeba* keratitis occurring with disposable contact lenses. *Am. J. Ophthalmol.* **108**, 453.

Fischer, F.P. (1928) Über die Darstellung der Hornhautoberfläche und ihrer veränderungen im reflexbild. *Archiv für Augenheilkunde.* **98**, 1-84.

Gartry, D.S., Kerr Muir, M. and Marshall, J. (1992a) Excimer laser photorefractive keratectomy. 18-month follow-up. *Ophthalmology.* **99,** :1209-1219.

Gartry, D.S., Kerr Muir, M., Lohmann, C.P. and Marshall, J. (1992b) The effect of topical corticosteroids on refractive outcome and corneal haze after photorefractive keratectomy. A prospective, randomized, double-blind trial. *Arch. Ophthalmol.* **110,** 944-52.

Gartry, D.S., Kerr Muir, M. and Marshall, J. (1993) The effect of topical corticosteroids on refraction and corneal haze following excimer laser treatment of myopia: an update. A prospective, randomised, double-masked study. *Arch. Ophthalmol.* **7,** 584-590.

Gonzalez, R.C. and Wintz, P. (1983a) Image Enhancement: Image smoothing. In: Anonymous *Digital Image Processing*, 6th edn. pp. 136-154. Reading, Massachusetts: Addison-Wesley Publishing Company.

Gonzalez, R.C. and Wintz, P. (1983b) Image enhancement: Image enhancement by histogram modification techniques. In: *Digital image processing*, 6th edn. pp. 118-136. Reading, Massachusetts: Addison-Wesley Publishing Company.

Goodman, G.L., Trokel, S.L., Stark, W.J., Munnerlyn, C.R. and Green, W.R. (1989) Corneal healing following laser refractive keratectomy. *Arch. ophthalmol.* **107**, 1799-1803.

Hanna, K.D., Pouliquen, Y.M., Waring III, G.O., Savoldelli, M., Fantes, F. and Thompson, K.P. (1992) Corneal wound healing in monkeys after repeated excimer laser photorefractive keratectomy. *Arch. Ophthalmol.* **110**, 1286-1291.

Ichijima, H., Petroll, W.M., Barry, P.A., Andrews, P.M., Dai, M., Cavanagh, H.D. and Jester, J.V. (1993) Actin filament organization during endothelial wound healing in the rabbit cornea: comparison between transcorneal freeze and mechanical scrape injuries. *Invest. Ophthalmol. Vis. Sci.* **34**, 2803-2812.

Jenkins, F.A. and White, H.E. (1985) Reflection. In: *Fundamentals of Optics*, pp. 523-526. McGraw HillBook Company.

Jester, J.V., Petroll, W.M., Feng, W., Essepian, J. and Cavanagh, H.D. (1992) Radial Keratotomy. 1. The wound healing process and measurement of incisional gape in two animal models using in vivo confocal microscopy. *Invest. Ophthalmol. Vis. Sci.* **33**, 3255-3270.

Jones, D.B. (1986) *Acanthamoeba*: the ultimate opportunist? *Am. J. Ophthalmol.* **102**, 527-530.

Kanski, J.J. (1992a) Glaucoma. In: *Clinical ophthalmology*, 2nd edn. pp. 181-231. Oxford: Butterworth-Heinemann Ltd.

Kanski, J.J. (1992b) The cornea and sclera. In: *Clinical ophthalmology*, 2nd edn. pp. 118-119. Oxford: Butterworth-Heinemann Ltd.

Katakami, C., Sahori, A., Kazusa, R. and Yamamoto, M. (1991) Keratocyte activity in wound healing after epikeratophakia in rabbits. *Invest. Ophthalmol. Vis. Sci.* **32**, 1837-1845.

Kino, G.S., Chou, C.H. and Xiao, G.K. (1988) Imaging theory for the scanning optical microscope. *Proc SPIE* **1028.**

Klyce, S.D. and Beuerman, R.W. (1988) Structure and function of the cornea. In: Kaufman, H.E., Barron, B.A. and McDonald, S.R. (Eds.) *The Cornea*, pp. 3-54. Churchill Livingstone.

Koester, C.J., Auran, J.D., Rosskothe, H.D. and Florakis, G. (1993) Clinical microscopy of the cornea utilizing optical sectioning and a high-numerical-aperture objective. *J. Opt. Soc. Am.* **10,** 1670-1679.

Laing, R.A., Sandstrom, M.M. and Leibowitz, H.M. (1975) In vivo photomicrography of the corneal endothelium. *Arch. ophthalmol.* **93**, 143-145.

Lawrenson, J.G., Corbett, M.C., O'Brart, D.P.S., Marshall, J. The effect of beam configuration on corneal sensitivity following excimer laser photorefractive keratectomy. *Invest. Ophthalmol. Vis. Sci.* 36(4), 714.

Lemp, M.A., Dilly, P.N. and Boyde, A. (1985) Tandem scanning (confocal) microscopy of the full thickness cornea. *Cornea* **4**, 205-209.

Lohmann, C.P., Gartry, D.S., Kerr Muir, M., Timberlake, G.T.F., Fitzke, F.W. and Marshall, J. (1991a) 'Haze' in photorefractive keratectomy: its origins and consequences. *Lasers Light Opthalmol.* **4**, 15-34.

Lohmann, C.P., Gartry, D.S., Kerr Muir, M., Timberlake, G.T.F., Fitzke, F.W. and Marshall, J. (1991b) Corneal haze after excimer laser refractive surgery: objective measurements and functional implications. *Eur. J. Ophthalmol.* **1**, 173-180.

Lohmann, C.P., MacRobert, I., Pattimore, A., O'Brart, D., Corbett, M.C., Kerr Muir, M. and Marshall, J. (1994) A histopathological study of surgical specimens of tissue responsible for haze and regression after excimer laser photokeratectomy. *Lasers Light Opthalmol.* **6**, 149-158.

Lohmann, C.P., Timberlake, G.T.F., Fitzke, F.W., Gartry, D.S., Kerr Muir, M. and Marshall, J. (1992) Corneal light scattering after excimer laser photorefractive keratectomy: the objective measurements of haze. *Refract. Corneal. Surg.* **8,** 114-121.

Lohmeyer, M., McNaughton, L., Hunt, S.P. and Workman, P. (1994) Stimulation of intracellular free calcium increases by platelet-activating factor in HT29 colon carcinoma cells. Spectrofluorimetric and preliminary spatio-temporal analysis using confocal laser scanning fluorescence imaging microscopy. *Biochem. Pharmacol.* **47,** 975-985.

Lucas, D.R. (1989) The conjunctiva, cornea and sclera. In: *Greer's ocular pathology*, 4th edn. pp. 45-80. Oxford: Blackwell Scientific Publications.

Marshall, J., Trokel, S., Rothery, S. and Krueger, R.R. (1986) Photoablative reprofiling of the cornea using an excimer laser: photorefractive keratectomy. *Lasers Opthalmol.* **1**, 21-48.

Marshall, J., Trokel, S., Rothery, S. and Schubert, H. (1985) An unltrastructural study of corneal incisions induced by excimer laser at 193 nm. *Opthalmology* **92**, 749-758.

Marshall, J., Trokel, S.L., Rothery, S. and Krueger, R.R. (1988) Long-term healing of the central cornea after photorefractive keratectomy using an excimer laser. *Ophthalmology* **95**, 1411-1421.

Masters, B.R. and Paddock, S. (1990) In vitro confocal imaging of the rabbit cornea. *J. Microscopy* **158**, 267-274.

Masters, B.R. (1994) Differentiation of basal epithelial cells to wing cells studied with real-time confocal microsocpy of *in*-vivo human cornea. Invest. Ophthalmol. Vis. Sci. **35(4)**, 1937.

Matsuda, H. (1967) Electron microscopic study of the corneal nerve with special reference to its endings. *Jap. J. Ophthalmol.* **12**, 163-173.

Maurice, D.M. (1968) Cellular membrane activity in the corneal endothelium of the intact eye. *Experimentia* **24**, 1094-1095.

Maurice, D.M. (1974) A scanning slit optical microscope. *Invest. Ophthalmol.* **13,** 1033-1037.

Maurice, D.M. and Giardini, A.A. (1950) A Simple Optical Apparatus for Measuring the Corneal Thickness, and the Average Thickness of the Human Cornea. *Brit. J. Ophthalmol.* **35**, 169-177.

Maurice, D.M. and Giardini, A.A. (1951) Swelling of the cornea in vivo after the destruction of its limiting layers. *Brit. J. Ophthalmol.* **35**, 791-797.

Minsky, M. (1988) Memoir on inventing the confocal scanning microscope. *Scanning* **10**, 128-138.

Møller-Pedersen, T., Ledet, T. and Ehlers, N. (1994) The keratocyte denisty of human corneas. *Current Eye Res.* **13**, 163-169.

O'Day, D., M. and Jones, B.R. (1990) *Herpes simplex* keratitis. In: Schwab, I.R. (Ed.) *Duane's clinical ophthalmology*, pp. 1-27. Philadelphia: Lippincott Company.

Pallikaris, I.G., Papatzanaki, M.E., Georgiadis, A. and Frenschok, O. (1990) A comparative study of neural regeneration following corneal wounds induced by argon fluoride excimer laser and mechanical methods. *Lasers Opthalmol.* **3**, 89-95.

Patel, S. (1992) An investigation of the optical zone of the human cornea and changes induced by excimer laser surgery. PhD Thesis, Glasgow Polytechnic. pp.67-98.

Petran, M. and Hadravsky, M. (1989) Tandem scanning microscope--a new tool for three-dimensional microanatomy. *Prog. Clin. Biol. Res.* **295,** 551-558.

Petran, M., Hadravsky, M., Benes, J. and Boyde, A. (1986) In vivo microscopy using the tandem scanning microscope. *Ann. N. Y. Acad. Sci.* **483,** 440-447.

Petran, M., Hadravsky, M., Benes, J., Kucera, R. and Boyde, A. (1985a) The tandem scanning reflected light microscope. Part 1 - the principle, and its design. *Proc. Roy. Mic. Soc.* **20**, 125-139.

Petran, M., Hadravsky, M., Boyde, A. and Mueller, M. (1985b) A tandem scanning reflected light microscope. In: *Science of Biological Specimen Preparation*, pp. 606-607. SEM Inc. AMF O'Hare, Chicago.

Petran, M., Hadravsky, M. and Egger, M.D. (1968) Tandem scanning reflected light microscopy. *J. Opt. Soc. Am.* **58**, 661-664.

Poole, C.A., Brookes, N.H. and Clover, G.M. (1993) Keratocyte networks visualised in the living cornea using vital dyes. *J. Cell Sci.* **106**, 685-692.

Prydal, J.I. (1991) Optical studies of the eye surface. PhD thesis, University of Cambridge.

Prydal, J.I., Artal, P., Woon, H. and Campbell, F.W. (1992) Study of human precorneal tear film thickness and structure using laser interferometry. *Invest. Ophthalmol. Vis. Sci.* **33,** 2006-2011.

Prydal, J.I. and Campbell, F.W. (1992) Study of precorneal tear film thickness and structure by interferometry and confocal microscopy. *Invest. Ophthalmol. Vis. Sci.* **33,** 1996-2005.

Prydal, J.I. and Dilly, P.N. (1994) Measurement of tear film thickness on the surface and under contact lenses. *Invest. Ophthalmol. Vis. Sci.* **35**, 1778.

Prydal, J.I., Kerr Muir, M. and Dilly, P.N. (1993) Comparison of tear film thickness in three species determined by the glass fibre method and confocal microscopy. *Arch. Ophthalmol.* **7,** 1472-1475.

Reinstein, D.Z., Silverman, R.H., Rondeau, M.J. and Coleman, D.J. (1994) Epithelial and corneal thickness measurements by high-frequency ultrasound digital processing. *Ophthalmology* **101**, 140-146.

Rözsa, A.J. and Beuerman, R.W. (1982) Density and organization of free nerve endings in the corneal epithelium of the rabbit. *Pain* **14,** 105-120.

Schlaegel, T.F. (1995) Uveitis associated with other bacterial infections. In: Schwab, I.R. (Ed.) *Duane's clinical opthalmology*, pp. 3-4. Philadelphia: Lippincott Company.

Tagawa, S. (1928) Über die Dispersion der Brechenden medien des Auges. *Archiv für Augenheilkunde* **99**, 587-610.

Trabucchi, G., Brancato, R., Verdi, M., Carones, F. and Sala, C. (1994) Corneal nerve damage and regeneration after excimer laser photokeratectomy in rabbit eyes. *Invest. Ophthalmol. Vis. Sci.* **35**, 229-235.

Whitear, M. (1960) An electron microscope study of the cornea in mice, with special reference to the innervation. *J. Anat. (Lond.)* **194**, 387-409.

Wilson, G., O'Leary, D.J. and Henson, D. (1980) Micropachometry: a technique for measuring the thickness of the corneal epithelium. *Invest. Ophthalmol. Vis. Sci.* **19**, 414-417.

Wilson, T. (1989) Trends in confocal microscopy. *TINS* **12**, 486-493.

Winchester, K., Mathers, W.D., Sutphin, J.E. and Daley, T.E. (1995) Diagnosis of *Acanthamoeba* keratitis in vivo with confocal microscopy. *Cornea* **14**, 10-17.

Wolff, E. (1968) The eyeball. In: Anonymous *Anatomy of the eye and orbit*, 6th edn. pp. 182-241. Philadelphia and Toronto: W.B. Saunders company.

Xiao, G.K., Corle, T.R. and Kino, G.S. (1988) Real-time confocal scanning optical microscope. *Appl. Phys. Lett.* **53**, 716-718.

Xiao, G.K. and Kino, G.S. (1987) A real-time confocal scanning optical microsocpe. In: Wilson, T. and Balk, L. (Eds.) *Proc SPIE 809*, 107-113.

Zander, E. and Weddell, G. (1951) Observations on the innervation of the cornea. *J. Anat. (Lond.)* **85**, 68-79.

ZIBL. LOKDIEL. UNIV.